



**Calhoun: The NPS Institutional Archive**  
**DSpace Repository**

---

Theses and Dissertations

1. Thesis and Dissertation Collection, all items

---

1956

Angular distributions of alpha particles  
scattered by light nuclei.

Watters, Harry J.

Massachusetts Institute of Technology

---

<http://hdl.handle.net/10945/13930>

---

*Downloaded from NPS Archive: Calhoun*



Calhoun is the Naval Postgraduate School's public access digital repository for research materials and institutional publications created by the NPS community. Calhoun is named for Professor of Mathematics Guy K. Calhoun, NPS's first appointed -- and published -- scholarly author.

**Dudley Knox Library / Naval Postgraduate School**  
**411 Dyer Road / 1 University Circle**  
**Monterey, California USA 93943**

<http://www.nps.edu/library>

**ANGULAR DISTRIBUTIONS OF ALPHA  
PARTICLES SCATTERED BY LIGHT NUCLEI**

**Harry J. Watters**



















ANGULAR DISTRIBUTIONS OF ALPHA PARTICLES  
SCATTERED BY LIGHT NUCLEI

by

Harry J. Watters

Lieutenant Commander, U. S. Navy

B. S. Purdue University (1949)

M. S. Massachusetts Institute of Technology (1953)

SUBMITTED IN PARTIAL FULFILLMENT OF THE  
REQUIREMENTS FOR THE DEGREE OF  
DOCTOR OF PHILOSOPHY

at the

MASSACHUSETTS INSTITUTE OF TECHNOLOGY  
1956



# ANGULAR DISTRIBUTIONS OF ALPHA PARTICLES SCATTERED BY LIGHT NUCLEI

Harry J. Watters

Submitted to the Department of Physics on 9 January 1956 in  
partial fulfillment of the requirements for the degree of  
Doctor of Philosophy

## ABSTRACT

A study has been made of the angular distributions obtained in the  $(\alpha, \alpha)$  and  $(\alpha, \alpha')$  interactions on  $\text{Li}^6$ ,  $\text{C}^{12}$ , and  $\text{Mg}^{24}$ . The M.I.T. cyclotron was utilized to obtain the 31.5-Mev alpha particles used in the bombardment of these target materials. Separation of the alpha particles from other products of the alpha induced reactions was accomplished by the use of a particle selection technique developed at the cyclotron laboratory. This equipment permitted the detection of groups of inelastically scattered alpha particles which were identified with known levels of excitation of the target nuclei.

Inelastic angular distributions were obtained for the following interactions:

$\text{Li}^6(\alpha, \alpha')\text{Li}^{6*}$	$Q = -2.18 \text{ Mev}$	$\text{C}^{12}(\alpha, \alpha')\text{C}^{12*}$	$Q = -7.65 \text{ Mev}$
$\text{Li}^6(\alpha, \alpha')\text{Li}^{6*}$	$Q = -4.5 \text{ Mev}$	$\text{Mg}^{24}(\alpha, \alpha')\text{Mg}^{24*}$	$Q = -1.37 \text{ Mev}$
$\text{C}^{12}(\alpha, \alpha')\text{C}^{12*}$	$Q = -4.43 \text{ Mev}$	$\text{Mg}^{24}(\alpha, \alpha')\text{Mg}^{24*}$	$Q = -4.12 \text{ Mev}$

The experimental results are shown to be in agreement with the angular distributions predicted for a direct surface interaction model.

The angular distributions of alpha particles elastically scattered by  $\text{Li}^6$ ,  $\text{C}^{12}$ , and natural Mg were also obtained. These data lend support to the increasing evidence that the nuclear elastic scattering of charged particles can be interpreted in terms of an optical model represented by a complex scattering potential.

In addition, it was determined that the excitation of isotopic spin prohibited levels in  $\text{Li}^6$  and in  $\text{N}^{14}$  occurred with a probability of less than about 5 percent that observed in the excitation of isotopic spin allowed levels of the same nuclei.

Thesis Supervisor: M. Stanley Livingston

Title: Professor of Physics

36226



# ANNUAL REPORT OF THE COMMISSIONER OF THE BUREAU OF MINES

1910-1911

Submitted to the Department of Mines on 1 January 1912 in  
partial fulfillment of the requirements for the degree of  
Doctor of Philosophy

## ABSTRACT

A study has been made of the angular distribution of  
rays in the (2,2) and (2,4) reflections of  $^{226}\text{Ra}$ . The  
W.L.T. system was utilized to obtain the 1.1-  
MeV alpha particles used in the experiment of these rays.  
Materials. Separation of the alpha particles from other pro-  
ducts of the alpha induced reactions was accomplished by the  
use of a certain technique developed at the University  
of California. This equipment permitted the detection of groups  
of isotopes scattered from particles with which they  
interacted with known levels of scattering of the target nuclei.

Isotopic angular distributions were obtained for the  
following isotopes:

$^{226}\text{Ra}$  (2,2)  $\alpha$  = -2.10 MeV  $C(2,2)(^{226}\text{Ra})$   
 $^{226}\text{Ra}$  (2,4)  $\alpha$  = -2.10 MeV  $C(2,4)(^{226}\text{Ra})$   
 $^{226}\text{Ra}$  (2,2)  $\alpha$  = -1.77 MeV  $C(2,2)(^{226}\text{Ra})$   
 $^{226}\text{Ra}$  (2,4)  $\alpha$  = -1.77 MeV  $C(2,4)(^{226}\text{Ra})$

The experimental results are shown to be in agreement with the  
angular distributions predicted for a direct nuclear interaction  
model.

The angular distribution of alpha particles is also  
scattered by  $^{226}\text{Ra}$ , and natural  $\text{Ra}$  was also obtained. These  
data are compared to the theoretical values for the nucleus  
elastic scattering of charged particles and is interpreted in  
terms of an optical model represented by a complex scattering  
potential.

In addition, it was determined that the scattering of iso-  
topic alpha particles levels in  $^{226}\text{Ra}$  and in  $^{228}\text{Ra}$  occurred at the  
probability of less than unity as observed in the  
scattering of isotopic alpha particles with the same model.

Thesis Department: M. Physics Department

Professor of Physics

1911

## ACKNOWLEDGMENT

The author wishes to thank his advisor, Prof. M. S. Livingston, for his valuable advice and counsel throughout the course of this investigation. He is also grateful to Prof. V. F. Weisskopf for many informative discussions and to Prof. Martin Deutsch for his frequent suggestions and for a critical analysis of the theoretical implications of the results of this experiment.

Sincere appreciation is extended to Prof. S. D. Drell, Dr. H. S. Hall, Dr. A. M. Lane, Dr. J. W. Haffner, and Mr. L. S. Rodberg for their continued interest and advice and for many helpful suggestions.

To Mr. E. White, Mr. F. Fay, and Mr. A. Nummola, of the M.I.T. cyclotron crew, the author wishes to express his most sincere gratitude for their continual efficient and untiring assistance.

Thanks is also due to Mr. J. B. Bulkley, Executive Officer of the Radioactivity Group, for his able assistance in initiating the preliminary research of this experiment.

Above all, the author would like to thank his wife whose patience, understanding, and encouragement were of invaluable assistance during the conduct of this investigation.

The report states that the investigation was conducted by the FBI, the Department of Justice, and the Department of Education. The report also states that the investigation was conducted by the FBI, the Department of Justice, and the Department of Education. The report also states that the investigation was conducted by the FBI, the Department of Justice, and the Department of Education.



## TABLE OF CONTENTS

I.	Introduction . . . . .	1
II.	Apparatus . . . . .	7
	A. Cyclotron and Emergent Beam . . . . .	7
	B. Scattering Chamber . . . . .	9
	C. Beam Monitor . . . . .	11
	D. Particle Selective Counter . . . . .	12
	E. Electronics . . . . .	15
III.	Preliminary Considerations . . . . .	21
	A. Beam Energy Determination . . . . .	21
	B. Energy Resolution . . . . .	23
	C. Target Choice . . . . .	26
	D. Target Preparation . . . . .	26
	E. Counter Zero Angle Determination . . . . .	30
IV.	Experimental Procedure . . . . .	32
	A. Identification of Alpha-Particle Groups . . . . .	32
	B. Angular Distribution Measurements . . . . .	39
	C. Cross Section Measurements . . . . .	45
	D. Back Angle Intensities . . . . .	47
	E. Energy Dependence of Angular Distributions . . . . .	50
	F. Experimental Uncertainties . . . . .	51
V.	Experimental Data . . . . .	57
VI.	Discussion of Results . . . . .	71
	A. Inelastic Scattering Process . . . . .	71



# TABLE IV. CONTENTS

I.	Introduction . . . . .	1
II.	General . . . . .	7
	1. General and Special . . . . .	7
	2. General . . . . .	7
	3. General . . . . .	12
	4. General . . . . .	12
	5. General . . . . .	12
III.	Particular . . . . .	23
	1. Particular . . . . .	23
	2. Particular . . . . .	23
	3. Particular . . . . .	23
	4. Particular . . . . .	23
	5. Particular . . . . .	23
IV.	General . . . . .	27
	1. General . . . . .	27
	2. General . . . . .	27
	3. General . . . . .	27
	4. General . . . . .	27
	5. General . . . . .	27
	6. General . . . . .	27
	7. General . . . . .	27
	8. General . . . . .	27
	9. General . . . . .	27
	10. General . . . . .	27
	11. General . . . . .	27
	12. General . . . . .	27
	13. General . . . . .	27
	14. General . . . . .	27
	15. General . . . . .	27
	16. General . . . . .	27
	17. General . . . . .	27
	18. General . . . . .	27
	19. General . . . . .	27
	20. General . . . . .	27
	21. General . . . . .	27
	22. General . . . . .	27
	23. General . . . . .	27
	24. General . . . . .	27
	25. General . . . . .	27
	26. General . . . . .	27
	27. General . . . . .	27
	28. General . . . . .	27
	29. General . . . . .	27
	30. General . . . . .	27
	31. General . . . . .	27
	32. General . . . . .	27
	33. General . . . . .	27
	34. General . . . . .	27
	35. General . . . . .	27
	36. General . . . . .	27
	37. General . . . . .	27
	38. General . . . . .	27
	39. General . . . . .	27
	40. General . . . . .	27
	41. General . . . . .	27
	42. General . . . . .	27
	43. General . . . . .	27
	44. General . . . . .	27
	45. General . . . . .	27
	46. General . . . . .	27
	47. General . . . . .	27
	48. General . . . . .	27
	49. General . . . . .	27
	50. General . . . . .	27
	51. General . . . . .	27
	52. General . . . . .	27
	53. General . . . . .	27
	54. General . . . . .	27
	55. General . . . . .	27
	56. General . . . . .	27
	57. General . . . . .	27
	58. General . . . . .	27
	59. General . . . . .	27
	60. General . . . . .	27
	61. General . . . . .	27
	62. General . . . . .	27
	63. General . . . . .	27
	64. General . . . . .	27
	65. General . . . . .	27
	66. General . . . . .	27
	67. General . . . . .	27
	68. General . . . . .	27
	69. General . . . . .	27
	70. General . . . . .	27
	71. General . . . . .	27
	72. General . . . . .	27
	73. General . . . . .	27
	74. General . . . . .	27
	75. General . . . . .	27
	76. General . . . . .	27
	77. General . . . . .	27
	78. General . . . . .	27
	79. General . . . . .	27
	80. General . . . . .	27
	81. General . . . . .	27
	82. General . . . . .	27
	83. General . . . . .	27
	84. General . . . . .	27
	85. General . . . . .	27
	86. General . . . . .	27
	87. General . . . . .	27
	88. General . . . . .	27
	89. General . . . . .	27
	90. General . . . . .	27
	91. General . . . . .	27
	92. General . . . . .	27
	93. General . . . . .	27
	94. General . . . . .	27
	95. General . . . . .	27
	96. General . . . . .	27
	97. General . . . . .	27
	98. General . . . . .	27
	99. General . . . . .	27
	100. General . . . . .	27

VI. B. Theoretical Angular Distribution and	
Comparison with Experiment . . . . .	74
C. Validity of Isotopic Spin Selection Rule . . .	89
D. Elastic Scattering . . . . .	90
VII. Conclusions . . . . .	99
Appendix I. Center-of-Mass Corrections for Angular	
Distribution Measurements . . . . .	105
Bibliography . . . . .	116
Biographical Note . . . . .	122

# VII. Theoretical and Experimental Results

Comparison with experiment . . . . .	10
5. Theory of the spin Hall effect . . . . .	11
6. Spin Hall effect . . . . .	12
VII. Conclusions . . . . .	13
Appendix I. Vector- and tensorial calculations for spin Hall effect	
Vectorial calculations . . . . .	14
Tensorial calculations . . . . .	15
References . . . . .	16

The spin Hall effect of light is a phenomenon that has been observed in a variety of contexts, including the propagation of light in anisotropic media, the scattering of light by small particles, and the interaction of light with matter. In this paper, we present a theoretical and experimental study of the spin Hall effect of light. We first review the basic theory of the spin Hall effect, and then present our experimental results. We find that the spin Hall effect is a universal phenomenon that can be observed in a wide range of systems. Our results provide a new way of understanding the spin Hall effect of light, and may have important implications for the development of new optical devices.

The spin Hall effect of light is a phenomenon that has been observed in a variety of contexts, including the propagation of light in anisotropic media, the scattering of light by small particles, and the interaction of light with matter. In this paper, we present a theoretical and experimental study of the spin Hall effect of light. We first review the basic theory of the spin Hall effect, and then present our experimental results. We find that the spin Hall effect is a universal phenomenon that can be observed in a wide range of systems. Our results provide a new way of understanding the spin Hall effect of light, and may have important implications for the development of new optical devices.

# LIST OF FIGURES

1. Schematic diagram of cyclotron and scattering chamber . . . . .	8
2. Photograph of scattering chamber . . . . .	10
3. Schematic drawing of particle selective counter . . .	14
4. a. Photograph of oscilloscope presentation of mass-energy spectrum of particles emitted from a $C^{12}$ target bombarded by 31.5-Mev alpha particles . .	19
b. Energy spectrum of alpha particles, shown in Fig. 4a, obtained by proper adjustment of bias voltage of multiplier pulse height analyzer . . . . .	19
5. Block diagram of electronic equipment . . . . .	22
6. Curve of proton pulse height ratios used in determination of beam energy . . . . .	24
7. Typical curve obtained in determining zero angle of the counter . . . . .	31
8. Photograph of oscilloscope presentation of mass-energy spectra of particles resulting from the 31.5-Mev alpha-particle bombardment of $Li^6$ , $C^{12}$ , and natural Mg . . . . .	34
9. Energy spectra of alpha particles shown in Figs. 8a, b, and c obtained by proper adjustment of bias voltage of multiplier pulse height analyzer . . . . .	36



- [illegible]

10.	Energy spectrum of alpha particles from $\text{Li}^6$ bombarded with 31.5-Mev alpha particles; counter angle 32 degrees . . . . .	28
11.	Energy spectrum of alpha particles from $\text{C}^{12}$ bombarded with 31.5-Mev alpha particles; counter angle 32 degrees . . . . .	43
12.	Energy spectrum of alpha particles from natural Mg bombarded with 31.5-Mev alpha particles; counter angle 32 degrees . . . . .	44
13.	Experimental angular distribution of alpha particles scattered inelastically from the 4.19-Mev level of $\text{Li}^6$ . . . . .	60
14.	Experimental angular distribution of alpha particles scattered inelastically from the 4.5-Mev level of $\text{Li}^6$ . . . . .	61
15.	Experimental angular distribution of alpha particles scattered inelastically from the 4.43-Mev level of $\text{C}^{12}$ . . . . .	62
16.	Experimental angular distribution of alpha particles scattered inelastically from the 7.65-Mev level of $\text{C}^{12}$ . . . . .	63
17.	Experimental angular distribution of alpha particles scattered inelastically from the 1.37-Mev level of $\text{Mg}^{24}$ . . . . .	64

15.	Heavy section of lime particles from 1A <sup>8</sup>
14.	Composed with 11.5-12.5% lime particles composed
13.	Heavy section of lime particles from 1A <sup>8</sup>
12.	Composed with 11.5-12.5% lime particles composed
11.	Heavy section of lime particles from 1A <sup>8</sup>
10.	Composed with 11.5-12.5% lime particles composed
9.	Heavy section of lime particles from 1A <sup>8</sup>
8.	Composed with 11.5-12.5% lime particles composed
7.	Heavy section of lime particles from 1A <sup>8</sup>
6.	Composed with 11.5-12.5% lime particles composed
5.	Heavy section of lime particles from 1A <sup>8</sup>
4.	Composed with 11.5-12.5% lime particles composed
3.	Heavy section of lime particles from 1A <sup>8</sup>
2.	Composed with 11.5-12.5% lime particles composed
1.	Heavy section of lime particles from 1A <sup>8</sup>



18.	Experimental angular distribution of alpha particles scattered inelastically from the 4.18-Mev level of $\text{Mg}^{24}$ . . . . .	65
19.	Experimental angular distribution of alpha particles elastically scattered by $\text{Li}^6$ . . . . .	66
20.	Experimental angular distribution of alpha particles elastically scattered by $\text{C}^{12}$ . . . . .	69
21.	Experimental angular distribution of alpha particles elastically scattered by natural Mg . . . . .	70
22.	Experimental data for the interaction $\text{Li}^6(\alpha, \alpha')\text{Li}^{6*}$ , $Q = -2.19$ Mev compared with theoretical angular distribution . . . . .	73
23.	Experimental data for the interaction $\text{Li}^6(\alpha, \alpha')\text{Li}^{6*}$ , $Q = -4.5$ Mev compared with theoretical angular distribution . . . . .	80
24.	Experimental data for the interaction $\text{C}^{12}(\alpha, \alpha')\text{C}^{12*}$ , $Q = -4.43$ Mev compared with theoretical angular distribution . . . . .	81
25.	Experimental data for the interaction $\text{C}^{12}(\alpha, \alpha')\text{C}^{12*}$ , $Q = -7.65$ Mev compared with theoretical angular distribution . . . . .	83
26.	Experimental data for the interaction $\text{Mg}^{24}(\alpha, \alpha')\text{Mg}^{24*}$ , $Q = -1.37$ Mev compared with theoretical angular distribution . . . . .	84

[illegible]

27.	Experimental data for the interaction $\text{Mg}^{24}(1,1')\text{Mg}^{24*}$ , $Q = -4.12$ Mev compared with theoretical angular distribution . . . . .	86
28.	Relative intensities of protons, deuterons, and alpha particles from the 31.5-Mev alpha-particle bombard- ment of $\text{Li}^6$ . . . . .	92
29.	Differential cross section ratio to coulomb for the elastic scattering of 31.5-Mev alpha particles from $\text{Li}^6$ , $\text{C}^{12}$ , and natural Mg . . . . .	100
30.	Angular relations between particle velocities in the laboratory and center-of-mass coordinate systems . . .	109
31.	Graphic representation of the angular relationship between laboratory and center-of-mass angles . . . . .	110
32.	Curves for the conversion of laboratory to center-of- mass angle for the reaction $\text{Li}^6(\alpha,\alpha')\text{Li}^6$ , $Q = 0$ , $\text{Li}^6(\alpha,\alpha')\text{Li}^{6*}$ , $Q = -2.19$ Mev, and $\text{Li}^6(\alpha,\alpha')\text{Li}^{6*}$ , $Q =$ $-4.52$ Mev . . . . .	111
33.	Graphic representation of equation (*) of App. I. . .	113
34.	Graphic representation of equation (5) of App. I . .	113
35.	Curves for the conversion of observed intensity to the center-of-mass system for the interaction $\text{Li}^6(\alpha,\alpha')\text{Li}^6$ , $Q = 0$ , $\text{Li}^6(\alpha,\alpha')\text{Li}^{6*}$ , $Q = -2.19$ Mev, and $\text{Li}^6(\alpha,\alpha')\text{Li}^{6*}$ , $Q = -4.52$ Mev . . . . .	115



[illegible]



## LIST OF TABLES

1. Angular positions of maxima and minima experimentally observed in the inelastic alpha-particle angular distribution . . . . . 66
2. Angular positions of maxima and minima of the inelastic alpha particle angular distributions compared with theoretical predictions for the direct surface interaction model . . . . . 88
3. Angular positions of the maxima observed in the elastic scattering angular distributions compared with those predicted for elastic scattering from an opaque sphere . . . . . 94
4. Angular positions of the maxima observed in the elastic scattering angular distributions compared with those predicted for elastic scattering from a square well potential . . . . . 98

1. The position of the system is determined by the position of the

center of mass of the system and the position of the

distances . . . . .

2. The position of the system is determined by the position of the

center of mass of the system and the position of the

distances . . . . .

3. The position of the system is determined by the position of the

center of mass of the system and the position of the

distances . . . . .

4. The position of the system is determined by the position of the

center of mass of the system and the position of the

distances . . . . .

5. The position of the system is determined by the position of the

center of mass of the system and the position of the

distances . . . . .

6. The position of the system is determined by the position of the

center of mass of the system and the position of the

distances . . . . .

7. The position of the system is determined by the position of the

center of mass of the system and the position of the

distances . . . . .

## I. INTRODUCTION

It has long been recognized that a direct experimental study of the scattering of charged particles by atomic nuclei provides a valuable source of information concerning the force field of the nucleus (B1). Subsequent to the classical investigations of Rutherford (R1) and Geiger and Marsden (G5), the alpha particles from radioactive substances were used intensively in studying this and other nuclear properties (B2, R3, D1). A renewal of interest in the scattering of alpha particles has been occasioned by the high energies to which they may be accelerated in the various types of particle accelerators. The stable 31.5-Mev high intensity alpha-particle beam, recently obtained at the M.I.T. cyclotron, has proven to be of great value in extending the scope of these investigations.

The primary object of this experiment is to obtain information concerning the inelastic scattering process. Relatively little data are available concerning the  $(\alpha, \alpha')$  interaction due to the experimental difficulties involved. The presence of elastically scattered alpha particles, as well as the reaction products from the  $(\alpha, p)$ ,  $(\alpha, d)$ , and  $(\alpha, t)$  interactions, makes identification of the inelastically scattered particles a major problem. This difficulty is





overcome by the use of a particle selection technique developed by Aschenbrenner (41). After suitable choice of target material (see Sec. IIIC), this technique permits the observation of separate alpha particle groups, each of which can be identified with a specific level of excitation in the target nucleus. The angular distributions of the inelastically scattered alpha particles can then be compared with those predicted by a theoretical treatment of the scattering process.

Nuclear interactions were, until recently, generally described by the compound nucleus model for nuclear reactions. This model was emphasized by Bohr in 1936 and has since been verified for a large class of nuclear reactions. It is assumed that when a target nucleus is bombarded by a charged particle, the two coalesce to form a compound nucleus in a state of excitation determined by the energy of the bombarding particle. A strong interaction between all the nucleons in the compound nucleus is assumed; the incident particle loses its independent identity and the total energy of the excited compound nucleus is shared in some way by all the nucleons present. It is postulated that the properties of the compound nucleus are independent of the mode of formation. Dissociation can occur in a great number of ways and competition among the various modes of dissociation does not



overcome by the use of a suitable solvent system  
developed by Langerman (11). After certain amount of  
target material (see sec. III C), this technique permits an  
observation of separate light scattering curves from which  
can be determined with a specific level of resolution in the  
target nucleus. The angular distribution of the scattered  
light scattered by the particles can then be compared with  
those predicted by a theoretical treatment of the scattering  
process.

Nuclear interactions were, until recently, generally de-  
scribed by the compound nucleus model for nuclear reactions.  
This model was established by Bohr in 1936 and has since been  
verified for a large class of nuclear reactions. It is as-  
sumed that when a target nucleus is bombarded by a charged  
particle, the two combine to form a compound nucleus in a  
state of excitation determined by the energy of the incident  
particle. A strong interaction between all the nucleons  
in the compound nucleus is assumed. The incident particle  
loses its independent identity and the total energy of the  
excited compound nucleus is shared in some way by all the  
nucleons present. It is postulated that the properties of  
the compound nucleus are independent of the mode of formation.  
Dissociation can occur in a great number of ways and under  
little energy the reverse mode of association does not

depend on the manner in which the compound nucleus was formed. Recent evidence has indicated that nuclear excitation may occur by processes which do not involve the formation of a compound nucleus. The results of the present experiment are not compatible with any known theory based on the compound nucleus interaction model.

Three interaction models are currently used to describe the excitation of atomic nuclei which results from a bombardment by charged particles (P2).

1. The statistical theory for nuclear reactions was proposed in 1940 (W4) and numerous experiments were designed to test its validity. Many of these experiments supported the theoretical predictions (B3, B4, D2). However, numerous reports such as those compiled by Cohen (C1) have disclosed discrepancies which are not explained by the statistical approach. This theory, whose model is the formation of a compound nucleus, predicts angular distributions which are symmetric about 90 degrees in the center-of-mass coordinates (H3) if:

- (a) the excitation levels of the compound nucleus are so closely spaced that they may be treated statistically or,
- (b) the levels are so widely separated that only one excitation level in the compound nucleus is involved in the interaction.

... report on the subject is that the ...  
... present evidence has indicated that ...  
... this can occur by ...  
... idea of a ...  
... systems are not ...  
... the ...  
... These ...  
... the ...  
... best by ...

1. The ...  
... proposed in ...  
... to test its ...  
... the ...  
... reports ...  
... distinguished ...  
... process. This ...  
... ground ...  
... which about 20 ...

(10) ...  
... (a) ...  
... are ...  
...  
... (b) ...  
... one ...  
... is ...



4

In certain special circumstances, the angular distribution need not be symmetric about 90 degrees in reactions involving formation of a compound nucleus.

2. A second model (H4, M3) is used to describe a reaction in which the target nucleus is excited through an electromagnetic interaction with the incident charged particle. The theory predicts angular distributions which depend on the energy of the incident particle and the multipole order involved in the transition.

3. As early as 1952 it was proposed (M2) that a model involving a direct interaction at the nuclear surface could be used to explain some of the experimental results which were not explained by either of the preceding theories. This concept was used with some success in studying the angular distributions obtained in (n,p) and (n, $\alpha$ ) reactions. The theory (A4) is analogous to the deuteron stripping calculations of S. T. Butler, and predicts the differential cross section for a reaction in which the residual nucleus is excited to a specific level. The angular distribution of the reaction products depends on the angular momenta and parity of initial and final levels of the residual nucleus. This direct interaction model, with certain modifications, has been used by others (B5, C2, G1, H2) in explaining experimental results which are not in agreement with the compound





nucleus or electric excitation models. Recent evidence of a direct interaction in the inelastic scattering process is illustrated in the  $\text{Fe}^{56}(\text{p}, \text{p}')\text{Fe}^{56*}$  data obtained by G. Schrank et al. (S2). The inelastic alpha-particle angular distributions obtained in the present investigation give strong support to the direct interaction process of nuclear excitation.

The properties of two of the nuclei chosen for investigation in this experiment permitted a test of the applicability of the isotopic spin selection rule in the  $(\alpha, \alpha')$  interaction. One of the conclusive verifications of the charge independence of nuclear forces is the validity of this selection rule in nuclear reactions (A5). Since the alpha particle and the ground levels of  $\text{Li}^6$  and  $\text{N}^{14}$  all have  $T = 0$ , according to the isotopic spin selection rule the low-lying  $T = 1$  levels of these nuclei should not be excited appreciably. The probability of excitation of these forbidden levels is compared experimentally with the probability for excitation of the allowed levels in the same nuclei to obtain a measure of the validity of this selection rule.

The angular distributions of alpha particles elastically scattered by  $\text{Li}^6$ ,  $\text{C}^{12}$ , and natural Mg were also obtained in this investigation. Numerous experiments have been performed to observe the elastic scattering of alpha particles by light nuclei (B7, F3, R4, W5). Deviations from coulomb scattering

[illegible]

at angles greater than about 30 degrees were noted in these data but no analyses of the observed structure were attempted. The angular distributions of elastically scattered protons (F3) exhibited a structure suggestive of a diffraction phenomenon. Using the optical model for nucleon scattering and following the method of Feshbach et al. (F4), a theoretical angular distribution was obtained (F5) which compared favorably with the experimental data. Recent progress in interpreting data (B6) obtained in the elastic scattering of alpha particles from heavy nuclei (F1, W3) has revived an interest in the elastic scattering by light nuclei. Diffraction patterns obtained in the elastic scattering of alpha particles by light nuclei have been compared with the diffraction of light by an opaque disc (E1, T2) and by an opaque sphere (F9). In the present investigation, the elastic alpha-particle angular distributions also exhibit a structure similar to that which occurs in optical diffraction. These experimental results are compared with the diffraction of light by an opaque sphere and this interaction model is shown to be consistent with the model employed to describe the inelastic scattering data. It is also shown, however, that the elastic angular distributions are not incompatible with the theoretical predictions for scattering by a square well potential.





## II. APPARATUS

### A. CYCLOTRON AND EMERGENT BEAM

The high-energy alpha particles used in these experiments were produced in the M.I.T. cyclotron (L1) by accelerating doubly ionized helium atoms to an energy of approximately 31.5 Mev. The cyclotron is surrounded by 4-foot thick concrete walls which act as a radiation shield for personnel and reduce the background radiation in the scattering chamber. The scattering chamber is located in an adjacent room which has 2-foot thick concrete walls providing protection from radiation originating in the chamber. By means of a focusing magnet located in the main cyclotron vault, the external beam is directed into the scattering chamber through a tube which passes through the walls of the main vault. This tube contains a series of tantalum baffles to prevent small angle scattered particles from reaching the target, and a defining and antiscattering slit system at the scattering chamber entrance. After passing through the target, located at the center of the scattering chamber, the beam terminates in the Faraday cup in the beam catcher. The adjustable focus magnet, remotely controlled from the outside area, is set for maximum beam current in the Faraday cup as measured by a sensitive



[illegible]

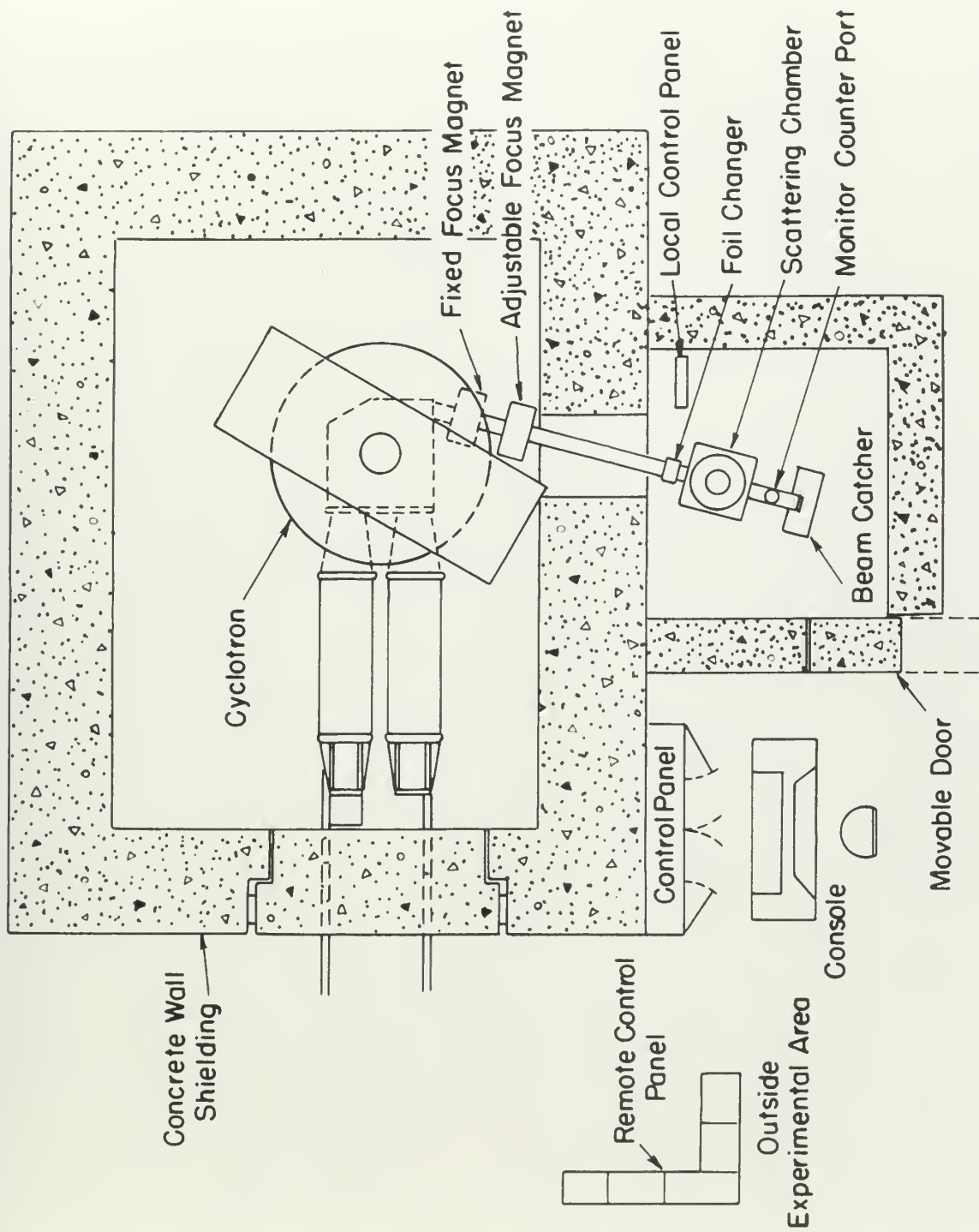


Figure 1



microammeter. The focusing system produces at the center of the target a spot which is  $1/4$  in. wide and  $5/16$  in. high. The foil changer contains a series of aluminum absorbers which can be inserted in or removed from the beam path by remote control, when it is desirable to vary the beam energy. A schematic diagram of the cyclotron and scattering chamber is shown in Fig. 1.

## B. SCATTERING CHAMBER

A photograph of the scattering chamber, previously described by Haffner (H1), is shown in Fig. 2. The main features of this chamber are:

1. The chamber contains mounting arms for two counters. Each arm can be rotated from 0 degrees to  $\pm 175$  degrees, with an accuracy of  $\pm 0.1$  degree. This provides versatility in that the arrangement is excellent for particle- $\gamma$  coincidence measurements and for angular correlation studies.
2. The target holder has a capacity of four and can be rotated through 360 degrees. Target choice and angular position can be controlled remotely from the outside area. The target holder can be raised into the bell jar hydraulically, in which position the scattering chamber is sealed off, and completely isolated from the bell jar. Targets can be changed

microscopy. The specimen is mounted on a slide of  
the target a root which is 1/4 in. thick and 1/16 in. wide.  
The foil chamber consists of a series of aluminum chambers  
which can be inserted as or removed from the main body  
very easily, when it is desirable to vary the beam energy.  
A schematic diagram of the operation and construction of the  
is shown in Fig. 1.

## 2. SCATTERING CHAMBER

A photograph of the scattering chamber, previously de-  
scribed by Bellner (2), is shown in Fig. 2. The main body  
of this chamber is:

1. The chamber contains mounting arms for the detectors.  
They can be rotated from 0 degrees to 15 degrees, with  
an accuracy of 0.1 degrees. This provides versatility in  
that the arrangement is simplified for the study of scattering  
measurements and for angular correlation studies.
2. The target holder has a capacity of four and can be  
rotated through 180 degrees. Target choice and angular posi-  
tion can be controlled remotely from the outside area. The  
target holder can be raised into the well for automaticity,  
in which position the scattering chamber is sealed off, and  
completely isolated from the hall air. Targets can be changed



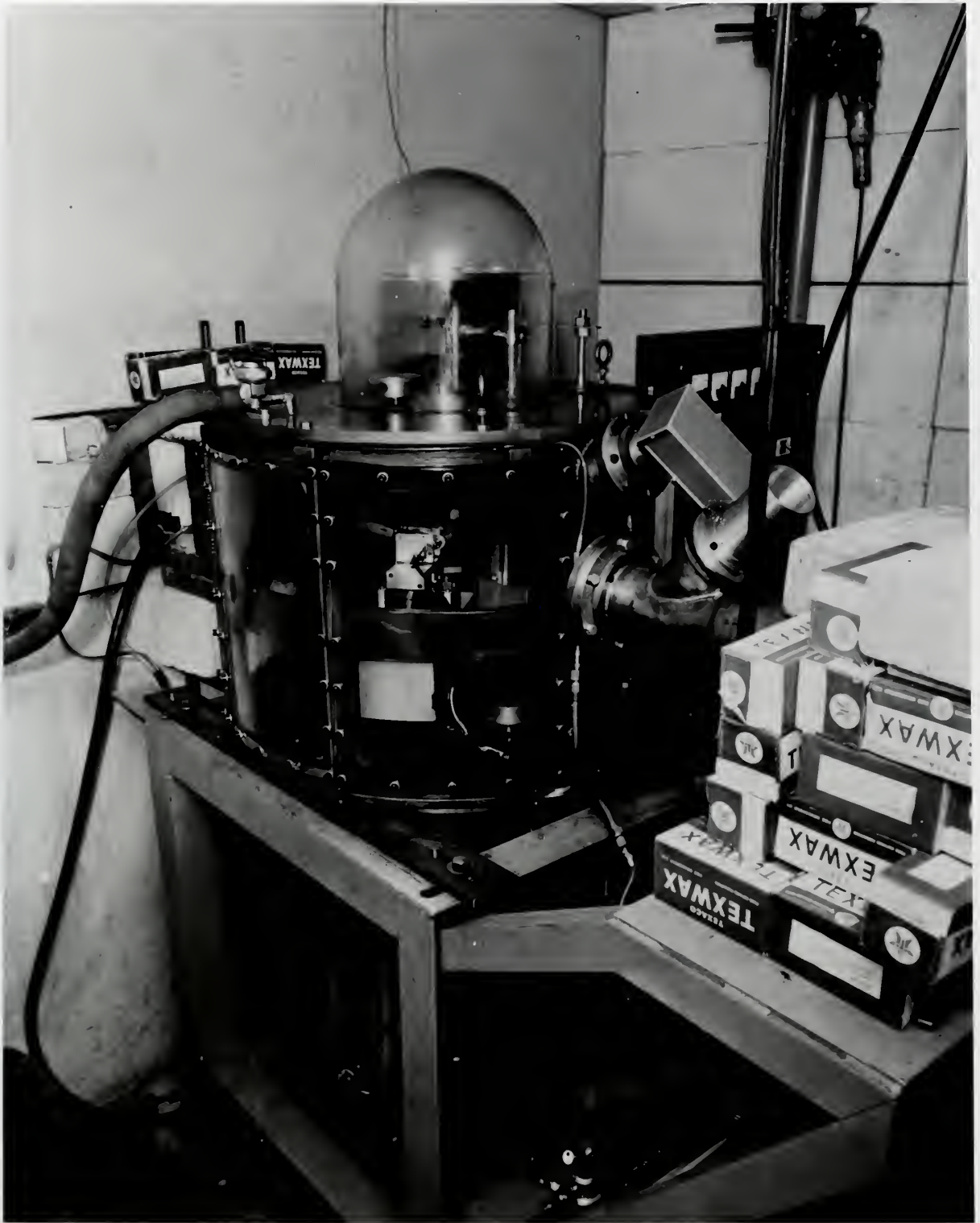


Figure 2



without affecting the scattering chamber vacuum. In addition, an evaporator is contained in the bell jar permitting targets to be made and subsequently bombarded without exposure to air.

3. The angular position of counter arms and target is measured by bridge circuits which contain precision helipot. This provides the positioning accuracy of 0.1 degree previously mentioned.

4. The angular position of counter arm or target and the choice of target can be controlled remotely from the outside area. In addition, these functions can be controlled from within the scattering chamber vault and the plexiglas windows permit visual observation of the scattering chamber interior.

#### C. BEAM MONITOR

The beam monitor consists of a scintillation counter mounted in a port, at an angle of 45 degrees from the incident beam, between the scattering chamber and the beam catcher. At this point a thin gold foil is fixed in the beam at an angle of 45 degrees, so that only particles scattered 45 degrees by the gold foil are "seen" by the monitor counter.

During the conduct of this experiment, the monitor discriminator was set so that the monitor scaler only counted

without affecting the monitoring channel system. In addition, no vaporizer is contained in the cell for preventing vapors to be made and subsequently condensed without exposure to air.

3. The angular position of counter arm and target is measured by bridge circuits which maintain constant deflection. This provides the positioning accuracy of 0.1 degree previously mentioned.

4. The angular position of counter arm or target and the choice of target can be controlled remotely from the outside area. In addition, these functions can be controlled from within the monitoring chamber via the electrical window panel which observation of the scattering chamber interior.

#### C. BEAM MONITOR

The beam monitor consists of a scintillation counter mounted in a box, at an angle of 45 degrees from the incoming beam, between the scattering chamber and the beam catcher. At this point a thin gold foil is fixed in the beam at an angle of 45 degrees, so that only particles scattered at 90 degrees by the gold foil are "seen" by the monitor counter. During the conduct of such experiments, the monitor discriminator was set so that the monitor counter only counted



the elastic alpha particles scattered at 45 degrees by the gold foil. The optics of this counter is similar to that described by Stoddart and Gove (21). The scintillation counter consists of a Dumont 6291 photomultiplier tube and a plastic\* scintillator.

#### D. PARTICLE SELECTIVE COUNTER

It is a well established fact that the specific energy loss in traversing matter of a nonrelativistic heavy particle of a given energy is dependent upon its mass. The expression for the specific energy loss given by Livingston and Bethe (12) can be written

$$-\frac{dE}{dx} = \frac{4\pi Z^2 z e^4 N M}{m E} \ln \left( \frac{4mE}{MI} \right)$$

where  $Ze$ ,  $M$ , and  $E$  are the charge, mass, and energy of the incident particle,  $Nz$  and  $I$  are the number of electrons per  $\text{cm}^3$  and the average excitation potential of the atom of the material traversed, and  $m$  is the electron mass. For a given substance,  $N$ ,  $z$ ,  $m$ , and  $e$  are constant and the logarithm term is practically constant over the energy range under consideration. Therefore to a good approximation, for nonrelativistic particles the above can be written

---

\* Pilot "B" - Pilot Chemicals, Inc., 47 Felton Street,  
Waltham, Mass.



$$\frac{dE}{dx} = \left(\frac{M_0^2}{E}\right)K$$

where  $K$  varies only slightly with energy. Then, if both  $dE/dx$  and the total energy  $E$  are known, the mass  $M$  of the particle can be determined.

A particle selection technique has been devised by Aschenbrenner utilizing the above principles. The detector consists of two scintillation counters, each using a Dumont 6291 photomultiplier tube (Fig. 3). The first crystal is a thin plastic (Pilot "B") scintillator which measures the initial specific ionization of the incident particles. The second is a thallium-activated sodium iodide crystal which measures the remaining energy of the particles after traversing the thin scintillator. The pulse height from the first photomultiplier is proportional to  $dE/dx$  since all particles traverse the same thickness of plastic scintillator. After amplification and pulse shaping, pulses from the two scintillators are added electronically to give a resultant pulse height proportional to the initial total energy  $E$  of the incident particle. The  $dE/dx$  and total energy  $E$  pulses are then multiplied electronically to give an output pulse proportional to







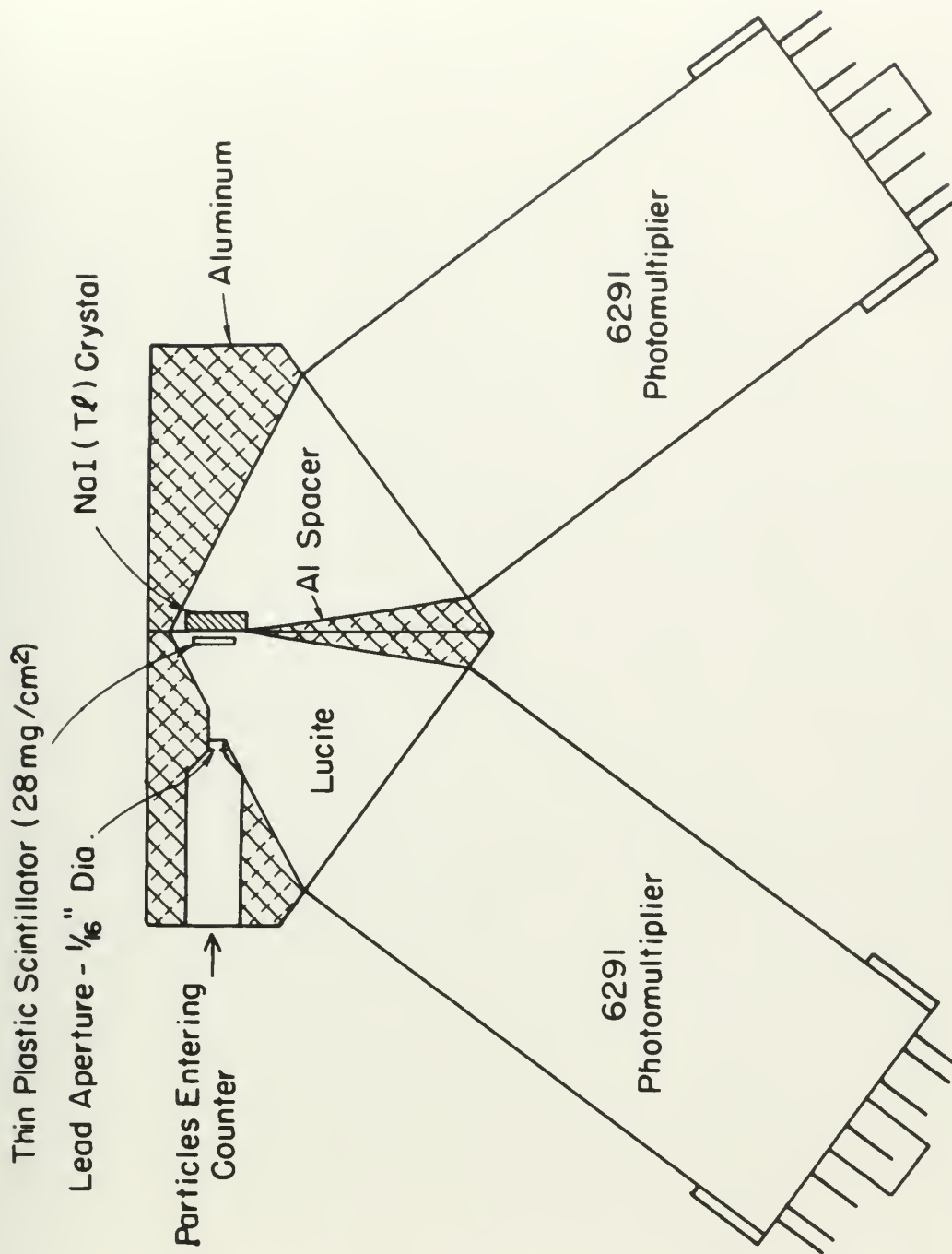


Figure 3

PARTICLE SELECTIVE COUNTER  
SCHEMATIC DIAGRAM



$$\frac{dE}{dx} \cdot E = \left(\frac{M_1^2}{E}\right) K \cdot E \propto Z^2 M$$

Theoretically then, these product pulses should occur in the ratio of 1:2:3:16 for incident protons, deuterons, tritons, and alpha particles of the same energy. Due to the nonlinear response of the plastic and sodium iodide scintillators, and other effects not considered in the approximations made, the observed ratio of pulse heights deviates somewhat from this theoretical ratio. However, since these pulses are used only to identify the reaction products, the deviations do not interfere with the particle selection technique.

## E. ELECTRONICS

The functions and over-all method of operation of the electronic equipment will be described for completeness. A detailed description of the electronic components including circuit diagrams has previously been described by Aschenbrenner (A1).

Pulses from the two photomultipliers feed directly into cathode followers (W1) mounted on the counter arm in the scattering chamber. The output signals are then fed to preamplifiers located in the scattering chamber vault. These three-stage preamplifiers invert the signals and the pulses

The deviations in the literature with the various papers  
these could be used only to identify the various programs  
which are somewhat from this theoretical point. However, since  
propositions which the various type of model have been  
rejection, and other criteria are considered in the ex-  
istence of various types of model have been followed  
the various types of model have been followed  
which are somewhat from this theoretical point. However, since  
propositions which the various type of model have been  
rejection, and other criteria are considered in the ex-  
istence of various types of model have been followed

The Inspector and several members of staff of the  
electronic equipment will be assigned for maintenance, a  
detailed description of the electronic equipment is  
being given and previously has been described by the Inspector.

[illegible]



are then conducted to the electronic apparatus located at the outside experimental area. Here, after suitable pulse shaping and linear amplification, the two output pulses are added electronically. This is accomplished by feeding the pulses into the grids of a double triode and superposing the plate currents through a common plate resistor. The adder output pulse is then fed to one side of the pulse multiplier. The shaped amplified pulse from the plastic scintillator provides the second input to the multiplier. Multiplication is accomplished by a  $5 \times 5$  array of matched 6BN6 tubes whose characteristics are such that the plate output pulses are proportional to the product of the pulses fed into the two grids over a range of 0 to 15.5 volts. Phototube high voltage and amplifier gain must be such that the multiplier inputs do not exceed this range. The multiplier output then consists essentially of pulses of three heights corresponding to the alpha particles, deuterons, and protons entering the counter.

The information obtained from the particle selective counter is displayed on an oscilloscope to permit visual observation during adjustment of electronic components. The multiplier output pulses, proportional to  $Z^2M$ , are fed through a single channel pulse height analyzer and a coincidence

the beam connected to the electrostatic deflection system is  
 the outside deflection system. After deflection the  
 scanning and linear amplifiers, and two other stages  
 are added electrically. This is accomplished by loading  
 the tubes into the grid of a double triode and connecting  
 the other output tube to a common plate resistor. The  
 other output tube is then fed from one side of the plate  
 resistor. The shaped amplified signal from the double  
 triode provides the second input to the amplifier.  
 Amplification is accomplished by a 2 x 2 stage of vacuum  
 tubes whose characteristics are such that the plate vol-  
 tage pulses are proportional to the product of the plate vol-  
 tage and the two grids over a range of 0 to 10 volts. There-  
 fore high voltage and amplifier gain must be such that the  
 amplifier inputs do not exceed this range. The amplifier  
 output then provides a series of pulses of three magnitudes  
 corresponding to the alpha particles, fission, and gamma  
 entering the counter.

The information obtained from the detector assembly  
 is displayed on an oscilloscope to which a series of  
 resistor divider networks of different components. The  
 amplifier output pulses, proportional to  $E^2$ , are fed through  
 a series channel pulse height analyzer and a coincidence

circuit to the Y axis of the oscilloscope. The shaped amplified NaI scintillator pulses, proportional to particle energy, provide the input to another single channel pulse height analyzer, then feed through the coincidence circuit to the X axis input. The coincidence circuit ensures that only those counts are registered which result from pulses occurring simultaneously at the two analyzer inputs. In addition, the coincidence pulses operate a trigger circuit which operates the intensifying control in the oscilloscope. Thus a particle which traverses the plastic scintillator and is stopped in the NaI crystal registers as a momentary spot on the oscilloscope face, the Y position indicating the mass and the X position the energy of the particle.

By visual observation of the oscilloscope face, the window width and bias of the pulse height analyzers can be set to exclude all but particles of a given mass, or all but particles of a given energy spread. This, of course, includes the possibility of counting all particles of a given mass and any energy or particles of any mass but with an energy which lies in a specific energy interval. Figure 4a is a photograph of the oscilloscope face showing the mass and energy spectrum of particles emitted from a  $C^{12}$  target under bombardment by 31.5-Mev alpha particles, observed at an angle of 17 degrees from the direction of the incident beam. The proton







501  
spectrum appears as a low-energy continuum with four distinguishable higher-energy groups of which the highest is the most intense. Three separate deuteron groups and four well separated alpha-particle groups are seen.

When the bias level and window width of the analyzer fed by the multiplier are set to exclude all but pulses due to alpha particles, the spectrum appears as shown in Fig. 4b. This energy spectrum is then scanned using a method in which a single channel pulse height analyzer performs the function of a 20-channel device. By use of an external battery box, a bias range, chosen to include the desired range of pulse heights, is applied to a voltage divider consisting of 20 precision resistors. The window width of the analyzer fed by the NaI scintillator is then adjusted to a value approximately 10 percent greater than one-twentieth of the bias range chosen. This ensures a slight overlap in scanning the energy spectrum. A relay, actuated by the output from the monitor counter scaler, then steps the analyzer window through the 20 individual bias voltage increments in turn, the number of pulses corresponding to each pulse height interval being counted in separate registers. The monitor scaler only counts the alpha particles elastically scattered at 45 degrees by a gold foil. Thus by using the monitor scaler to actuate the stepping relay we ensure that each of the 20 bias increments

...the most common. These are the ...  
...well ...  
...the ...  
...by the ...  
...also ...  
...This ...  
...a ...  
...of a ...  
...a ...  
...which ...  
...increased ...  
...so the ...  
...help ...  
...chosen. ...  
...spectrum. ...  
...counter ...  
...to ...  
...values ...  
...counted ...  
...the ...  
...will ...  
...because ...

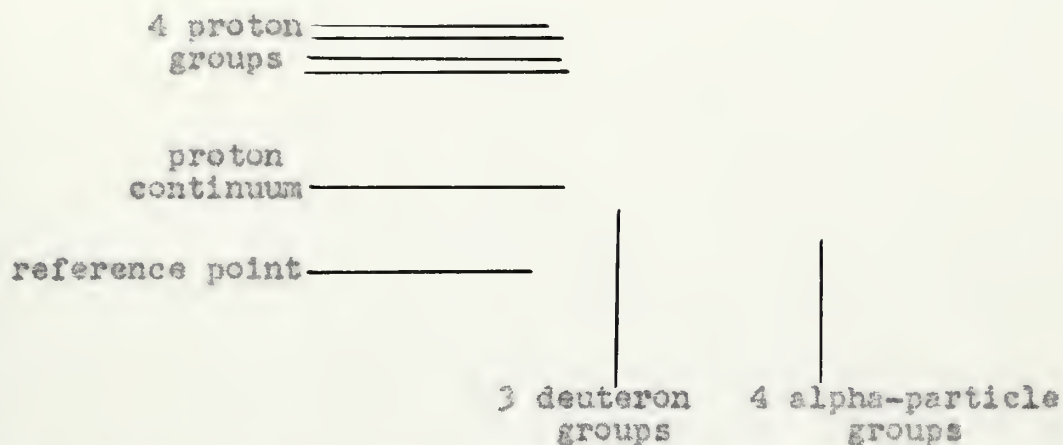


Fig. 4a. Photograph of oscilloscope presentation of mass-energy spectrum of particles emitted from a  $C^{12}$  target bombarded by 31.5-Mev alpha particles.

Fig. 4b. Energy spectrum of alpha particles, shown in Fig. 4a, obtained by proper adjustment of bias voltage of multiplier pulse height analyzer.

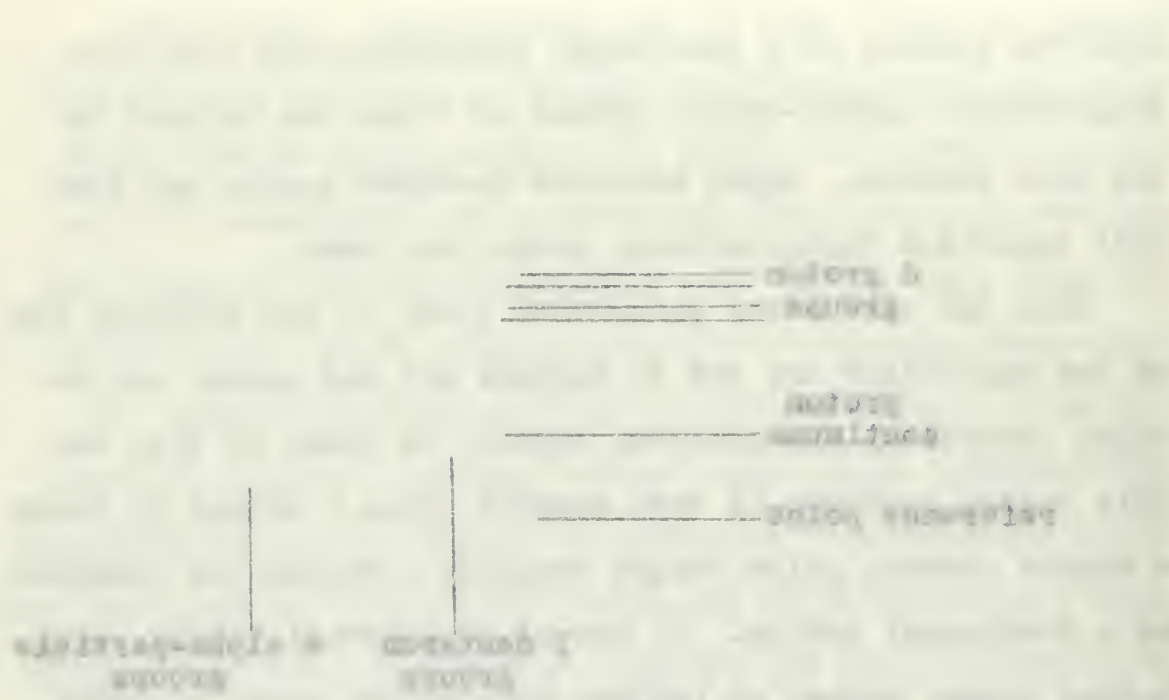
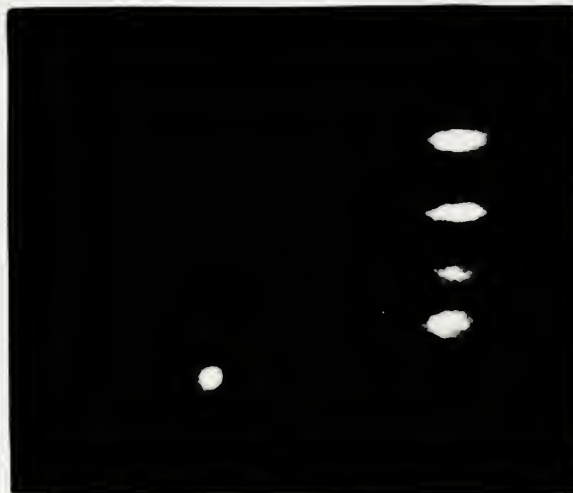
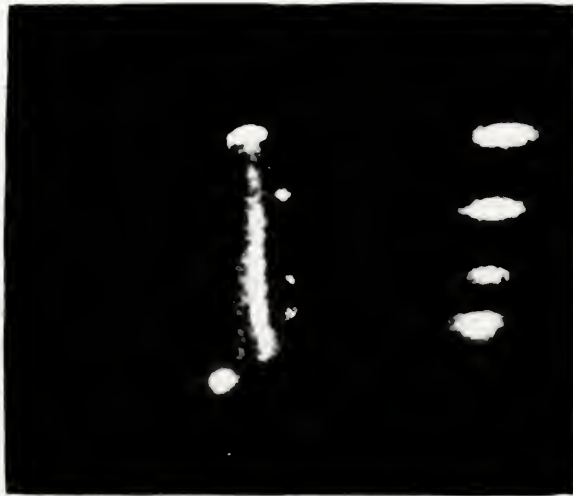


Fig. 10. Diagram of vertical axis. The axis is divided into four segments by horizontal lines. The segments are labeled 'a-b', 'b-c', 'c-d', and 'd-e' from top to bottom. The labels 'a' and 'b' are on the left side of the axis, and 'c' and 'd' are on the right side. The labels 'a-b', 'b-c', 'c-d', and 'd-e' are on the right side of the axis.

Fig. 10. Diagram of vertical axis. The axis is divided into four segments by horizontal lines. The segments are labeled 'a-b', 'b-c', 'c-d', and 'd-e' from top to bottom. The labels 'a' and 'b' are on the left side of the axis, and 'c' and 'd' are on the right side. The labels 'a-b', 'b-c', 'c-d', and 'd-e' are on the right side of the axis.







is observed for the same length of time in terms of total number of particles in the incident beam. This automatically compensates for changes in intensity of the beam during a given observation. The experimental assembly of equipment is shown functionally in the block diagram of Fig. 5.

### III. PRELIMINARY CONSIDERATIONS

#### A. BEAM ENERGY DETERMINATION

A 1.4-mil thick natural lithium target was placed in the scattering chamber perpendicular to the beam. The particle selective counter was then used to identify the two proton groups resulting from the reaction  $\text{Li}^7(\alpha, p)\text{Be}^{10}$   $Q = -2.56$  Mev and  $\text{Li}^7(\alpha, p)\text{Be}^{10*}$   $Q = -5.94$  Mev. It was experimentally observed that the intensity of these two groups varied considerably with angle and that the ratio of intensities was smallest at about 28 degrees. The counter was then set at 28 degrees and was used to obtain the energy spectrum of protons after they pass through an aluminum absorber placed in front of the counter aperture. A linear pulse generator was used to calibrate the single channel pulse height analyzer since zero bias on this analyzer does not correspond to zero

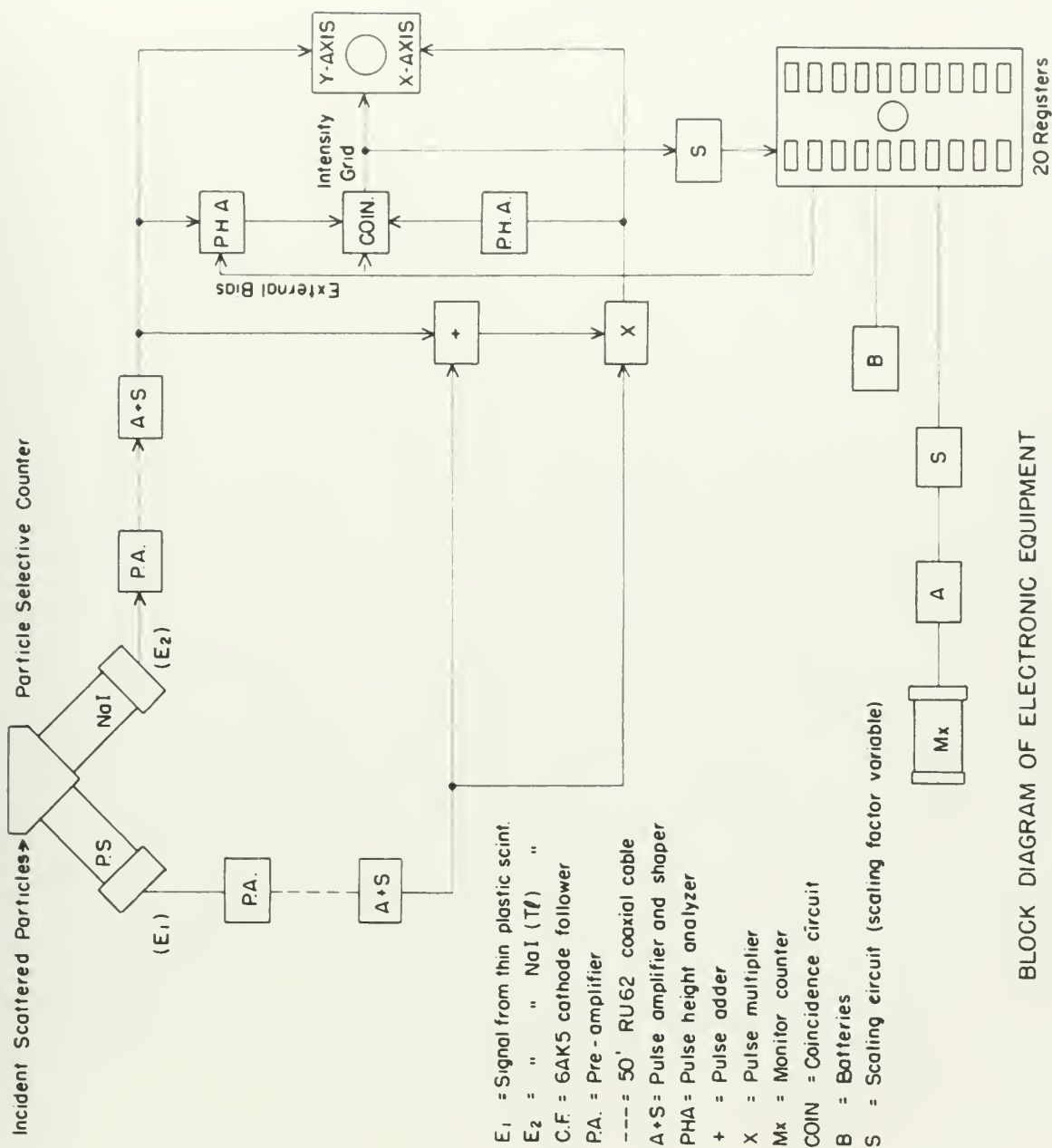
is observed for the same length of time in terms of total number of particles in the incident beam. This is especially convenient for changes in intensity of the beam having a given observation. The experimental assembly of apparatus is shown schematically in the block diagram of Fig. 2.

### III. PRELIMINARY OBSERVATIONS

#### A. BEAM ENERGY DETERMINATION

A 1.4-mil thick natural lithium target was placed in the scattering chamber perpendicular to the beam. The resulting selective counter was then used to identify the two proton groups resulting from the reaction  $Li(p, \alpha)He$   $Q = -2.12$  Mev and  $Li(p, \alpha)He$   $Q = -2.94$  Mev. It was experimentally observed that the intensity of these two groups varied considerably with angle and that the ratio of intensities was smallest at about 30 degrees. The counter was then set at 30 degrees and was used to obtain the energy spectrum of protons after they pass through an aluminum absorber placed in front of the counter aperture. A linear pulse generator was used to calibrate the single channel pulse height analyzer since zero bias on this analyzer does not correspond to zero





BLOCK DIAGRAM OF ELECTRONIC EQUIPMENT

Figure 5



pulse height. Spectra including these two proton peaks were taken using aluminum absorber of thicknesses 274 mg/cm<sup>2</sup> and 330 mg/cm<sup>2</sup>.

If we define  $E_p$  and  $E_{p'}$  as the energies of the protons incident on the NaI(Tl) crystal from the ground and first excited levels of Be<sup>10</sup> respectively, then the beam energy can be determined by the ratio  $E_p/E_{p'}$ ; since this ratio varies with beam energy as shown in Fig. 6. The beam energy was measured at frequent intervals and the 64 measurements obtained approximate a normal distribution about 31.5 Mev with 41 measurements falling inside one standard deviation. The error assigned in the energy determination includes the straggling effect in the absorbing material traversed.

## B. ENERGY RESOLUTION

Since the particle selective detector consists of two scintillation counters it seemed advisable to determine the highest resolution attainable with the NaI(Tl) crystal and then to determine the effect of introducing the plastic scintillator. The plastic scintillator was removed and the counter positioned at an angle of 30 degrees with the beam. A freshly cleaved NaI(Tl) crystal was used and extreme care was taken so that the crystal had six perfectly cleaved sides

gamma rays. The gamma rays are produced in the decay of the  $^{60}\text{Co}$  source. The gamma rays are detected by the NaI(Tl) crystal. The gamma rays are detected by the NaI(Tl) crystal. The gamma rays are detected by the NaI(Tl) crystal.

It is defined  $E_D$  and  $E_C$  as the energies of the gamma rays incident on the NaI(Tl) crystal from the source and the scattered levels of  $^{60}\text{Co}$  respectively. From the beam energy can be determined by the ratio  $E_D/E_C$  since this ratio varies with beam energy as shown in Fig. 6. The beam energy was measured at frequent intervals and the NaI(Tl) crystal was placed approximately a normal distribution about 11.5 cm with of measurements taking inside one standard deviation. The error associated in the energy determination includes the straggling effect in the absorbing material traversed.

## B. BEAM MONITORING

Since the particle sensitive detector consists of two scintillation counters it seems advisable to determine the highest resolution attainable with the NaI(Tl) crystal and then to determine the effect of introducing the plastic scintillator. The plastic scintillator was removed and the counter positioned at an angle of 30 degrees with the beam. A freshly cleaved NaI(Tl) crystal was used and extreme care was taken so that the optical and air perfectly aligned glass



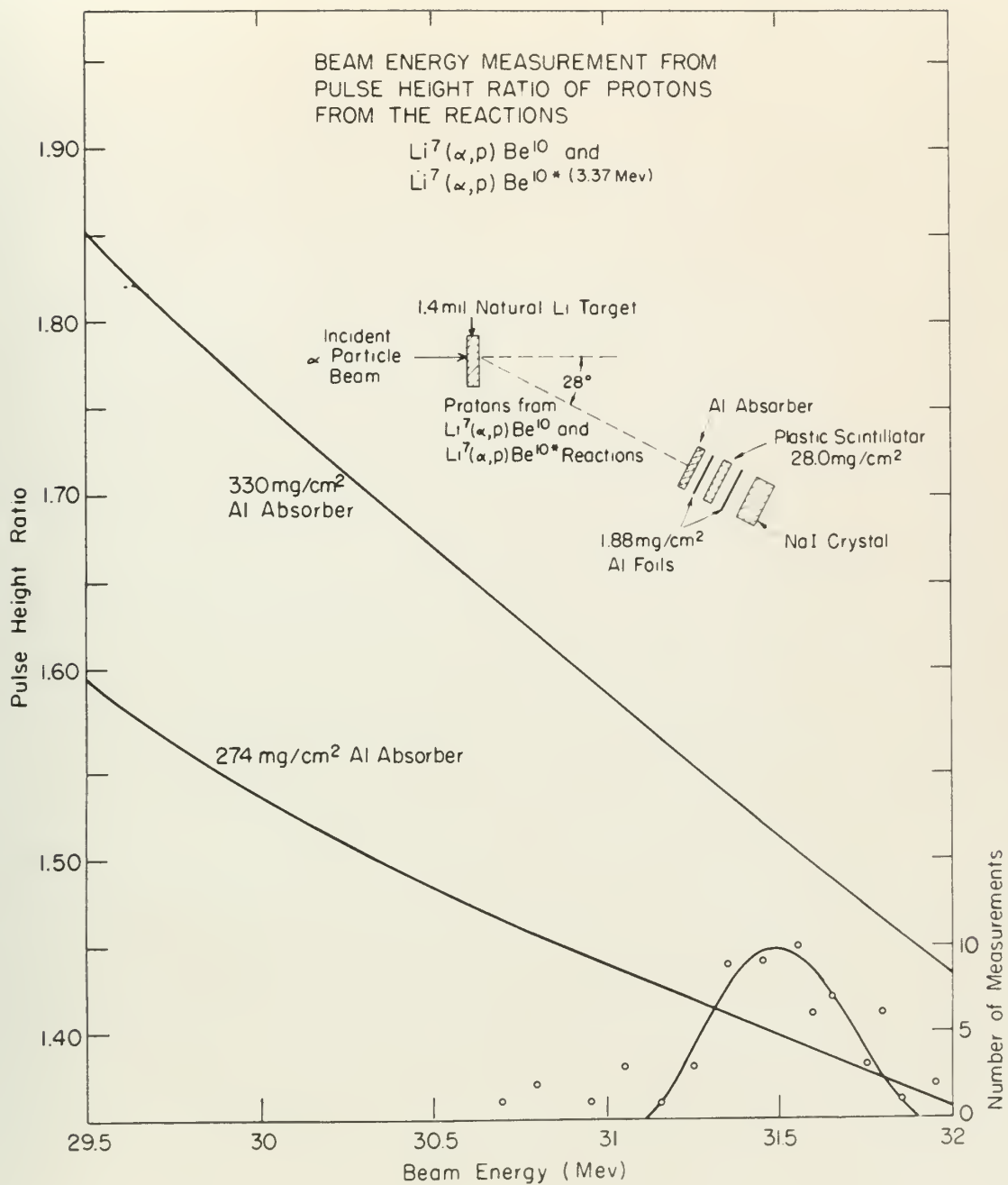


Figure 6



with no visible imperfections of any kind. A thin ( $0.2 \text{ mg/cm}^2$ ) gold foil target was then positioned at an angle of 15 degrees with the beam to minimize the target thickness effect on resolution. By use of the linear pulser, the window width of the NaI pulse height analyzer was set to a minimum value which still gave a definite overlap, and the analyzer was calibrated over the 20-channel range. The energy spectrum of alpha particles was then taken and the highest attainable resolution (full width at half maximum) was found to be 1.7 percent. The plastic scintillator was then placed in position in the counter and the spectrum was taken again with identical electronic equipment settings. Under these ideal conditions of target thickness, target angle, and minimum window width, the best resolution attainable was found to be 3.8 percent. A working resolution of 4 percent was assumed which was frequently verified during subsequent experimental work.

### C. TARGET CHOICE

The 4-percent energy resolution of the equipment immediately placed a limit on the number and characteristics of the target nuclei to be studied. First of all, the excitation energies of the levels to be investigated must be known. The targets should not consist of compounds but of a single element.

with no visible indication of any kind. A scan (0.5  
sec/cm) gold foil target was then positioned in an angle  
of 15 degrees with the beam to minimize the target thickness  
effect on resolution. By use of the linear plot, the scan  
how wide of the foil target target analyzer was set to a scan-  
rate value which still gave a definite overlap, and the analyzer  
was calibrated over the 10-degree range. The energy spectrum  
of alpha particles was then taken and the highest attainable  
resolution (full width at half maximum) was found to be 1.7  
percent. The linear plot was then placed in position  
in the counter and the spectrum was taken again with identical  
electronic equipment settings. Under these ideal conditions  
of target thickness, target angle, and minimum window width,  
the best resolution attainable was found to be 1.5 percent.  
A working resolution of 4 percent was assumed when the  
previously verified during subsequent experimental work.

### C. TARGET CHOICE

The 4-percent energy resolution of the equipment imme-  
diately placed a limit on the number and characterization of  
the target nuclei to be studied. First of all, the excitation  
energies of the levels to be investigated must be known. The  
targets should not consist of compounds but of a single element.



The presence of hydrogen contamination was permissible, however, since the elastic scattering of alpha particles from hydrogen does not occur at laboratory angles greater than 14.5 degrees.

Since it was desired to investigate at least two excited levels in each nucleus, the first four energy levels must be separated at least by about 1.2 Mev in order that they might be resolved. Also, depending on the relative positions of the excited levels of the stable isotopes, some targets must consist of a single isotope to permit resolution of the inelastic alpha-particle groups. In addition, the isotopic spin of some of the levels must be known since it was desired to check the validity of the isotopic spin selection rules in these interactions. With these restrictions in mind, the nuclei chosen for investigation were  $\text{Li}^6$ ,  $\text{C}^{12}$ ,  $\text{N}^{14}$ , and  $\text{Mg}^{24}$ .

#### D. TARGET PREPARATION

All targets were 1 1/8 in. by 1 1/8 in. in size, self-supporting, free of any backing material and were mounted in aluminum target frames. It was experimentally determined that a thickness of from 1.0 to 2.0 mils, depending on the target nucleus, gave the best compromise between an acceptable resolution and good counting statistics. Thinner targets

The presence of hydrogen contamination was verified, however, since the elastic scattering of alpha particles from hydrogen does not occur at laboratory angles greater than 18.5 degrees.

Since it was desired to investigate at least two angular levels in each nucleus, the first four energy levels must be separated at least by about 1.2 Mev in order that they might be resolved. Also, depending on the relative positions of the excited levels of the nuclei isotopes, some isotopes must consist of a single isotope to permit resolution of the inelastic alpha-particle groups. In addition, the isotopic spin of some of the levels must be known since it was desired to check the validity of the isotopic spin selection rules in these transitions. With these restrictions in mind, the nuclei chosen for investigation were  $Li$ ,  $C$ ,  $N$ ,  $O$ ,  $F$ ,  $Ne$ ,  $Na$ ,  $Mg$ ,  $Al$ ,  $Si$ ,  $P$ ,  $S$ ,  $Cl$ ,  $Ar$ ,  $K$ ,  $Ca$ ,  $Sc$ ,  $Ti$ ,  $V$ ,  $Cr$ ,  $Mn$ ,  $Fe$ ,  $Co$ ,  $Ni$ ,  $Cu$ ,  $Zn$ ,  $Ga$ ,  $Ge$ ,  $As$ ,  $Se$ ,  $Br$ ,  $Kr$ ,  $Rb$ ,  $Sr$ ,  $Zr$ ,  $Nb$ ,  $Mo$ ,  $Tc$ ,  $Ru$ ,  $Rh$ ,  $Pd$ ,  $Ag$ ,  $Cd$ ,  $In$ ,  $Sn$ ,  $Sb$ ,  $Te$ ,  $I$ ,  $Xe$ ,  $Ba$ ,  $La$ ,  $Ce$ ,  $Pr$ ,  $Nd$ ,  $Pm$ ,  $Sm$ ,  $Eu$ ,  $Gd$ ,  $Tb$ ,  $Dy$ ,  $Ho$ ,  $Er$ ,  $Tm$ ,  $Yb$ ,  $Lu$ ,  $Hf$ ,  $Ta$ ,  $W$ ,  $Re$ ,  $Os$ ,  $Ir$ ,  $Pt$ ,  $Au$ ,  $Hg$ ,  $Tl$ ,  $Pb$ ,  $Bi$ ,  $Po$ ,  $At$ ,  $Rn$ ,  $Ac$ ,  $Th$ ,  $Pa$ ,  $U$ ,  $Np$ ,  $Pu$ ,  $Am$ ,  $Cm$ ,  $Bk$ ,  $Cf$ ,  $Es$ ,  $Fm$ ,  $Md$ ,  $No$ ,  $Lr$ .

#### D. TARGET PREPARATION

All targets were 1/8 in. by 1/8 in. in size, self-supporting, free of any backing material and were mounted in aluminum target frames. It was experimentally determined that a thickness of from 1.0 to 2.0 mils, depending on the target nucleus, gave the best compromise between an adequate resolution and good counting statistics. Targets targets

would increase the statistical errors in a reasonable counting time and thicker targets made resolution of the separated particle groups less accurate.

1. Mg<sup>24</sup>. This was the simplest target to obtain and prepare. A foil of 1.5 mils thickness, 99.8 percent pure magnesium was commercially obtained.\* Surface oxidation was removed by lapping in jeweler's rouge and the completed target was either kept under vacuum or in a dry atmosphere. The percent abundance and level structure of the Mg<sup>25</sup> and Mg<sup>26</sup> is such that their presence in the target was of no consequence in this experiment.

2. Li<sup>6</sup>. The separated isotope was obtained from the Atomic Energy Commission in a pure metallic form. Targets of 1.0 to 1.4 mils thickness were formed by rolling the lithium between sheets of thin aluminum using a set of micrometer-controlled rollers. The material was rolled under dried Nujol to prevent oxidation from exposure to air. The Nujol was removed by immersion in successive baths of thoroughly dried naphtha after which the lithium target was kept in a high vacuum. The targets maintained a bright metallic luster throughout their use indicating the absence of oxidation.

---

\* Magnesium foil obtained from A. O. Mackay, Inc., 198 Broadway, New York 38, N. Y.







3. C<sup>13</sup>. The negligible percentage abundance of C<sup>13</sup> permits the use of natural carbon; however, the problem of preparing a contaminant-free self-supporting thin sheet of carbon of the size required was quite troublesome. Using a pair of hardened steel dies in a 40-ton press, it was possible to form 2.5-mil targets from a special spectroscopic graphite powder.\* The resolution obtained with these targets was relatively poor and they were discarded.

After experimenting with several different colloidal graphite dispersions, the "Dag No. 154"\*\*\* was found to be quite satisfactory, and self-supporting targets of from 0.3 to 1.5 mils were prepared. Dag No. 154 consists of colloidal graphite dispersed in alcohol with a particle size of 1 micron or less and a solid content of less than 10 percent. No contaminant was experimentally observable using targets prepared from this material in the following manner.

- (a) The colloid is further diluted by the addition of two parts alcohol (isopropanol). Using an artist's air brush with a fine nozzle\*\*\* and a

---

\* Special graphite spectroscopic powder (suitable for pelleting) obtained from National Carbon Company.

\*\* Dag dispersion obtained from Acheson Colloids Co., Port Huron, Michigan.

\*\*\* Paasche type H air brush and H3 nozzle obtained from B. L. Makepeace, Inc., Boston, Mass.



30 psi supply of dry nitrogen, the solution is sprayed so as to uniformly cover the face of a mirror on which a thin film of detergent has been applied and thoroughly dried. The dry nitrogen causes the highly volatile lique to solidify almost on contact and with practice, uniform layers of almost any desired thickness can be obtained.

- (b) An infrared heat lamp is used to thoroughly dry the layer and then the mirror is immersed in water. The thin layer separates from the mirror floating to the surface of the water. The film is transferred directly to a target frame and dried under a heat lamp after which it is ready for use.

4. N<sup>14</sup>. This was the only target material used which could not be obtained in pure form. The substance with the highest nitrogen content suitable for use as a target was found to be a melamine formaldehyde resin "Melmac 404"\* which is a filler-free thermal setting plastic. It was impossible to mould this material to less than 8 mils thickness because the powder would set before sufficient pressure

---

\* Obtained from American Cyanamid Company, Research Division, Stamford, Conn.



to get enough of the nitrogen, the solution  
is exposed to air to uniformly cover the sides  
of a vessel in which a thin film of nitrogen  
has been applied and thoroughly dried. The  
dry nitrogen causes the nitric oxide to be  
oxidized almost to constant rate with oxygen,  
nitrous fumes of almost any desired thickness  
can be obtained.

(v) An improved method is used in preparing the  
gas layer and then the nitric oxide is introduced in  
water. The gas layer separates from the nitric  
oxide to the surface of the water. The film  
is transferred directly to a heated iron and  
dried under a low vacuum after which it is ready  
for use.

4. 2. This was the only method reported here which  
could not be obtained in any form. The substance with the  
highest nitrogen content suitable for use as a rocket was  
found to be a substance containing 70% nitrogen oxide  
which is a liquid-type chemical reaction. It was not  
possible to make this material to less than 8 min. which  
was because the gases would not before without pressure

-----  
\* Obtained from American Chemical Company, Boston, Mass.  
Boston, Mass.



could be applied. However, several pieces of 4-mil thickness, resulting from the "flash" obtained in a bar mould, were lapped down to uniform thicknesses varying from 1.5 to 2.0 mils using various abrasives.\*

E. COUNTER ZERO ANGLE DETERMINATION

A 0.2-mg/cm<sup>2</sup> gold target was positioned perpendicular to the beam, the angular position being determined optically. With the cyclotron set to produce a steady beam in the scattering chamber, the energy spectrum of alpha particles scattered by gold was taken. This measurement was repeated at 1.8 degree intervals as the counter was rotated from an angle of approximately 25 degrees to 45 degrees on each side of the assumed direction of the beam. The intensity at each angular setting, as determined by the area under the elastic peak, was then plotted against the setting of the 1000-division helipot which determines the angular position of the counter. The intersection of the curves taken on each side of the assumed beam direction thus located the setting corresponding to zero angle as shown in Fig. 7. This measurement was repeated at frequent intervals during the conduct of the experiment.

-----

\* Obtained from the Plastics Laboratory, National Bureau of Standards, Washington, D. C.

could be applied. In fact, every point of the surface  
resulting from the film obtained in a few weeks, was applied  
down to uniform thicknesses varying from 1.5 to 1.8 mils with  
various solvents.

#### 2. COUNTER AND ANGLE ESTIMATION

A 0.2-mg/cm<sup>2</sup> gold target was positioned perpendicular to  
the beam, the angular position being determined optically.  
With the crystal set to produce a sharp spot in the dif-  
fracting chamber, the crystal position of about 10 degrees was  
taken by gold as target. This measurement was repeated at  
1.8 degree intervals as the counter was rotated from an angle  
of approximately 15 degrees to 45 degrees on one side of the  
assumed direction of the beam. The distance at each angular  
setting, as determined by the size of the spot, was  
was then plotted against the setting in the low-angle dif-  
fracting chamber the angular position of the counter. The  
intersection of the curve taken on each side of the assumed  
beam direction then located the actual direction of the  
angle as shown in Fig. 7. This measurement was repeated at  
1.8 degree intervals during the course of the experiment.

\* Obtained from the Physics Department, National Bureau of  
Standards, Washington, D. C.

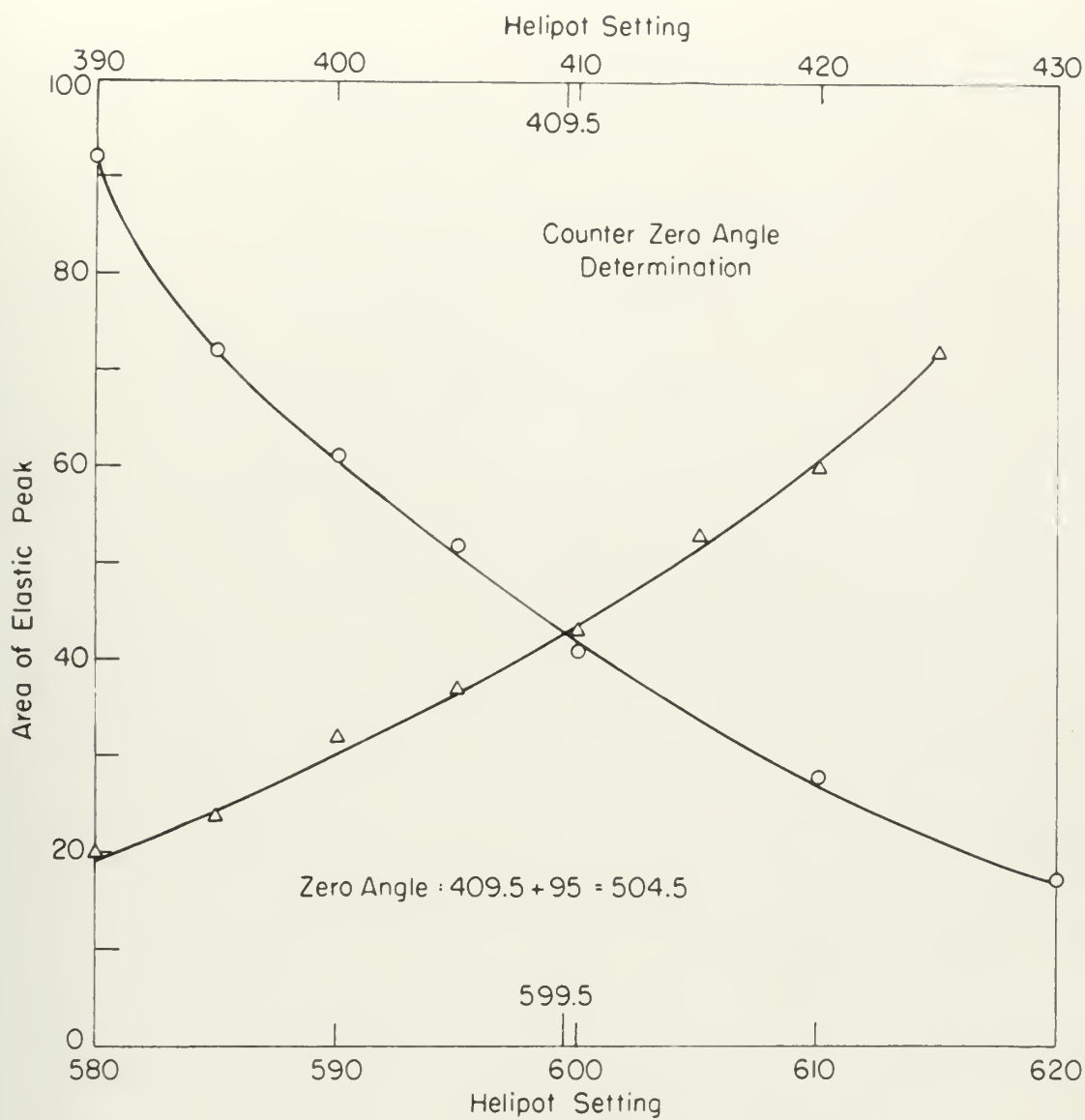


Figure 7





#### IV. EXPERIMENTAL PROCEDURE

##### A. IDENTIFICATION OF ALPHA PARTICLE GROUPS

The theory and method of operation of the particle selective counter were outlined in Sec. IID. There is no difficulty in separating the alpha particles from the protons and deuterons resulting from the bombardment. Figure 8a, b, and c shows the complete mass-energy spectra of particles resulting from the 31.5-Mev alpha particle bombardment of  $\text{Li}^6$ ,  $\text{C}^{12}$ , and natural magnesium respectively. Figure 9a, b, and c shows only the alpha particle spectra, obtained by proper setting of the bias level of the pulse height analyzer fed by the plastic scintillator. The energies of the separated alpha-particle groups must be determined in order to identify them as being associated with a given level of excitation in the target nuclei.

The bias level of the plastic scintillator analyzer is set to exclude all but alpha particles, as shown in Fig. 2. A bias level and window width, chosen to include at least two alpha-particle groups, is set on the NaI(Tl) pulse height analyzer. The energy pulse height spectrum of the alpha-particle groups is then taken with the counter set at a forward

# A. IDENTIFICATION OF ALPHA PARTICLE GROUPS

The theory and method of operation of the particle selective counter were outlined in Sec. III. There is no difficulty in separating the alpha particles from the gamma and neutron sources resulting from the bombardment. Figures 2a, b, and c show the complete mass-energy spectra of particles resulting from the 11.2-MeV alpha particle bombardment of  $^{23}\text{U}$ ,  $^{235}\text{U}$ , and natural mendelevium respectively. Figure 2a, b, and c shows only the alpha particle spectra, obtained by proper setting of the bias level of the pulse height analyzer fed by the plastic scintillator. The energies of the recorded alpha-particle groups must be determined in order to identify them as being associated with a given level of excitation in the target nuclei.

The bias level of the plastic scintillator analyzer is set so include all but alpha particles, as shown in Fig. 3. A bias level and window width, chosen so include at least two alpha-particle groups, is set on the VAX(T) pulse height analyzer. The energy pulse height spectrum of the alpha-particle groups is then read with the counter set at a forward

Photographs of  
oscilloscope  
presentation  
of mass energy  
spectra of  
particles re-  
sulting from  
the 31.5-Mev  
alpha-particle  
bombardment of  
 $\text{Cl}^6$ ,  $\text{C}^{12}$ , and  
natural Mg.

Fig. 8a  $\text{Li}^6$

Fig. 8b  $\text{C}^{12}$

Fig. 8c natural Mg

# THEORY OF THE

THEORY OF THE

THEORY OF THE

THEORY OF THE

THEORY OF THE

THEORY OF THE

THEORY OF THE

THEORY OF THE

THEORY OF THE

THEORY OF THE

THEORY OF THE

THEORY OF THE

THEORY OF THE

THEORY OF THE

THEORY OF THE

THEORY OF THE

THEORY OF THE

THEORY OF THE

THEORY OF THE

THEORY OF THE







Fig. 8a  $\text{Li}^6$ 

Energy spectra  
of alpha par-  
ticles shown  
in Figs. 8a,  
b, and c, ob-  
tained by  
proper adjust-  
ment of bias  
voltage of  
multiplier  
pulse height  
analyzer.

Fig. 8b  $\text{C}^{12}$ 

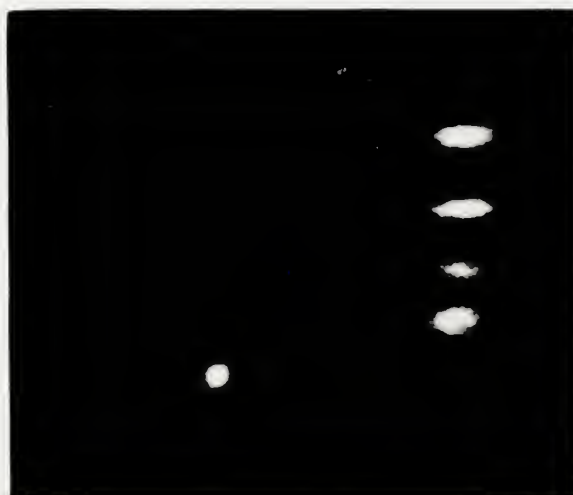
Fig. 8c natural Mg

Fig. 3a 11°

Fig. 3b 11°

Energy spectra  
of alpha par-  
ticles known  
in Fig. 3a  
and b, ob-  
tained by  
proper adjust-  
ment of bias  
voltage of  
multiplier  
pulse height  
analyzer.







angle chosen such that the intensity ratio of the groups is small. The target is then replaced by a gold foil of approximately equal thickness, in  $\text{mg}/\text{cm}^2$ , and the elastic peak of the alpha particles scattered by gold is obtained. With no change in electronic settings, the effective 20 channels of the NaI(Tl) single channel analyzer are calibrated using a linear pulse generator. The resultant positions of the alpha-particle groups, on a linear voltage scale, then correspond to the energies of the alpha particles at the NaI(Tl) crystal. With the beam energy known, and assuming that the interaction occurs at the center of the target, the energy of the alpha particles elastically scattered by gold at the angle of the counter can be computed. By use of range-energy curves, the resultant alpha-particle energy at the NaI(Tl) crystal is obtained and the energy calibration of the effective 20-channel analyzer is accomplished. Then by extrapolation through known range-energy relationships, the center-of-target energies of the unidentified alpha-particle groups may be found and the groups identified with known levels in the target nucleus. Figure 10 shows the result of such a calibration in the case of  $\text{Li}^6$ . The computed energies of the alpha particles from the ground, first, and third levels of  $\text{Li}^6$  all agree within 2 percent with the calibration against gold. Figure 10 also shows that excitation to the second excited

angle shows that the normally part of the process is small. The target is then treated by a Gold foil of approximately equal thickness, in which, and the elastic part of the alpha particles scattered by Gold is measured. With no change in electronic stopping, the difference in thickness of the foil (II) alpha channel analysis are calculated using a linear pulse generator. The resultant position of the alpha-particle group, on a linear voltage scale, then corresponds to the energies of the alpha particles as the foil (II) is varied. With the same energy range, and assuming that the interaction occurs at the center of the target, the energy of the alpha particles classically scattered by Gold at the angle of the detector can be computed. By use of computer-aided techniques, the resultant alpha-particle energy at the foil (II) is obtained and the energy calibration of the alpha-particle channel analysis is established. Then by extrapolation through known range-energy relationships, the computed target energies of the unidentified alpha-particle group may be found and the group identified with known levels in the target nucleus. Figure 10 shows the result of such a calibration in the case of  $Li^6$ . The computed energies of the alpha particles from the ground, first, and third levels of  $Li^6$  are given within 2 percent with the calibration against Gold. Figure 10 also shows that variation in the spread existed



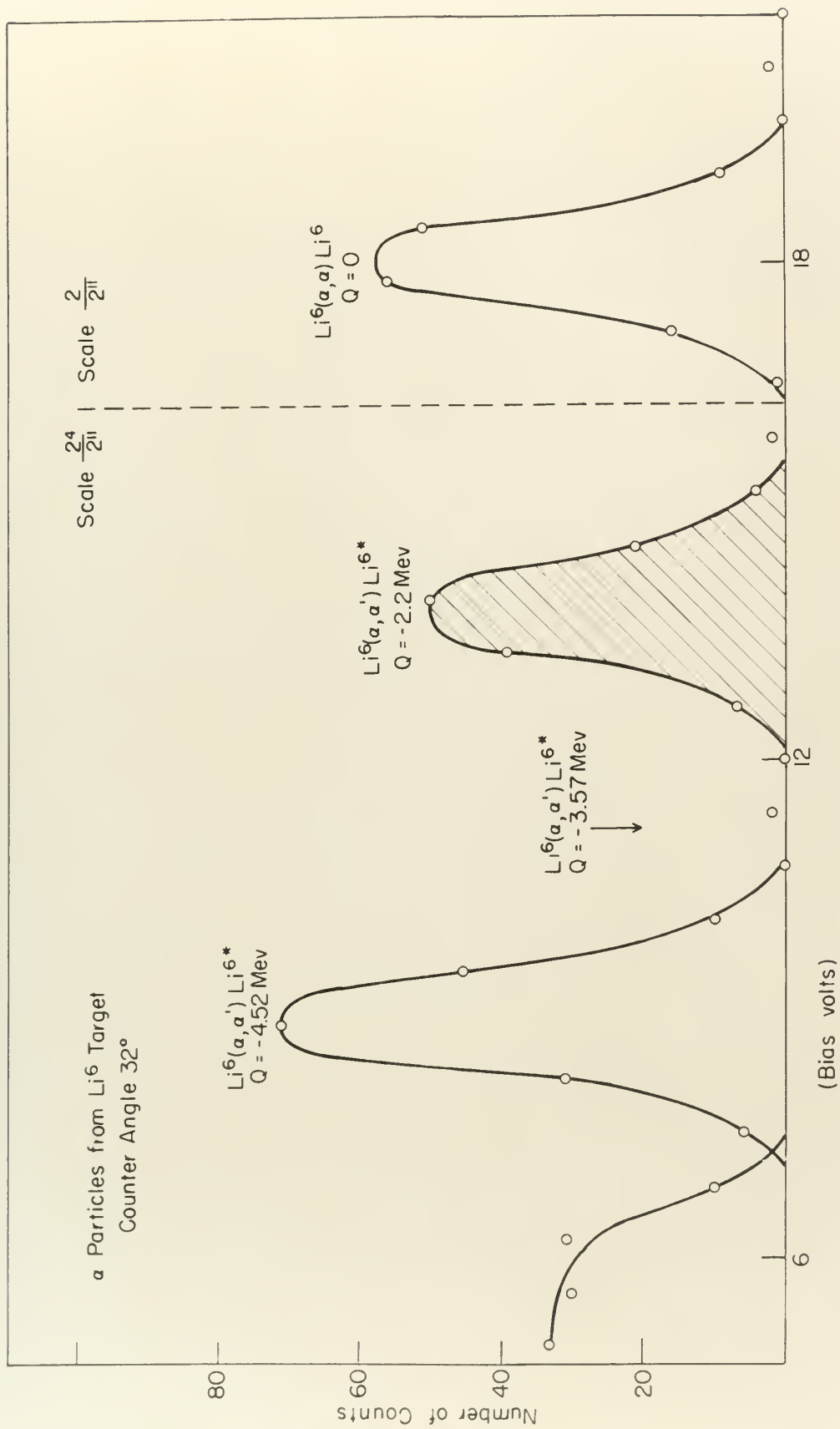


Figure 10



level has an extremely low probability of occurrence.

## B. ANGULAR DISTRIBUTION MEASUREMENTS

To obtain an angular distribution one must measure the number of alpha particles of a given energy, corresponding to a specific excitation level of the target nucleus, scattered into unit solid angle at a given mean angle, over a specific angular range. All angular distribution measurements were made with the target normal set at an angle of 45 degrees with the incident beam. This permitted observation of the entire forward quadrant without the necessity of rotating the target. With the bias level of the plastic scintillator pulse height analyzer set to exclude all but alpha particles, as shown in Fig. 4b, the bias voltage range was chosen so that the resulting spectrum would include two peaks. As an example, intensity measurements of the alpha-particle groups corresponding to the elastic and first excited levels were included in one bias range. The peak corresponding to the first excited level was also included in the intensity measurement of the group corresponding to the next higher excited level, etc. This afforded a continuous check on the reproducibility of the measurement, on the linearity over the bias range, and on the stability of the window width.

level was an extremely low probability of occurrence.

## B. ANGULAR DISTRIBUTION MEASUREMENTS

To obtain an angular distribution one must measure the number of alpha particles at a given energy, corresponding to a specific excitation level of the target nucleus, scattered into unit solid angle at a given mean angle, over a specific angular range. All angular distribution measurements were made with the target normal and at an angle of 45 degrees with the incident beam. This permitted observation of the entire forward quadrant without the necessity of rotating the target. With the bias level of the plastic scintillator pulse height analyzer set to exclude all low alpha particles, as shown in Fig. 4b, the bias voltage range was chosen so that the resulting spectrum would include two peaks. As an example, intensity measurements of the alpha-particle groups corresponding to the elastic and first excited levels were included in one bias range. The bias corresponding to the first excited level was also included in the intensity measurement of the group corresponding to the next alpha excited level, etc. This afforded a continuous check on the reproducibility of the measurement, as the intensity over the bias range, and on the stability of the window width.



Early in the experiment it was found that the intensities of the separated alpha-particle groups varied rapidly with angle. To ensure that none of the structure was missed, intensity measurements were made at angular intervals of 1.8 degrees (5 helipot units). To prevent errors due to pulse pile-up in the multiplier circuit at excessive counting rates, resulting from the rapidly increasing intensity of elastic alpha particles at forward angles, the incident beam intensity had to be decreased to a very low value ( $< 0.0001$  microampere). As a result, one to three hours of steady operation were required to obtain a statistically significant cross section measurement at a forward angle. At large angles, where the scattered intensity was greatly decreased, considerable time was also required to accumulate statistically acceptable data. To ensure proper matching of curves to make up the total angular distribution, all partial curves obtained on different runs were matched over an angular region of at least 3 degrees, chosen so that the intensity permitted a rapid accumulation of data and the intensity variation with angle produced a well defined maximum or minimum to facilitate the matching.

An initial energy spectrum, containing the desired alpha-particle group, was run with the counter set at an angle of 30 degrees. The spectrum was then taken at intervals of 1.8

... which is the assumption is made throughout the paper that  
of the separated light-particle groups varied rapidly with  
angle. To ensure that none of the spectrum was missed, in-  
tegrity measurements were made at angular intervals of 1.5  
degrees (5 half-degree units). To prevent errors due to false  
build-up in the multi-layer circuit, an excessive counting rate,  
resulting from the rapidly increasing intensity of elastic  
alpha particles at forward angles, was included even when  
it had to be decreased to a very low value ( $< 0.001$  counts  
per second). As a result, one to three hours of steady operation  
were required to obtain a statistically significant cross  
section measurement at a forward angle. At large angles,  
where the scattered intensity was greatly decreased, considera-  
ble time was also required to accumulate statistically accep-  
table data. To ensure proper matching of curves to make up  
the total angular distribution, all partial curves obtained  
on different runs were averaged over an angular region of at  
least 5 degrees, chosen so that the intensity variation was  
rapid accumulation of data and the inevitable variation with  
angle produced a well defined maximum or minimum to facilitate  
the matching.

An initial energy spectrum, considering the best fit al-  
pha particle group, was run with the counter set at an angle of  
30 degrees. The spectrum was then taken at intervals of 1.5



degrees as far forward as possible without having the particles enter the counter so rapidly that pulse pile-up occurred. The limit was determined to be 1000 particles per second for a maximum acceptable counting error of 1 percent. The counter was then repositioned at 30 degrees and the spectrum verified with the initial measurement. Then the spectrum was taken at intervals of 1.8 degrees as the angle was increased to a value where the lowered intensity of the scattered group necessitated an increase in incident beam intensity. The power level of the cyclotron was then raised, the counter rotated 9 degrees forward to ensure a match with the previous data at the old cyclotron power level, and the measurements continued. The angle of observation was increased in this way until the energy of the alpha group under observation had decreased to a point where the peak could no longer be detected or until the time required for the collection of statistically acceptable data was considered excessive. The cyclotron power level was then decreased until the intensity was well below the initial value, spectrum was again checked at 30 degrees, and the forward angle measurements were made, decreasing the incident beam intensity as necessary and requiring a match of the curves at each new power level. In addition to the numerous checks at 30 degrees and the matching over a 9-degree range, the spectrum was also frequently checked at various angles on the

degrees as the forward is possible within the available  
 angle the counter is ready that angle will be counted. The  
 limit was determined to be 1000 particles per second for a  
 maximum acceptable counting error of 1 percent. The counter  
 was then recalibrated at 10 degrees and the spectrum verified  
 with the initial measurement. Then the spectrum was taken at  
 intervals of 1.8 degrees as the angle was increased to a value  
 where the lowered intensity of the scattered group necessitated  
 an increase in incident beam intensity. The lower level of  
 the spectrum was then raised, the counter revealed a decrease  
 forward to ensure a count with the previous value at the old  
 position lower level, and the measurements continued. The  
 angle of observation was increased in this way until the en-  
 try of the alpha group under observation had decreased to a  
 point where the peak could no longer be detected by itself the  
 time required for the collection of statistically acceptable  
 data was considered excessive. The spectrum taken level was  
 then decreased until the intensity was well below the initial  
 value, spectrum was again checked at 10 degrees, and the for-  
 ward angle measurements were made, decreasing the intensity  
 was intensity as necessary and repeating a count at the counter  
 at each new lower level. In addition to the spectrum counts  
 at 10 degrees and the spectrum over a 0-degree range, the  
 spectrum was also frequently checked at various angles as the



opposite side of the zero angle of the beam. This verified the zero angle determination previously described and insured that no particles were scattered into the aperture from the asymmetric small angle scattering shield. Each complete angular distribution was taken at least two times and the positions of maxima and minima were verified at least three additional times for each distribution.

When the data for a complete angular distribution had been obtained, the counts recorded in the 20 registers were plotted versus bias voltage for each angle of observation and the areas under the peaks corresponding to the identified alpha-particle groups were taken as a measure of their relative intensities. The areas under the peaks were measured, after graphical resolution where necessary, using a polar planimeter.

The cross-hatched areas shown in Figs. 10-12 correspond to the relative intensities of the indicated groups at the angle specified. The relative intensities were thus obtained as a function of laboratory angle. These data must be corrected for two effects before they are subject to comparison with any theoretical interpretation. Since the solid angle subtended by the counter in the particle or center-of-mass coordinates differs from the angle subtended in the laboratory coordinates and also varies with angle, the observed intensities must be corrected for this effect. In addition, the angles of observation must be transposed from the laboratory to the center-of-mass

opposite side of the same angle of the same, this position  
 the more easily accessible position, and the more  
 that no particles were emitted from the position from the  
 apparatus until after the position had been  
 again distributed and taken at least two times and the  
 positions of motion and motion with respect to the same  
 additional time for each distribution.

When the time for a number of days was distributed and some  
 obtained, the number of days in the position was given  
 versus the value of the angle of observation and the value  
 under the same distribution of the position of the position  
 group were given as a result of each position obtained.  
 The group under the same position, after the position was  
 then made necessary, using a value obtained.

The cross-section area shown in Fig. 10-15 corresponds  
 to the relative intensity of the incident waves of the  
 angle specified. The relative intensity was then obtained  
 as a function of the angle of the angle. This was done by  
 for two angles before the angle is specified and the  
 theoretical distribution, from the value of the angle  
 for the number in the position of the position of the position  
 after the angle was specified in the position of the position  
 and also with the angle, the value of the angle was  
 corrected for the angle, in addition, the value of the  
 then must be transferred from the position to the position of the

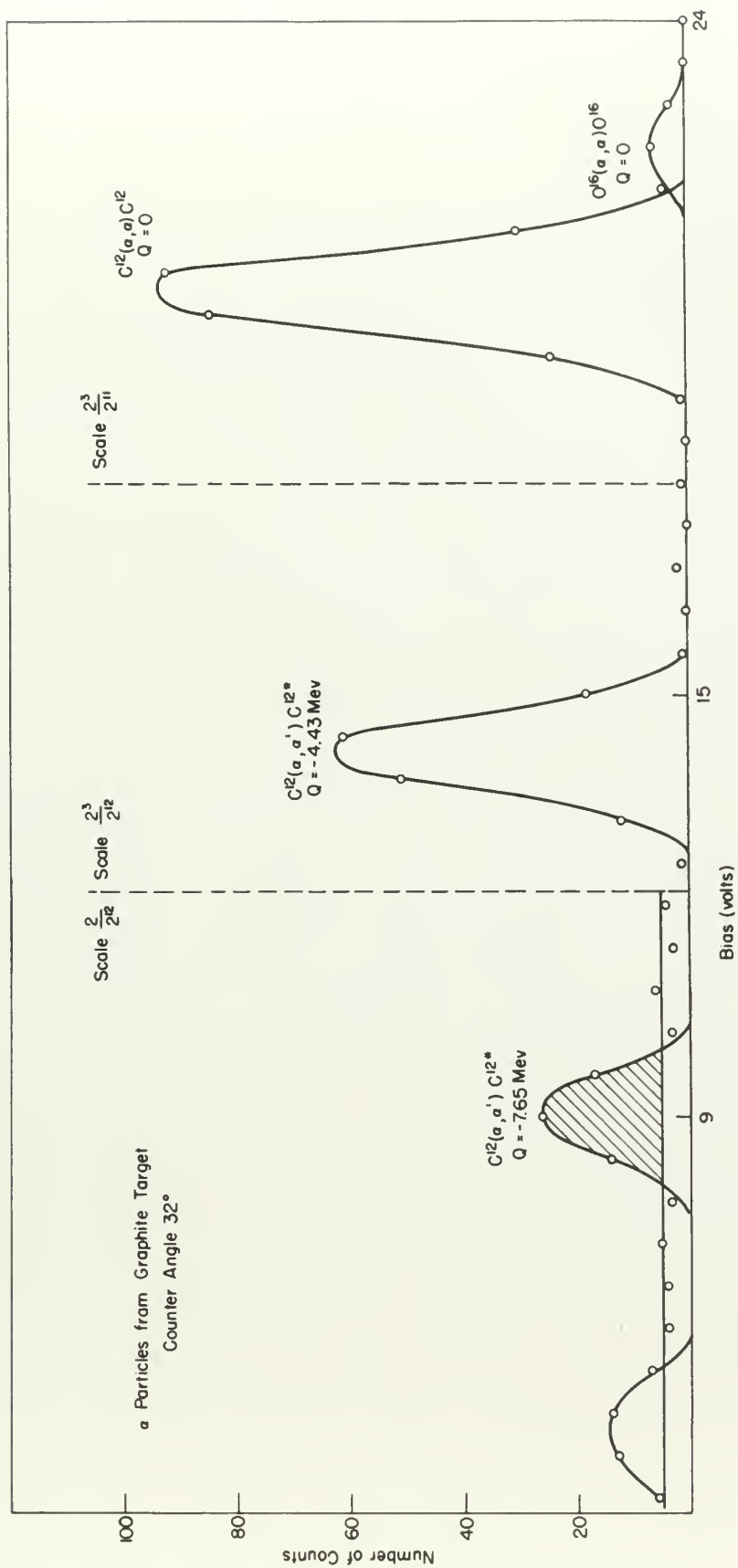


Figure 11





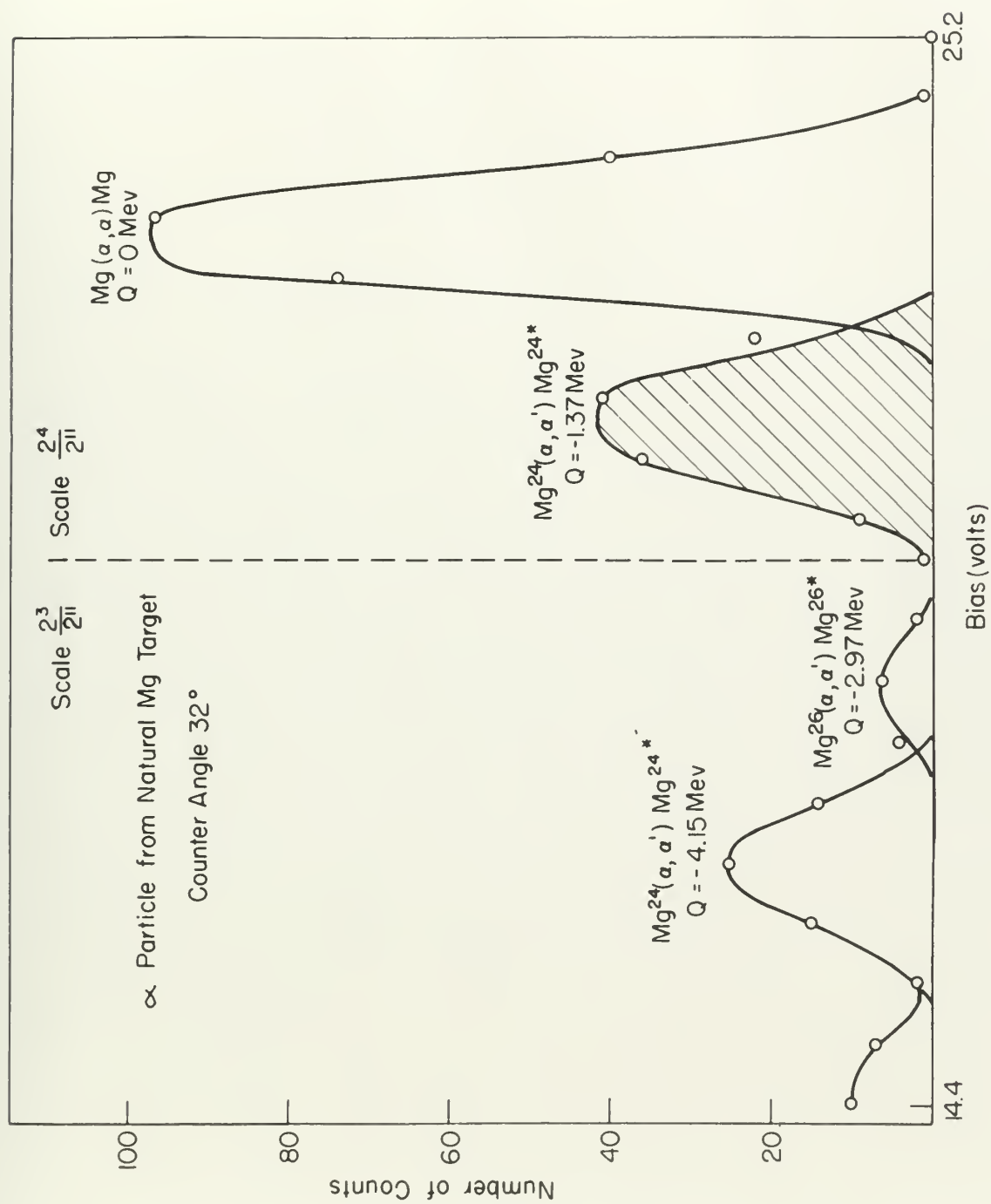


Figure 12



coordinate system. These corrections are derived and typical conversion curves are shown in Appendix 1. The angular distributions are thus obtained after the data have been corrected for these effects. The relative intensity measurements are converted to an absolute differential cross section by the method described in the following section.

### C. CROSS SECTION MEASUREMENTS

As described in Sec. IIC, the beam monitor consists of a plastic scintillator which observes only the particles scattered at an angle of 45 degrees with the incident beam by a thin gold foil. The bias level of the monitor counter is adjusted so that it counts only those pulses of a height corresponding to the elastically scattered alpha particles. Since the monitor counter does not measure the alpha-particle beam directly, the differential cross sections were determined by comparing the intensities of the observed alpha-particle groups with the intensity of the alpha particles elastically scattered by a gold target. Recent experiments (W2, S3) have shown that the elastic scattering of energetic alpha particles from heavy elements agrees with the coulomb differential cross section (R1) at small angles. The angular distribution of 31.5-Mev alpha particles elastically scattered from gold was taken over an angular range of from 14.8 degrees to 60 degrees, and

coordinate system. These coordinates are derived and digital  
converted curves are shown in Figure 1. The former dis-  
tributions are then obtained after the data have been cor-  
rected for these effects. The relative intensity distributions  
are converted to an absolute differential cross section by the  
method described in the following section.

#### C. CROSS SECTION MEASUREMENTS

As described in Sec. III, the beam monitor consists of  
a plastic scintillator which observes only the particles scat-  
tered at an angle of 45 degrees with the incident beam by a  
thin gold foil. The bias level of the monitor counter is set  
just so that it counts only those pulses of a height cor-  
responding to the elastically scattered alpha particles. Since  
the monitor counter does not measure the alpha-particle beam  
directly, the differential cross section was determined by  
comparing the intensities of the observed alpha-particle groups  
with the intensities of the alpha particles elastically scattered  
by a gold target. Recent experiments (17, 18) have shown that  
the elastic scattering of energetic alpha particles from heavy  
elements agrees with the absolute differential cross section  
(19) at small angles. The angular distribution of 3.6-MeV  
alpha particles elastically scattered from gold was taken over  
an angular range of from 1.8 degrees to 60 degrees, and



observed intensities were found to agree with the Rutherford scattering equation, within 5 percent, back to 30 degrees. Accordingly, all intensity comparisons used to determine absolute differential cross sections were made at angles smaller than 30 degrees.

An energy spectrum which includes the desired alpha-particle group was taken at an angle of 30 degrees as described in Sec. IVB. The target under investigation was then replaced by a gold foil of approximately the same thickness in  $\text{mg}/\text{cm}^2$ . This limitation on the thickness of the gold foil is necessary for two reasons. The width of the peak in the energy spectrum is dependent on the straggling effect in traversing the target and therefore if targets of different thickness are used, the calibration made by comparing the areas under the peaks would not be correct. In addition, since some small fraction of the beam incident on the counter aperture undergoes significant small angle scattering by the plastic scintillator, a more accurate comparison is obtained if the scattered particles have traversed the same effective scattering thickness of target material. Using the area under the elastic gold peak as a standard, the differential cross section of the alpha-particle group under investigation can be expressed in terms of this standard as follows (A1):

observed intensities were found to agree with the theoretical  
calculations, within 5 percent, down to 10 degrees.  
Accordingly, all intensity calculations used in determining  
associated differential cross sections were made on basis  
of the theoretical values.  
In energy spectra which include the desired alpha-  
particle group was taken at an angle of 90 degrees as described  
in Sec. IV. The target under investigation was then replaced  
by a gold foil of approximately the same thickness as before.  
This variation in the thickness of the gold foil is neces-  
sary for two reasons. The width of the peak in the energy  
spectrum is dependent on the statistical effect in measuring  
the target and therefore it is necessary to adjust the thickness  
of the foil, the calibration made by comparing the energy width  
of the peaks would not be correct. In addition, since the cross  
section of the peak incident on the detector is proportional to  
the square of the thickness of the foil, the energy width of the  
peak, a more accurate comparison is obtained if the same  
gold particles have traversed the same relative thickness.  
Thickness of target material. Since the area under the alpha  
gold peak is a standard, the differential cross section of  
the alpha-particle group under investigation may be expressed  
in terms of gold standard as follows (11):  
The differential cross section for the alpha-particle group

$$\frac{d\sigma}{d\Omega} = \frac{C/N}{C_s/N_s} \frac{A/T}{A_s/T_s} \frac{\cos \varphi}{\cos \varphi_s} \left( \frac{d\sigma}{d\Omega} \right)_s$$

where

$\frac{d\sigma}{d\Omega}$  = differential cross section in millibarns/steradian-atom in the laboratory coordinates

C = area under the differential spectrum curve

N = number of incident alpha particles

A = atomic weight of target material

T = target thickness in mg/cm<sup>2</sup>

$\varphi$  = angle between target normal and direction of incident alpha-particle beam

s = subscript indicates the values applicable to the gold target used as a standard

The ratio  $N_s/N$  is determined by the ratio of scaling factors used on the monitor counter. This, of course, assumes that interchanging the two targets does not affect the intensity of the beam incident on the gold foil observed by the monitor. The comparisons were made with both targets at the same angle which eliminated any error in the ratio  $\cos \varphi / \cos \varphi_s$ , due to errors in the angular positioning of the target.

#### D. BACK ANGLE INTENSITIES

The report of a recent experiment (R2), involving the bombardment of C<sup>12</sup> with 22-Mev alpha particles, indicates







a strong maximum at 150 degrees in the angular distribution of the inelastic alpha group corresponding to the 4.43-Mev excitation level in the target nucleus. Some equipment modification was necessary to investigate the intensity of alpha particles scattered at back angles in the present experiment.

A particle entering the aperture of the counter must traverse two 1.88-mg/cm<sup>2</sup> aluminum foils, used as light shields, and a 28.8-mg/cm<sup>2</sup> thickness of plastic scintillator, as shown in Fig. 6, before striking the NaI(Tl) crystal. After traversing this thickness of absorbing material, the particle must have sufficient energy remaining to produce a scintillation in the NaI(Tl) crystal which can be distinguished above the gamma-ray background, since chance coincidences between gamma rays and alpha particles are appreciable at the low end of the energy spectrum. As this investigation involves the bombardment of light nuclei with a relatively heavy particle, the decrease in energy of the inelastically scattered particles as the angle of observation increases is quite rapid. The result of these considerations is that a limitation is placed on the maximum angle of observation permissible using this particular method of particle detection.

The plastic scintillator was removed from the particle selective counter and only the NaI(Tl) scintillator was used



for particle detection. This eliminated  $26.4 \text{ mg/cm}^2$  of absorbing material and removed the previous limitation on the maximum permissible angle of observation. The maximum proton and deuteron energies and the energies of the alpha-particle groups resulting from the bombardment of a  $\text{C}^{12}$  target were computed over the angular range of from 90 degrees to 180 degrees. The response of NaI(Tl) to protons, deuterons, and alpha particles has been determined (Tl). By using these response curves in conjunction with known range-energy relations (A2) it was possible to choose a set of aluminum absorbers such that the percentage change in pulse height, produced by inserting these absorbers in front of the counter aperture, permitted identification of the particle producing the pulse, over this 90-degree angular range. The three alpha-particle groups observed in the bombardment of  $\text{C}^{12}$  and previously studied with the particle selective counter were identified using this method. Since these peaks were superposed on a background of protons, deuterons, and low-energy alpha particles, the intensity measurements obtained were assigned an experimental uncertainty of 50 percent. Nevertheless, by scanning the back angles, it was possible to ascertain that the differential cross section for scattering of any detectable alpha-particle group at angles greater than 90 degrees was less than 0.9 percent the value of that for



[illegible]



the ground level at 28 degrees, i.e., less than 0.8 millibarns/steradian-atom. From this it appeared that, at least in the case of  $C^{12}$ , the scattering is primarily confined to the forward quadrant.

#### E. ENERGY DEPENDENCE OF ANGULAR DISTRIBUTIONS

The data previously mentioned (R2, P1) indicated a very sensitive energy dependence in the angular distributions of 32-Mev alpha particles scattered by  $C^{12}$ . In the present experiment, the beam energy was known to vary as much as 0.4 percent (H1) depending on the power level of the cyclotron. This is largely due to variations in the r.f. heating and the subsequent mechanical motion of the dees. The continuous reproducibility of data, regardless of the cyclotron power level, implied that this strong energy dependence was not a factor in the present work. To verify the insensitivity to small changes in beam energy, angular distributions of the alpha groups corresponding to the ground, first, and second excited levels in both  $C^{12}$  and  $Mg^{24}$  were also taken with reduced beam energies of 30.9 Mev and 30.4 Mev. The reduction in energy was accomplished by insertion of 3.76-mg/cm<sup>2</sup> and 6.28-mg/cm<sup>2</sup> aluminum absorbers in the beam. Angular distributions obtained at both energies fell within the experimental uncertainties of those taken at 31.5 Mev.

The energy level at 10.5 eV, however, is not seen in the  
photoelectron spectrum. This fact is somewhat surprising  
in the case of  $C_{60}$ , the structure is relatively compact so  
the forward geometry.

2. ENERGY DISTRIBUTION OF PHOTOELECTRONS

The data previously mentioned (Fig. 1) indicated a very  
sensitive energy dependence in the angular distribution of  
photoelectrons ejected by  $C_{60}$ . In the present  
experiment, the beam energy was fixed at 10.5 eV and the  
angle  $\theta$  was varied in the range 0 to 90 degrees.  
This is largely due to variations in the e.f.f. between the  
the subsequent necessary motion of the beam. The maximum  
reproducibility of data, regardless of the electron beam  
level, implies that this photoelectron spectrum was not a  
factor in the present work. To verify the insensitivity to  
small changes in beam energy, angular distribution of the  
photoelectrons corresponding to the ground, first, and second  
excited levels in both  $C_{60}$  and  $Ag^+$  were also taken with  
reduced beam energies of 10.5 eV and 11.5 eV. The photo-  
electron energy was accompanied by insertion of 1.75 eV/cm<sup>2</sup>  
and 8.75 eV/cm<sup>2</sup> aluminum electrodes in the beam. Angular  
distributions obtained at these energies fell within the  
experimental uncertainties of those taken at 10.5 eV.

## F. EXPERIMENTAL UNCERTAINTIES

Only those sources of error which have an appreciable effect on the experimental data are mentioned. These are discussed with respect to their effect on the experimental measurements made.

1. Errors in Particle Selection. The separation of alpha particles from the protons and deuterons from all of the targets studied was quite satisfactory. Figures 8 and 9 show this separation as observed on the oscilloscope face while Fig. 28 shows the pulse height separation in terms of analyzer bias. Due to the long resolving time required in the coincidence circuit, chance coincidences between alpha particles and  $\gamma$  rays are possible. However, these chance coincidences are appreciable only at the low end of the energy spectrum where the  $\gamma$ -ray intensity is high (A1). The individual alpha-particle groups were, in general, cleanly separated from each other. Thus it was usually possible to graphically eliminate the chance coincidence rate by treating it as a continuous background over the specific low-energy range where it occurred. This procedure is shown in Fig. 11 where the cross-hatched area indicates the relative intensity of the alpha group corresponding to the 7.65-Mev level in Cl<sup>35</sup> after background subtraction.



1. Errors in Particle Selection. The separation of alpha particles from the protons and deuterons from all of the targets studied was quite satisfactory. Figure 2 and 3 show this separation as observed in the coincidence runs while Fig. 4 shows the same height separation in terms of analyzer bias. Due to the long resolving time involved in the coincidence circuit, chance coincidences between alpha particles and  $\gamma$  rays are possible. However, these chance coincidences are negligible only at the low end of the  $\gamma$ -ray spectrum where the  $\gamma$ -ray intensity is low (a). The individual alpha-particle groups were, in general, always separated from each other. Thus it was usually possible to establish definitely the chance coincidences rate in terms of a continuous measurement over the specified low-energy range where it occurred. This procedure is shown in Fig. 5 where the photo-peaked rate indicates the relative intensity of the alpha group compared to the  $\gamma$ -ray level in the photo-peaked region.



2. Errors in Beam Energy Determination. After consideration of all the sources of error, it is estimated that the beam energy measurement is correct to well within  $\pm 400$  kev. This is approximately twice one standard deviation as indicated in the distribution of energy measurements shown in Fig. 6. The sources of error in the determination of beam energy are:

- (a) Errors in thickness measurements of target, plastic scintillator, and aluminum foils in the counter, and the aluminum absorbers used in front of the counter aperture. These measurements were made by two methods. First, the thickness was measured directly with a vernier micrometer and converted to  $\text{mg}/\text{cm}^2$ . Then the various materials were weighed using an accurate analytical balance and the  $\text{mg}/\text{cm}^2$  thickness determined by dividing this weight by the cross sectional area. The estimated error in determining the thickness of the aluminum foils is  $\pm 1.0$  percent, but because these foils were extremely thin compared with the other absorbing material, this inaccuracy had a negligible effect on the energy determination. The thickness of the plastic



scintillator was determined to within  $\pm 0.3$  percent but this inaccuracy is quite small compared with the uncertainty in the plastic scintillator range-energy relations. For the same reason, the small error involved in determining the thickness of the aluminum absorbers may also be neglected.

- (b) Errors in range-energy curves. The range-energy curves (A2) were determined as follows. The rate of energy loss was computed from the theoretical formula (L3). Range-energy values were then obtained by numerical integration of the reciprocal of this rate with respect to energy. Low-energy values were based on experimental data rather than theoretical calculation. Range-energy relations for the plastic scintillator were calculated by a method previously described (A1). Due to inaccuracies in these calculations, they are estimated to be correct within 4 percent over the range of proton energies incident on the plastic scintillator. This inaccuracy permits an error of  $\pm 100$  kev in the beam energy determination.



scintillation and absorption as a light body  
parent but this indicates it is a light  
compound with the possibility of the kinetic  
recombination energy-energy relation. For the  
same reason, the small energy observed in  
determining the existence of the element  
absorption may also be neglected.

(c) Error in range-energy curves. The range-  
energy curves (12) were determined as follows.  
The rate of energy loss was computed from the  
theoretical formula (13). Range-energy values  
were then obtained by numerical integration  
of the reciprocal of this rate with respect  
to energy. Low-energy values were based on  
experimental data rather than theoretical  
calculation. Range-energy relations for the  
plasma scintillator were calculated by a  
method previously described (11). Due to in-  
homogeneities in these calculations, they are  
estimated to be correct within 4 percent over  
the range of photon energies involved on the  
elastic scintillator. This uncertainty results  
an error of 100 eV in the low energy range  
minimum.



- (c) Variation in incident beam energy. The mechanical motion of the dees previously mentioned produced a variation of  $\pm 125$  kev in the incident alpha-beam energy.
- (d) Error in  $Q$  values. The proton groups used for this energy calibration were from the reactions  $\text{Li}^7(\alpha, p)\text{Be}^{10}$  and  $\text{Li}^7(\alpha, p)\text{Be}^{10*}$ . The  $Q$  values for these reactions (A3) are known to within 20 kev and introduce a negligible error in the energy determination.
- (e) Nonlinear response of NaI(Tl) crystals. Over the range of proton energies used in this experiment, the response of NaI(Tl) has been shown to be linear within 2 percent (Tl). This is a small error compared with those previously mentioned.
- (f) Error in locating the center of the proton peaks. The full width at half maximum of the observed proton peaks was approximately 500 kev. It was therefore possible to locate the maximum to within 50 kev. The nonlinearity of the pulser used to calibrate the energy scale was determined to be negligible.

- [illegible]

3. Errors in Angular Positioning. The angular position of the counter is determined by balancing a bridge circuit whose variable element consists of a precision helipot connected to the arm on which the counter is mounted. With this method of control, the counter angle can be set to within  $\pm 0.1$  degree. The method described in Sec. III E for determining the zero angle is believed to be correct only to within  $\pm 0.3$  degree. The finite area of the beam on the target permits a maximum angular uncertainty of  $\pm 0.5$  degree. The collective effect of these possible errors limits the precision of angles measured relative to the beam to  $\pm 0.6$  degree. Due to the continuous reproducibility of results, especially when measuring coulomb scattering in the sensitive region of the  $[\sin^4(\theta/2)]^{-1}$  factor, it was concluded that angles could be set relative to one another to well within  $\pm 0.3$  degree.

Since the target was initially set perpendicular to the beam by optical means, a possible error of  $\pm 2$  degrees is assigned for this angular position. This error is insignificant, however, when the effect of the resultant error, a change in effective target thickness, is considered. In the few instances where the target angle was changed during an experiment, the correction for effective target thickness invariably fell within the statistical error of the data.

4. Errors in Relative Intensity Measurements. The most important error introduced in the measurement of relative



whose various agent consists of a certain policy and

referred to the way in which the analysis is conducted. With

25.1 decibel. The method described in sec. 1115 for determining the method of control, the number and the size of the

40.5 degree. The first step of the plan of the second was  
ending the first step is believed to be correct step in action

and a maximum angular uncertainty of  $\pm 0.5$  degrees. The two

of which measured relative to the mean of all values, the

the following conditions are satisfied in the case of the system (1) and (2):

Let  $\mathcal{R}$  be the set of all relations  $R$  on  $A$  such that  $R$  is reflexive and symmetric. Then  $\mathcal{R}$  is a lattice under the relation  $\subseteq$ .

beams of optical energy, a possible error of 25 percent is not  
claimed for this number position. This error is insignificant.

However, you are asked to be careful of the following points:

NOT THE PERSONS FOR WHOM THE ABOVE IS INTENDED



intensities was that due to the method of comparison. The area under a given peak was measured by a polar planimeter and this measurement is estimated to be correct to within 3 percent. Due to the small area of the target subtended by the beam, errors due to target thickness variations are estimated to be less than 1 percent. Compared to the above, those errors due to monitor discriminator stability and the inherent statistical counting errors are considered to be negligible.

5. Errors in Cross Section Measurement. As previously described in Sec. C, the cross section measurement depends on a comparison of plotted areas which represent relative intensities. The standard of comparison was that area under a peak corresponding to a differential cross section for coulomb scattering. This standard intensity was always obtained in a region where the variation with angle followed the  $[\sin^4(\theta/2)]^{-1}$  relationship within statistical counting error limits. The assumption was made that in this region, the Rutherford differential cross section formula (R1) is correct. Then, consideration of the errors previously described in this section places an upper limit of  $\pm 7$  percent on the accuracy of the differential cross section values.

[illegible]

8. Error in Error Section Measurement. As previously mentioned in sec. 5, the error section measurement depends on a comparison of shifted areas which represent relative positions. The accuracy of comparison was found to be about 1% when comparing to a differential area section for comparison. This standard indicates the degree of error in the region where the variation was greatest. The relationship between the shifted areas was found to be 1% and the error in the region was found to be 1%.

## V. EXPERIMENTAL DATA

The nuclei chosen for investigation afforded two opportunities for observing the validity of the isotopic spin selection rule in this experiment. In the reaction  $\text{Li}^6(\alpha, \alpha')\text{Li}^{6*}$ , excitation from the  $T = 0$  ground level to the 2.19-Mev and 4.52-Mev levels, both of isotopic spin  $T = 0$ , are allowed since the bombarding alpha particle is also  $T = 0$ . However, excitation to the  $T = 1$ , 3.57-Mev level is prohibited by this selection rule. Figure 10 shows the spectrum of alpha particles, observed at an angle of 30 degrees, which results from the bombardment of a 1.4-mil  $\text{Li}^6$  target. It is clearly evident that excitation of the 3.57-Mev level is almost entirely nonexistent. A study of the spectrum at all angles of observation indicates that excitation of this level has a probability of occurrence of less than 4 percent that of either of the two allowed levels which were excited.

A similar investigation was made to determine the probability of excitation of the  $T = 1$ , 2.31-Mev level in  $\text{N}^{14}$  compared with that of the  $T = 0$ , 3.95-Mev level. The only target material suitable for the study of nitrogen was melamine (see Sec. IIID), which contained a high percentage of carbon.



The model chosen for investigation allowed the user to simulate the operation of the system in the following manner. The system is represented by a set of states, each of which is a vector of the form  $(x, y, z, w)$ , where  $x, y, z, w$  are integers between 0 and 10. The initial state is  $(0, 0, 0, 0)$ . The system evolves according to the following rules: (1) If  $x > 0$ , then  $x$  is decremented by 1. (2) If  $y > 0$ , then  $y$  is decremented by 1. (3) If  $z > 0$ , then  $z$  is decremented by 1. (4) If  $w > 0$ , then  $w$  is decremented by 1. (5) If  $x = y = z = w = 0$ , then the system is in a terminal state. The system is simulated for a given number of steps, and the final state is reported. The results of the simulation are shown in Table I.

Table I. Results of the simulation for various initial states.

Initial State	Final State	Number of Steps
(0, 0, 0, 0)	(0, 0, 0, 0)	0
(1, 0, 0, 0)	(0, 0, 0, 0)	1
(0, 1, 0, 0)	(0, 0, 0, 0)	1
(0, 0, 1, 0)	(0, 0, 0, 0)	1
(0, 0, 0, 1)	(0, 0, 0, 0)	1
(1, 1, 0, 0)	(0, 0, 0, 0)	2
(1, 0, 1, 0)	(0, 0, 0, 0)	2
(0, 1, 1, 0)	(0, 0, 0, 0)	2
(1, 0, 0, 1)	(0, 0, 0, 0)	2
(0, 1, 0, 1)	(0, 0, 0, 0)	2
(0, 0, 1, 1)	(0, 0, 0, 0)	2
(1, 1, 1, 0)	(0, 0, 0, 0)	3
(1, 0, 1, 1)	(0, 0, 0, 0)	3
(0, 1, 1, 1)	(0, 0, 0, 0)	3
(1, 1, 0, 1)	(0, 0, 0, 0)	3
(1, 0, 0, 1)	(0, 0, 0, 0)	3
(0, 1, 0, 1)	(0, 0, 0, 0)	3
(0, 0, 1, 1)	(0, 0, 0, 0)	3
(1, 1, 1, 1)	(0, 0, 0, 0)	4

The results show that the system always reaches a terminal state, and the number of steps required to reach the terminal state is at most 4. This is consistent with the theoretical analysis of the system.



Combined with the poor resolution of the equipment, the proximity of the excitation levels of carbon and nitrogen did not permit taking clean angular distributions of the alpha particles scattered by  $N^{14}$ . However, it was possible to place an upper limit on the excitation of one forbidden level as follows. The alpha-particle groups elastically scattered by carbon and nitrogen were unresolved as were those groups corresponding to the 4.43-Mev level in  $C^{12}$  and the 3.95-Mev allowed level in  $N^{14}$ . The unresolved peaks were calibrated, as described in Sec. IVC, in terms of an absolute total differential cross section for both interactions. The  $C^{12}$  cross sections, separately obtained using a pure carbon target of a thickness determined by the carbon content of the melamine target, were then subtracted out. By this expedient it was determined that excitation of the isotopic spin prohibited 2.31-Mev level in  $N^{14}$  occurred with a probability of less than 6 percent that of the allowed 3.95-Mev level over an angular range of observation of from 14.8 degrees to 64.1 degrees.

Figure 11 shows the alpha-particle groups observed at an angle of 32 degrees with the beam when a carbon target is bombarded by 31.5-Mev alpha particles. The alpha particles elastically scattered by oxygen contamination of the target show up as a clearly separated group just above the elastic  $C^{12}$  group.

Combined with the good reproduction of the specimens, the  
proximity of the activated levels of carbon and nitrogen  
has been tested using angular distributions of the  
alpha particles emitted at  $15^\circ$ . However, it has been  
found that the angular distribution of the alpha particles  
level is higher. The alpha-particle group is  
characterized by energy and angular distribution in the  
cross section, indicating that the  $15^\circ$  level is  
the  $15^\circ$  level in  $15^\circ$ . The angular distribution  
characterized, as determined in the  $15^\circ$  level, in terms of an  
alpha-particle cross section for both isotopes. The  
 $15^\circ$  cross section, experimentally determined using a  
range of a detector, determined by the angular distribution of  
the alpha particles, with some exceptions. By this  
method it was determined that the angular distribution  
of the alpha particles in  $15^\circ$  was compared with a  
value of less than 1 percent that of the alpha-particle  
level over an angular range of observation of from  $15^\circ$   
between to  $60^\circ$  degrees.

Figure 11 shows the alpha-particle cross section of  
in terms of 15 degrees with the  $15^\circ$  level. The  
is bounded by  $15^\circ$  level. The alpha-particle  
characterized by energy and angular distribution of the  
cross section is a highly sensitive probe for the  
group.

The alpha-particle spectrum shown in Fig. 12 results from the 31.5-Mev alpha-particle bombardment of a natural magnesium target. The elastic peak includes the elastic scattering from all three stable magnesium isotopes while the inelastic groups are due only to the individual isotopes indicated in the figure.

The angular distributions of alpha particles scattered inelastically by  $\text{Li}^6$ ,  $\text{C}^{12}$ , and  $\text{Mg}^{24}$  are shown in Figs. 13-18. The well defined maxima and minima are suggestive of a direct interaction, as discussed later in Sec. VI. The data of G. Schrank et al. (82), obtained for the interaction  $\text{Fe}^{56}(\text{p}, \text{p}')\text{Fe}^{56*}$ , show a similar structure and are interpreted as indicative of a direct interaction. The errors indicated in Figs. 13-18 include all uncertainties affecting a comparison of relative intensities. Where no errors are indicated, the uncertainty lies within the limits of the finite size of the points on the curve. An additional error of 2 percent should be added to account for the uncertainty in absolute differential cross section values. The positions of maxima and minima for each observed inelastic angular distribution are indicated in Table I.

The angular distributions obtained for the elastically scattered alpha particles are shown in Figs. 19-21 where the calculated coulomb cross sections are indicated by a dashed line.



The above-mentioned specimens were in the 100 series from the 11-12 New York-Florida boundary at a distance of 100 miles. The results have indicated the above-mentioned specimens were in the 100 series from the 11-12 New York-Florida boundary at a distance of 100 miles.

The general distribution of light within the system is characterized by  $E_{10}^0$ ,  $E_{10}^{10}$ , and  $E_{10}^{20}$  and shown in Figs. 1-3. The well defined maxima and minima are suggestive of a limited interference, as discussed below in Sec. VI. The value of

Indicated in Fig. 2-4 is the relationship between the intensity of a given radiation, the energy to (2.2) by the known energy density and the intensity of radiation at 100% efficiency for the interaction.

indicated, the uncertainty limit within the limits of the  
finite size of the particle on the curve. An additional error  
of 1.5 percent should be added to account for the uncertainty

in absolute ethanol. The solution of acetic acid and water was added to the solution of the ester in absolute ethanol. The solution of the ester in absolute ethanol was added to the solution of the ester in absolute ethanol.

1. The first step is to identify the problem or question that needs to be answered. This involves understanding the context and the specific requirements of the task.



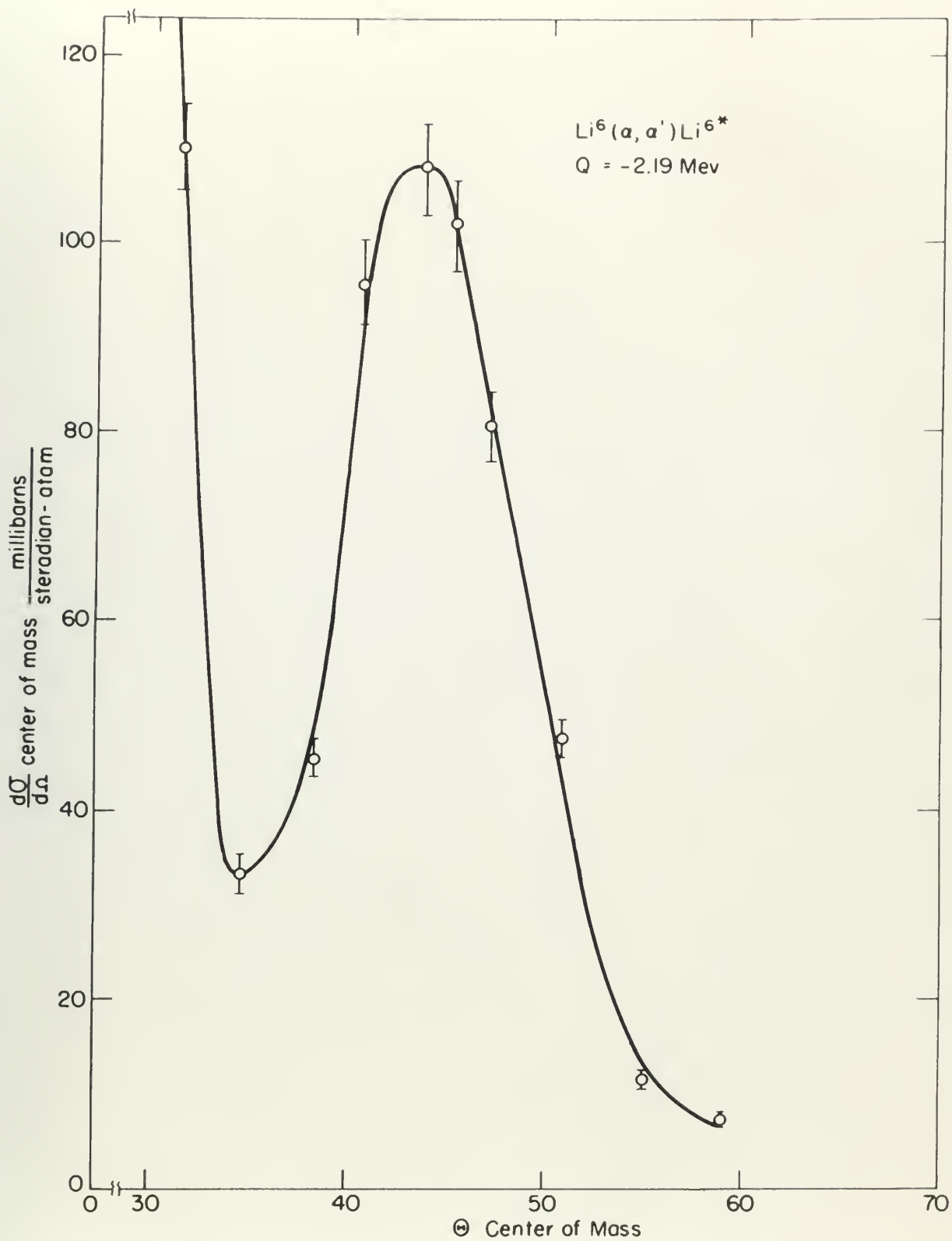


Figure 13



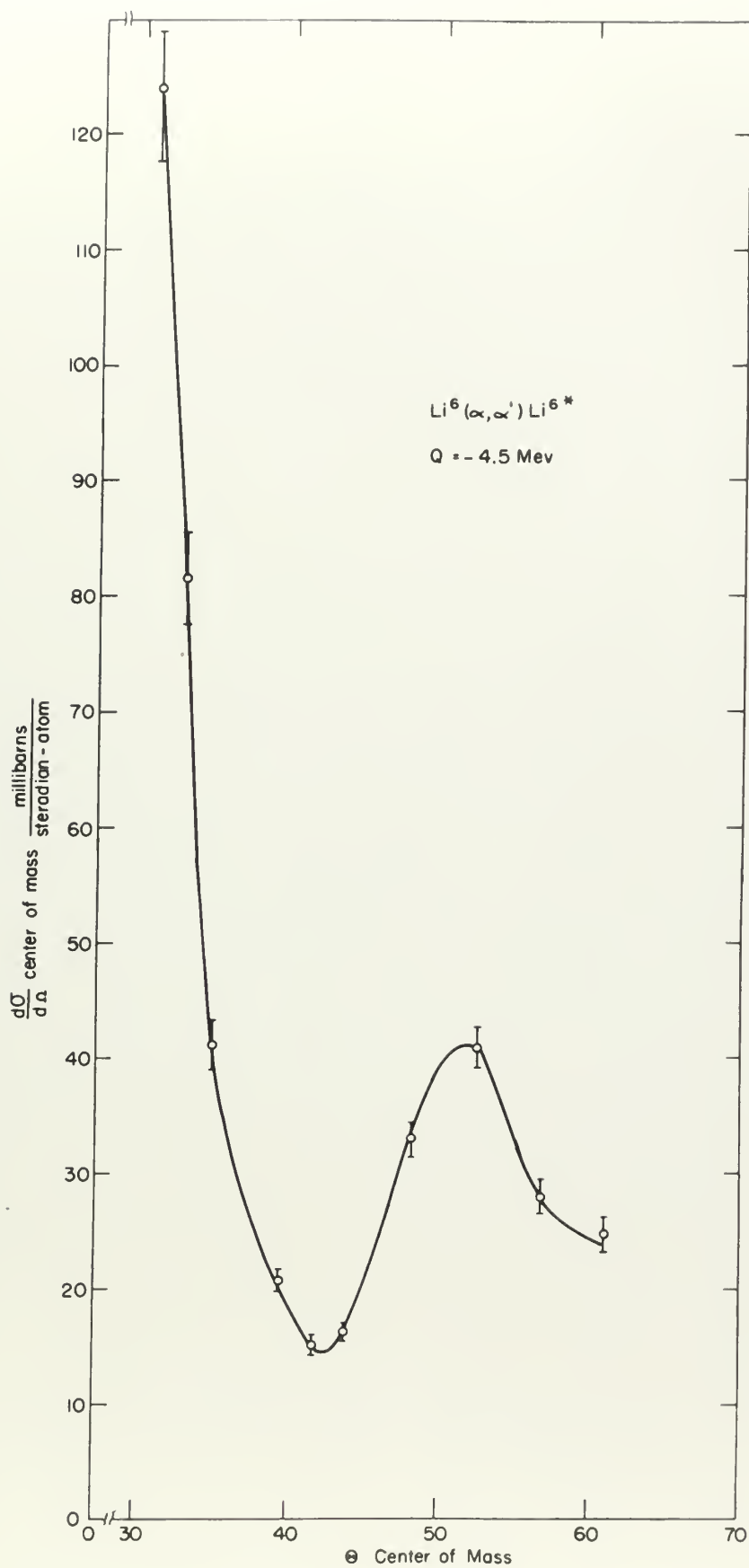


figure 14





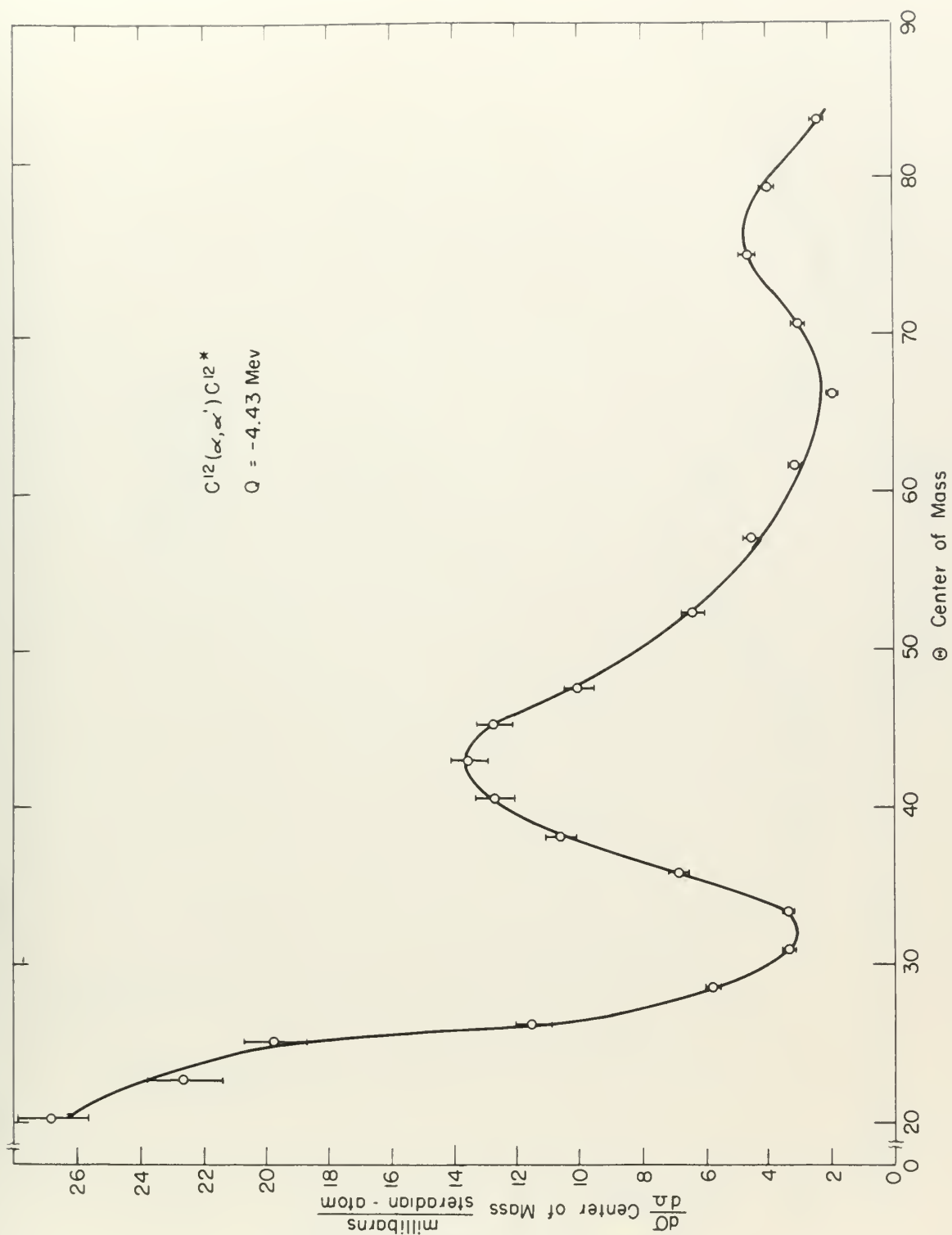


Figure 15



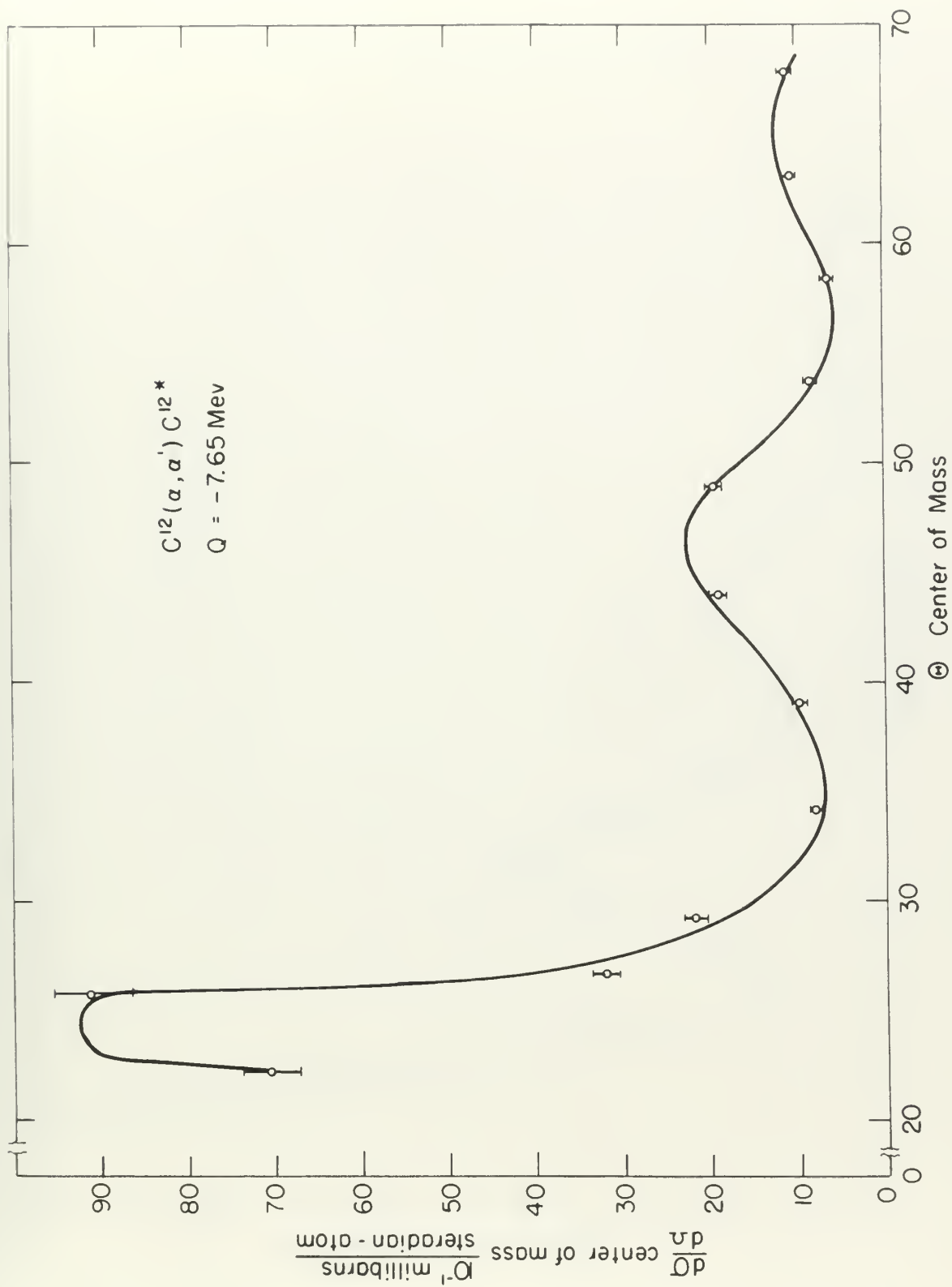


Figure 16





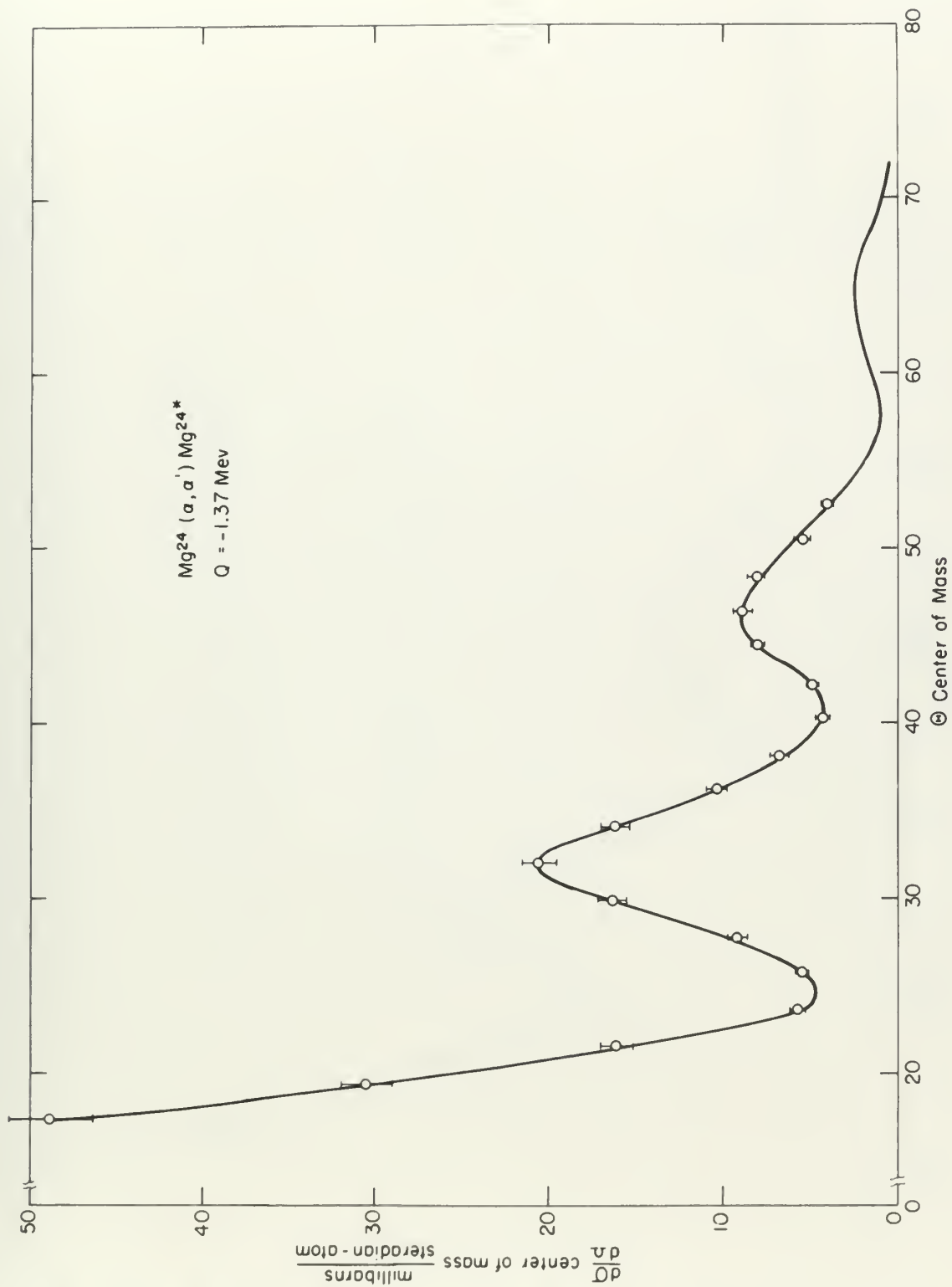


Figure 17



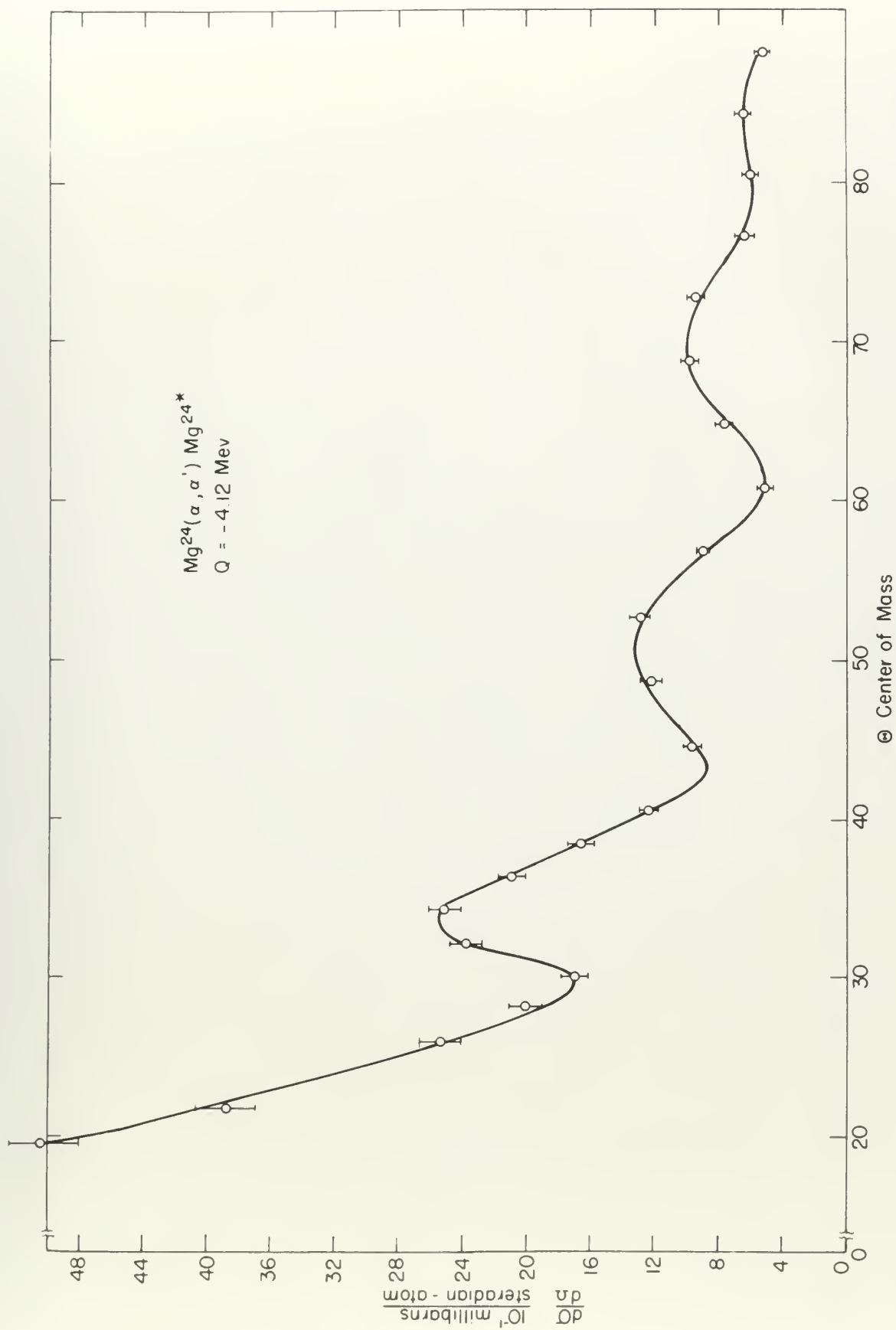


Figure 18





Table 1. Angular positions of maxima and minima experimentally observed in the inelastic alpha-particle angular distributions.

<u>Target nucleus</u>	<u>Excitation level (Kev)</u>	<u>Maximum or minimum</u>	<u>Angle C.M.</u>	<u>Intensity millibarns/steradian-stop</u>
$\text{Li}^6$	2.19	min	34.5	33
	2.19	max	44.0	108
	4.5	min	48.5	14
	4.5	max	52	41
$\text{C}^{12}$	4.43	min	32	3
	4.43	max	43	13.5
	4.43	min	66	2.0
	4.43	max	75	4.8
	7.65	max	24.5	9.25
	7.65	min	35	0.75
	7.65	max	46	2.25
	7.65	min	56.5	0.60
	7.65	max	65	1.25

Table 1. Angular positions of maxima and minima experimentally observed in the isotactic polypropylene region.

Target angles	Excitation level (V <sub>0</sub> )	Maximum of minima	Angle V <sub>0</sub>	Intensity of maxima-minima
15°	0.10	min	10.0	10
	0.10	max	11.0	100
	0.0	min	10.0	10
	0.0	max	10	10
15°	0.0	min	10	10
	0.0	max	10	10
	0.0	min	10	10
	0.0	max	10	10
15°	0.0	min	10	10
	0.0	max	10	10
	0.0	min	10	10
	0.0	max	10	10
15°	0.0	min	10	10
	0.0	max	10	10
	0.0	min	10	10
	0.0	max	10	10
15°	0.0	min	10	10
	0.0	max	10	10
	0.0	min	10	10
	0.0	max	10	10
15°	0.0	min	10	10
	0.0	max	10	10
	0.0	min	10	10
	0.0	max	10	10

Table 1 (cont.)

<u>Target nucleus</u>	<u>Excitation level (Mev)</u>	<u>Maximum or minimum</u>	<u>Angle C.M.</u>	<u>Intensity millibarns/steradian-atom</u>
$Mg^{24}$	1.37	min	25	4.5
	1.37	max	32	50.5
	1.37	min	40.5	4.0
	1.37	max	46.5	9.0
	1.37	min	57	1.0
	1.37	max	64.5	2.5
	4.12	min	29.5	1.70
	4.12	max	33.5	2.56
	4.12	min	43	0.68
	4.12	max	51	1.32
	4.12	min	60.5	0.52
	4.12	max	69	1.00
	4.12	min	80	0.60

TABLE I (Contd.)

TABLE I (Contd.)

TABLE I (Contd.)

TABLE I (Contd.)

TABLE I (Contd.)

TABLE I (Contd.)

TABLE I (Contd.)

TABLE I (Contd.)

TABLE I (Contd.)

TABLE I (Contd.)

TABLE I (Contd.)

TABLE I (Contd.)

TABLE I (Contd.)

TABLE I (Contd.)

TABLE I (Contd.)

TABLE I (Contd.)

TABLE I (Contd.)

TABLE I (Contd.)

TABLE I (Contd.)

TABLE I (Contd.)

TABLE I (Contd.)

TABLE I (Contd.)

TABLE I (Contd.)

TABLE I (Contd.)

TABLE I (Contd.)

TABLE I (Contd.)

TABLE I (Contd.)

TABLE I (Contd.)

TABLE I (Contd.)



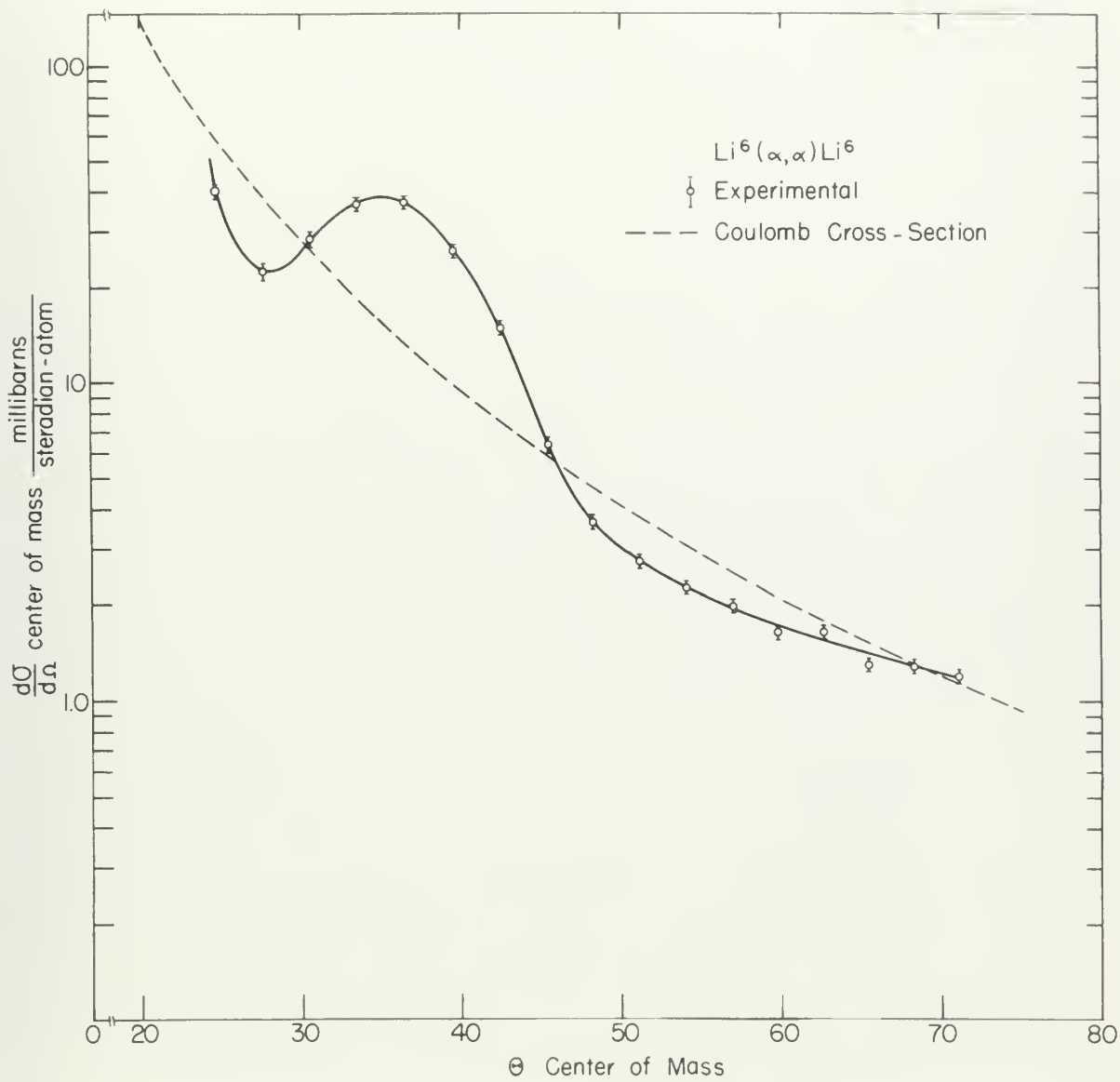


Figure 10



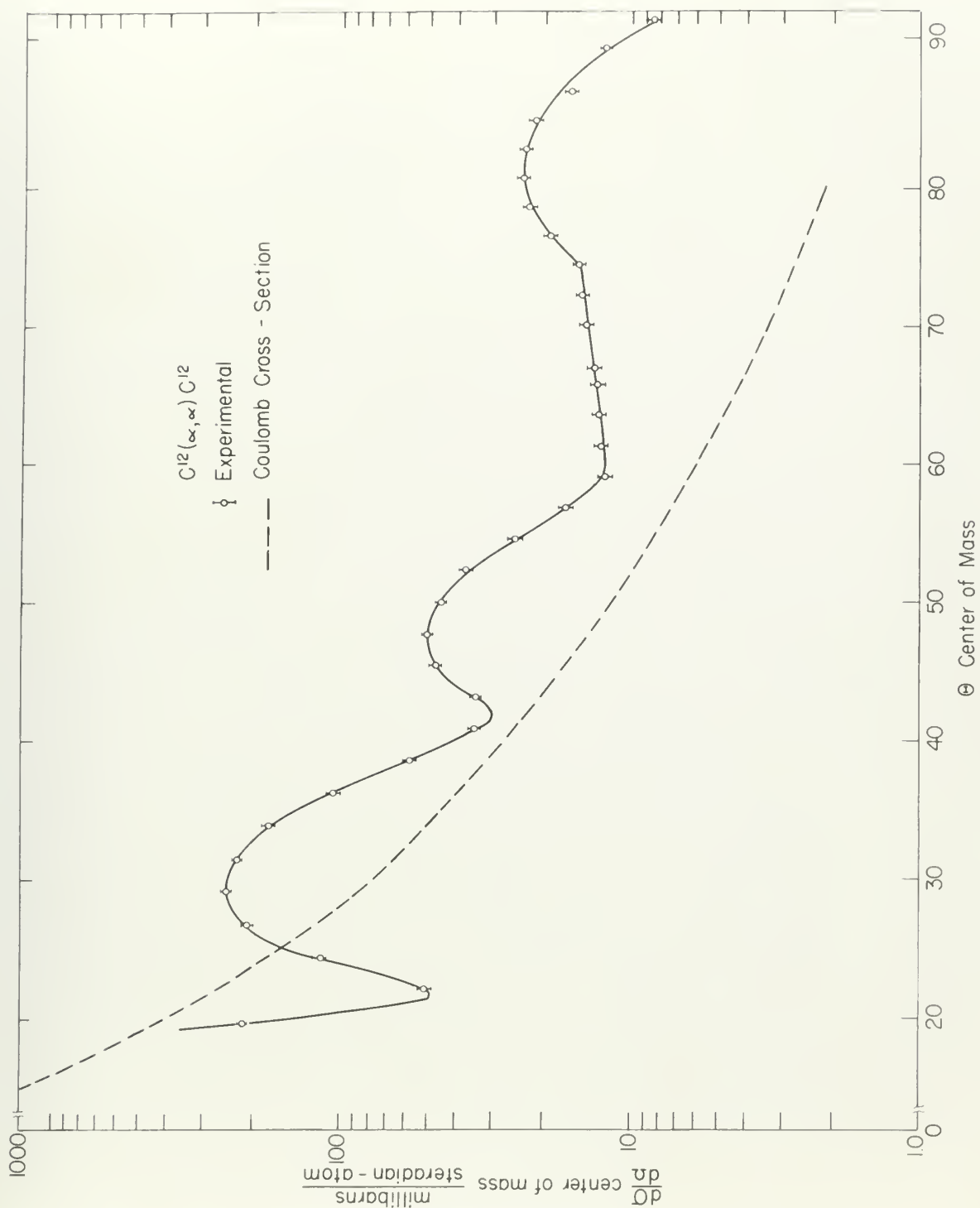


FIGURE 20





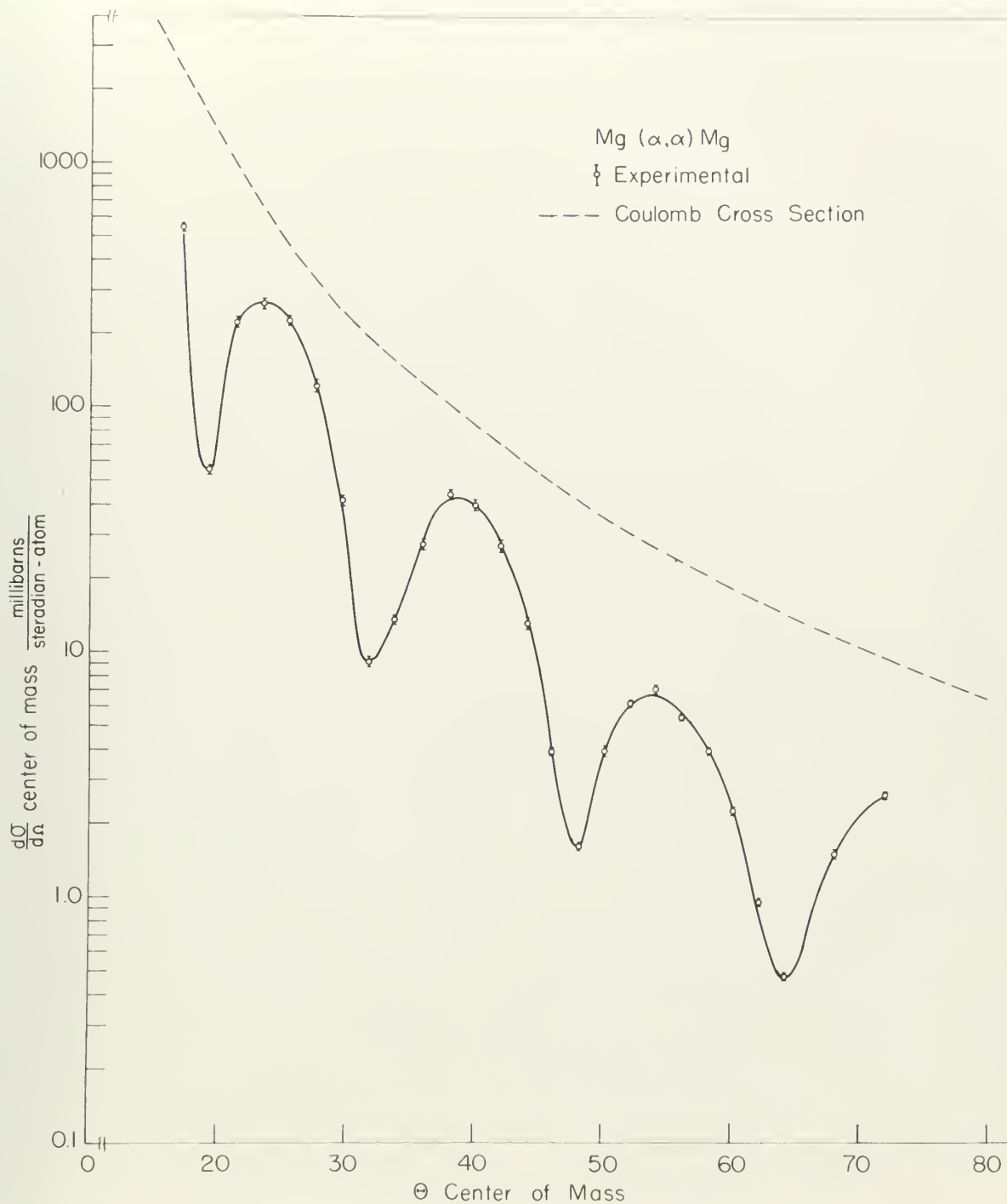


Figure 21



## VI. DISCUSSION OF RESULTS

### A. INELASTIC SCATTERING PROCESS

The well defined structure evident in the inelastic angular distributions of Figs. 13-18 is suggestive of the theoretical predictions for a direct interaction. This is more definitely indicated when we consider that, in the case of  $C^{12}$ , the cross section for scattering at angles greater than 90 degrees was found to be negligible compared with the values observed in the forward quadrant. As mentioned in Sec. I, there are three processes currently accepted as possible mechanisms for the excitation of nuclei by charged particles. Predictions of the theory for each process, when compared with the experimental data, should permit an estimate of the contribution due to each method of excitation.

If excitation occurred by the formation of a compound nucleus, the nuclei involved would be  $B^{10}$ ,  $O^{16}$ , and  $Si^{28}$ . A study of the level spacing in these nuclei ( $A3$ ,  $E3$ ), at the excitation levels involved, clearly indicates that a statistical treatment is not valid. Even if we did assume that the statistical theory was applicable, any reasonable level density function (W6) predicts inelastic scattering cross sections much smaller than the observed values.

## A. ELASTIC SCATTERING PROCESSES

The well defined structure evident in the inelastic angular distribution at  $15^\circ$ ,  $17-18^\circ$  is indicative of the theoretical prediction for a direct interaction. This is more definitely indicated when we consider that, in the case of  $^{12}\text{C}$ , the cross section for scattering at angles greater than  $90^\circ$  degrees was found to be negligible compared with the values observed in the former experiment. It mentioned in Sec. I, that the three processes previously accepted as possible mechanisms for the excitation of nuclei by charged particles. Prediction of the theory for each process, when compared with the experimental data, should permit an analysis of the contribution due to each method of excitation.

If excitation occurred by the formation of a compound nucleus, the nuclei involved would be  $^{12}\text{C}$ ,  $^{13}\text{C}$ , and  $^{14}\text{C}$ . A study of the level spacing in these nuclei (12, 13) as the excitation levels increase, clearly indicates that a statistical treatment is not valid. Even if we had shown that the statistical theory was applicable, any reasonable level density function (14) would indicate scattering cross sections much smaller than the observed values.



72

From a consideration of the energy spread in the incident beam, it is also apparent that the interactions could not involve the excitation of only a single level in the compound nucleus. The possibility still exists that an angular distribution which is not symmetric about 90 degrees in the center-of-mass coordinates could result from a compound nucleus interaction (M3). However, the experimental angular distributions were shown to be insensitive to significant changes in beam energy. It is concluded that no contributions to the observed angular distributions from compound nucleus interactions were experimentally observable.

It is assumed that a contribution to the observed cross sections due to electric excitation would not be of sufficient magnitude to permit detection. This assumption is believed to be valid for the following reasons.

- (a) The electric excitation mechanism is most important when the bombarding energies are below the coulomb barrier, a condition not fulfilled in this experiment.
- (b) For bombarding energies above the barrier, the electric excitation effect would probably be masked by the large nuclear scattering (M4, M3).

From a consideration of the results shown in the preceding  
 figures, it is also apparent that the information which can  
 involve the analysis of only a single level in the spectrum  
 mechanism. The possibility still exists that an analysis of the  
 spectrum which is not symmetric about the center is the  
 center-of-mass coordinate could result from a spectrum analysis  
 interaction (11). However, the experimental results obtained in  
 these were shown to be insensitive to significant changes in  
 beam energy. It is concluded that no correlation of the  
 observed angular distribution from spectrum analysis with  
 sections were experimentally observed.

It is assumed that a correlation in the energy of the  
 sections due to electric interaction would not be observed  
 sections to permit detection. This interaction is believed  
 to be valid for the following reasons:

(a) The electric interaction mechanism is over the  
 system and the resulting electric field is  
 the electric field, a correlation of the  
 in this experiment.

(b) For bounding energies above the barrier, the  
 electric interaction effect would probably be  
 caused by the large electric interaction (12),  
 (13).

From the above it is concluded that the electric interaction

- (c) If we optimize conditions of bombarding energy and order of multipole moment involved, the theoretical maximum total cross section for electric excitation is less than most of the differential cross sections obtained for excitation of the individual levels observed.

The early direct interaction models (B5, G1) had considerable success in explaining experimental angular distributions despite their somewhat crude approach. A theory based on the Born approximation (H2) was quite successful in explaining the (d,d') angular distributions obtained in excitation of the 1.38-Mev level in  $Mg^{24}$ . The recent theory of Austern et al. (A4) proposes a mechanism by which the reaction proceeds by a direct interaction between the incoming particle and one of the nucleons at the surface of the nucleus rather than with the nucleus as a whole. The theory predicts a differential cross section for a reaction in which the residual nucleus is left in an excited state. The theory given in the following section closely follows this treatment and was derived (R5) in an attempt to explain the inelastic angular distributions obtained in this experiment.



(c) If we assume that the distribution of the

not only of the total number of events, but

theoretical maximum value of the

electric field is less than that of the

theoretical maximum value of the

electric field is less than that of the

The only direct experimental evidence for the

success in explaining experimental results is the

old theory of the distribution of the

the distribution of the

the distribution of the

the distribution of the

the distribution of the

the distribution of the

one of the results of the

with the results of the

collisions of the

curve is left in the

the following results of the

derived (2) in an attempt to explain the

distribution of the



## B. THEORETICAL ANGULAR DISTRIBUTION AND COMPARISON WITH EXPERIMENT

The cross section for the interaction can be written

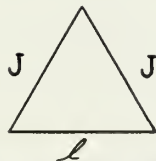
$$\frac{d\sigma}{d\Omega} = \frac{1}{2J+1} \sum_{M, M'} |f_{M', M}(\theta)|^2$$

where we have averaged over the initial (unprimed) magnetic quantum numbers and summed over the final (primed) ones.

Using the Born (plane wave) and impulse (unperturbed nuclear states) approximations (C3)

$$f_{M', M}(\theta) = \int d\vec{r}_1 \dots d\vec{r}_A d\vec{r} \psi_{J', M'}(A) \mathcal{E}^{-i\vec{k}' \cdot \vec{r}} V(r, A) \psi_{J, M}(A) \mathcal{E}^{i\vec{k} \cdot \vec{r}}$$

in which we have assumed that the spinless alpha particle is a point particle.  $\psi_{J, M}(A)$  and  $\psi_{J', M'}(A)$  are the initial and final nuclear states and the exchange of particles is neglected. To conserve angular momentum the alpha particle must undergo a change in angular momentum equal, and opposite in direction, to that of the nucleus. In other words,  $J$ ,  $J'$ , and  $\ell$  must satisfy the triangular inequalities



$$\begin{aligned} J + J' &\geq \ell \\ J + \ell &\geq J' \\ J' + \ell &\geq J \end{aligned}$$

Another selection rule, which results from a consideration of

# 3. THEORETICAL ANALYSIS OF THE EXPERIMENT

The cross section for the interaction can be written

$$\sigma = \frac{4\pi}{\Omega} \sum_{\mathbf{k}, \mathbf{k}'} \frac{1}{\Omega} |\langle \mathbf{k} | \hat{V} | \mathbf{k}' \rangle|^2$$

where we have averaged over the initial (incoming) momenta and summed over the final (outgoing) momenta. Using the Born (plane wave) and Fermi (degenerate electron) statistics (C)

$$\langle \mathbf{k} | \hat{V} | \mathbf{k}' \rangle = \int d\mathbf{r} \psi_{\mathbf{k}}^*(\mathbf{r}) \hat{V}(\mathbf{r}) \psi_{\mathbf{k}'}(\mathbf{r}) = \int d\mathbf{r} \psi_{\mathbf{k}}^*(\mathbf{r}) \psi_{\mathbf{k}'}(\mathbf{r}) \hat{V}(\mathbf{r})$$

in which we have assumed that the electron wave function is a point particle.  $\psi_{\mathbf{k}}(\mathbf{r})$  and  $\psi_{\mathbf{k}'}(\mathbf{r})$  are the initial and final electron states and the electron wave function is neglected. To conserve energy momentum for each particle must undergo a change in energy momentum equal and opposite in direction to that of the electron. In other words,  $\mathbf{k}$  and  $\mathbf{k}'$  must satisfy the triangular inequalities

$$\begin{aligned} k &\leq k' + 1 \\ k' &\leq k + 1 \\ 1 &\leq k + k' \end{aligned}$$



Another selection rule, which results from a consideration of

parity, is that  $\ell$  is odd for a nuclear parity change and  $\ell$  is even if the nuclear parity is unchanged in the reaction.

To see the results of the above, we abandon the independent particle model of the nucleus and consider the nucleus as a whole. Then

$$f_{M',M}(\theta,\varphi) = \int d\vec{r}_N \int d\vec{r} \psi_{J',M'}^*(\vec{r}_N) \mathcal{E}^{-i\vec{k}' \cdot \vec{r}} V(\vec{r} - \vec{r}_N) \psi_{JM}(\vec{r}_N) \mathcal{E}^{i\vec{k} \cdot \vec{r}} \\ = \int d\vec{r}_N \psi_{J',M'}^*(\vec{r}_N) \psi_{JM}(\vec{r}_N) \mathcal{E}^{i(\vec{k}-\vec{k}') \cdot \vec{r}_N} \int d\vec{x} \mathcal{E}^{-i\vec{k}' \cdot \vec{x}} V(\vec{x}) \mathcal{E}^{i\vec{k} \cdot \vec{x}}$$

where  $\vec{x} = \vec{r} - \vec{r}_N$ . We set  $V(\vec{x}) = V_0 \delta(\vec{x})$ , and expand the plane wave obtaining

$$f_{M',M}(\theta,\varphi) = V_0 \sum_{\ell} i^{\ell} \sqrt{4\pi(2\ell+1)} \int d\vec{r}_N \psi_{J',M'}^*(\vec{r}_N) \psi_{JM}(\vec{r}_N) j_{\ell}(Kr_N) Y_{\ell}^0(\theta_N)$$

where  $K = |\vec{k} - \vec{k}'| = \sqrt{k^2 + k'^2 - 2kk' \cos \Theta}$  and from the selection rule previously discussed,  $\ell$  is restricted to the "triangular values". Separating angular and radial integrals

$$f_{M',M}(\theta,\varphi) = \sum_{\ell} S(J,J',M,M',\ell) \int_R^{\infty} r_N^2 dr_N f'(\vec{r}_N) f(\vec{r}_N) j_{\ell}(Kr_N)$$

where we restrict the integration to the region outside the nucleus. If the integration includes the nuclear volume, the resulting angular distribution has much too little structure to be compared with the experimental data (T3). By assuming that the alpha particle does not penetrate the nucleus we imply a direct "surface" interaction.



device, is that  $\delta$  is not for a nucleus with charge  $Z$   
 and even if the nucleus is considered in the region,  
 To see the results of this theory, we assume the  
 constant particle model of the nucleus and consider the  
 as a whole. Then

$$\begin{aligned}
 \psi_{\vec{r}}(\vec{r}) &= \frac{1}{\sqrt{V}} \sum_{\vec{k}} \psi_{\vec{k}}(\vec{r}) = \frac{1}{\sqrt{V}} \sum_{\vec{k}} \psi_{\vec{k}}(\vec{r}) \\
 &= \frac{1}{\sqrt{V}} \sum_{\vec{k}} \psi_{\vec{k}}(\vec{r}) = \frac{1}{\sqrt{V}} \sum_{\vec{k}} \psi_{\vec{k}}(\vec{r}) \\
 &= \frac{1}{\sqrt{V}} \sum_{\vec{k}} \psi_{\vec{k}}(\vec{r}) = \frac{1}{\sqrt{V}} \sum_{\vec{k}} \psi_{\vec{k}}(\vec{r})
 \end{aligned}$$

$$\begin{aligned}
 \psi_{\vec{r}}(\vec{r}) &= \frac{1}{\sqrt{V}} \sum_{\vec{k}} \psi_{\vec{k}}(\vec{r}) = \frac{1}{\sqrt{V}} \sum_{\vec{k}} \psi_{\vec{k}}(\vec{r}) \\
 &= \frac{1}{\sqrt{V}} \sum_{\vec{k}} \psi_{\vec{k}}(\vec{r}) = \frac{1}{\sqrt{V}} \sum_{\vec{k}} \psi_{\vec{k}}(\vec{r}) \\
 &= \frac{1}{\sqrt{V}} \sum_{\vec{k}} \psi_{\vec{k}}(\vec{r}) = \frac{1}{\sqrt{V}} \sum_{\vec{k}} \psi_{\vec{k}}(\vec{r})
 \end{aligned}$$

where  $E = \sqrt{k^2 + m^2}$  is the energy of the particle  
 and  $\vec{r}$  is the position vector. The resulting  
 wave function is then given by  

$$\psi_{\vec{r}}(\vec{r}) = \frac{1}{\sqrt{V}} \sum_{\vec{k}} \psi_{\vec{k}}(\vec{r})$$
 where we have used the identity  $\sum_{\vec{k}} \psi_{\vec{k}}(\vec{r}) = \psi_{\vec{r}}(\vec{r})$ .  
 If the interaction is considered as a whole,  
 the resulting wave function is then given by  

$$\psi_{\vec{r}}(\vec{r}) = \frac{1}{\sqrt{V}} \sum_{\vec{k}} \psi_{\vec{k}}(\vec{r})$$
 where we have used the identity  $\sum_{\vec{k}} \psi_{\vec{k}}(\vec{r}) = \psi_{\vec{r}}(\vec{r})$ .  
 The resulting wave function is then given by  

$$\psi_{\vec{r}}(\vec{r}) = \frac{1}{\sqrt{V}} \sum_{\vec{k}} \psi_{\vec{k}}(\vec{r})$$
 where we have used the identity  $\sum_{\vec{k}} \psi_{\vec{k}}(\vec{r}) = \psi_{\vec{r}}(\vec{r})$ .



If the nuclear wave function falls off sufficiently rapidly outside the nucleus we can approximate it by the value of the integrand at  $r_N = R$ . Then

$$f_{M',M}(\theta, \varphi) = \sum_{\ell} \beta(J, J', M, M', \ell) g(R) j_{\ell}(KR)$$

and if  $\ell$  is restricted by the previous selection rules to a single value

$$f_{M',M}(\theta) = \beta(J, J', M, M', \ell) g(R) j_{\ell}(KR)$$

and

$$\frac{ds}{d\Omega} \propto |j_{\ell}(KR)|^2$$

This restriction of  $\ell$  to a single value will occur only if either  $J$  or  $J'$  is zero. Otherwise there may be two or more possibilities. These can be further restricted, however, if we use the independent particle model of the nucleus. Assume that the nucleus consists of one or more closed shells with a number of nucleons in the orbital angular momentum state  $\lambda$  outside the last closed shell. Then if we assume two particle interactions between the incident alpha particle and the individual nucleons,  $f_{M',M}(\theta)$  will involve integrals of the form  $\int Y_{\lambda m} Y_{\lambda m'} Y_{\ell 0} d\Omega$ , having the value zero unless  $\ell = 0, 2, \dots, 2\lambda$ . This additional selection rule is usually sufficient to eliminate all but a single value of  $\ell$ .

It can be shown that the value of the function  $f(x)$  is constant for all values of  $x$  and is equal to 1. This can be seen by considering the value of the function at  $x = 0$  and  $x = 1$ .

$$f(0) = \sum_{k=0}^{\infty} \frac{1}{2^k} = 1 + \frac{1}{2} + \frac{1}{4} + \dots = 2$$

and it is also true that  $f(1) = 1$ . This is because the function is defined as  $f(x) = \sum_{k=0}^{\infty} \frac{1}{2^k} x^k$  and for  $x = 1$  we have  $f(1) = \sum_{k=0}^{\infty} \frac{1}{2^k} = 2$ .

$$f(x) = \sum_{k=0}^{\infty} \frac{1}{2^k} x^k = \frac{1}{1 - \frac{x}{2}} = \frac{2}{2 - x}$$

and

$$\frac{d}{dx} f(x) = \frac{2}{(2-x)^2}$$

This function is a geometric series and it can be shown that it converges for all values of  $x$  such that  $|x| < 2$ . The sum of the series is  $\frac{2}{2-x}$  and this can be seen by considering the value of the function at  $x = 0$  and  $x = 1$ . It is also true that  $f(1) = 1$  and  $f(2) = 2$ . This is because the function is defined as  $f(x) = \sum_{k=0}^{\infty} \frac{1}{2^k} x^k$  and for  $x = 1$  we have  $f(1) = \sum_{k=0}^{\infty} \frac{1}{2^k} = 2$  and for  $x = 2$  we have  $f(2) = \sum_{k=0}^{\infty} \frac{1}{2^k} 2^k = \sum_{k=0}^{\infty} 1 = \infty$ . The function is also differentiable for all values of  $x$  such that  $|x| < 2$  and its derivative is  $\frac{d}{dx} f(x) = \frac{2}{(2-x)^2}$ . This can be seen by considering the value of the derivative at  $x = 0$  and  $x = 1$ . It is also true that  $f'(0) = \frac{2}{4} = \frac{1}{2}$  and  $f'(1) = \frac{2}{1} = 2$ . The function is also continuous for all values of  $x$  such that  $|x| < 2$  and this can be seen by considering the value of the function at  $x = 0$  and  $x = 1$ . It is also true that  $f(0) = 2$  and  $f(1) = 1$ . This is because the function is defined as  $f(x) = \sum_{k=0}^{\infty} \frac{1}{2^k} x^k$  and for  $x = 0$  we have  $f(0) = \sum_{k=0}^{\infty} \frac{1}{2^k} 0^k = \sum_{k=0}^{\infty} \frac{1}{2^k} = 2$  and for  $x = 1$  we have  $f(1) = \sum_{k=0}^{\infty} \frac{1}{2^k} = 2$ .

The predictions of this theory are now to be compared with the experimental data. It must be stated that, because of the plane wave approximation, these results are not expected to give accurate angular distributions. The predictions are most accurate at the forward angles and the position of the first maximum is most desirable for determining the value of  $\ell$  involved.

Experimental difficulties prohibited observations at laboratory angles less than 14.8 degrees, an angle greater than the predicted position of the first maxima in most of the interactions. In all but one case studied here, however, the  $\ell$  values can be obtained since the quantum numbers of the levels involved have been determined in other experiments (A3). The theoretical curves were compared with the experimental data using a value of  $R$  which gave the best fit with the first observable maximum and minimum.

1.  $\text{Li}^6(\alpha, \alpha')\text{Li}^6$ \*. The ground level of  $\text{Li}^6$  has  $J = 1$ , the 2.19-Mev level  $J = 3$ , and the 4.5-Mev level  $J = 2$ , all of even parity. In both cases the theory predicts an angular distribution which varies as  $|j_2(KR)|^2$ . The values of  $R$  required to fit the data are quite large. However, this is not considered too serious since the "radius" of  $\text{Li}^6$  is a rather nebulous concept. Using the relationship  $R = r_0 A^{1/3}$  with  $r_0 = 1.5 \times 10^{-13}$  cm, alpha-particle radii of  $3.0 \times 10^{-13}$







cm and  $3.9 \times 10^{-13}$  cm were required to fit the data for the 4.5-Mev and 5.19-Mev levels. There is some evidence (16, 38) for a large alpha-particle radius based on (n, $\alpha$ ) scattering experiments. However, the values given above are considered excessive. The fit obtained is quite good, however, and is shown in Figs. 22 and 23.

2.  $C^{12}(\alpha, \alpha') C^{12*}$   $Q = -4.43$  Mev. The theory predicts an angular distribution varying as  $|j_2(KR)|^2$  for excitation from the  $J = 0^+$  ground level to the  $J = 2^+$  first excited level in  $C^{12}$ . Figure 24 shows the fit with experimental observations and also illustrates the sensitivity of the spherical Bessel function to a small change in R. The value of R which gave the best agreement at forward angles required an alpha-particle radius of  $2.5 \times 10^{-13}$  cm for  $r_0 = 1.5 \times 10^{-13}$  cm. This is not incompatible with the previously mentioned evidence for a large alpha-particle radius. It is noted that the data deviate from the theoretical curve at angles greater than 50 degrees as expected from the discussion of its range of validity.

3.  $C^{12}(\alpha, \alpha') C^{12*}$   $Q = -7.65$  Mev. In this case a  $|j_0(KR)|^2$  curve is predicted since the ground and second excited levels are both  $J = 0^+$ . Agreement between theory and experiment are illustrated in Fig. 25 where the fit is seen to be extremely good. The value of R is the same as

[illegible]

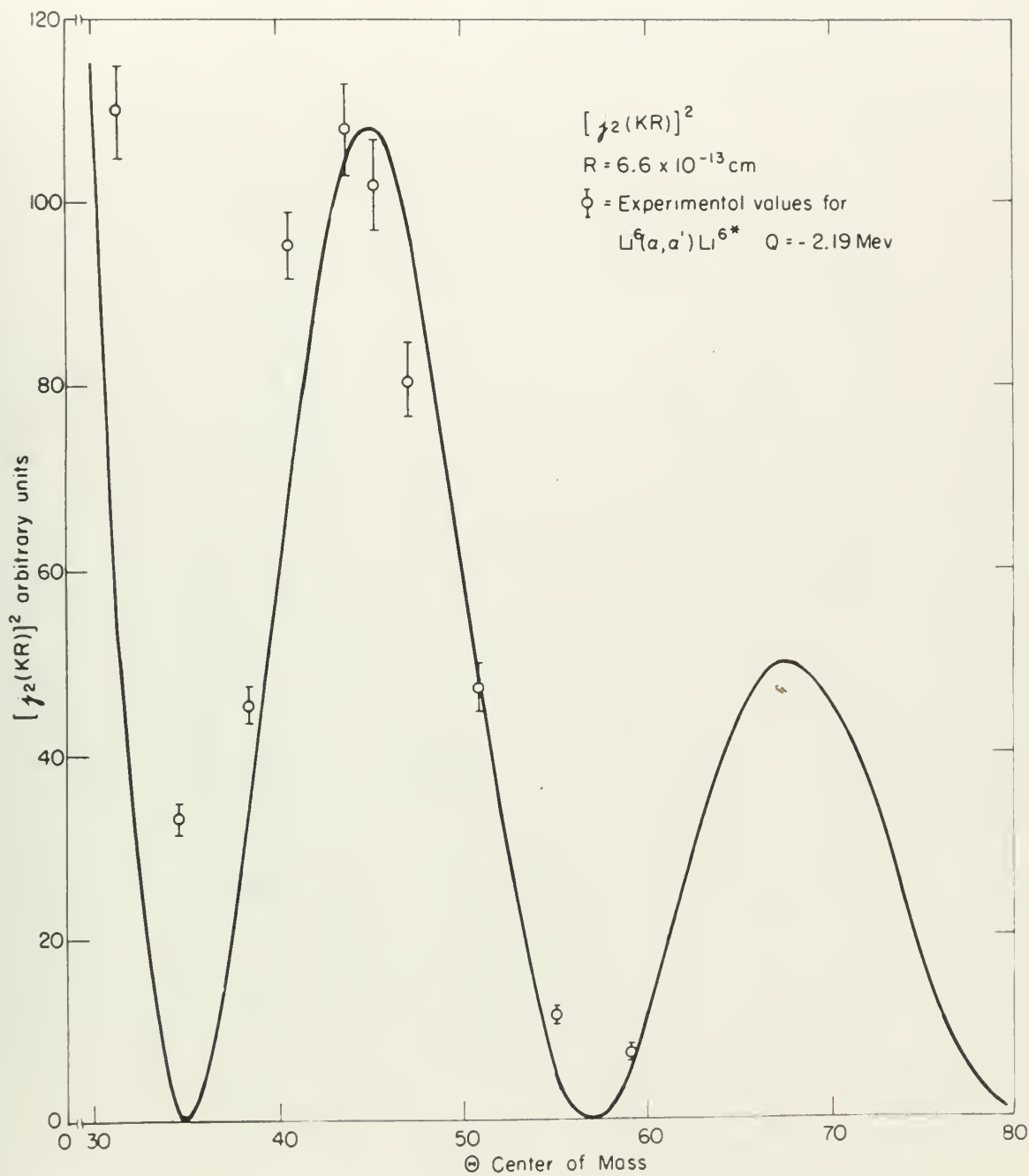


Figure 10





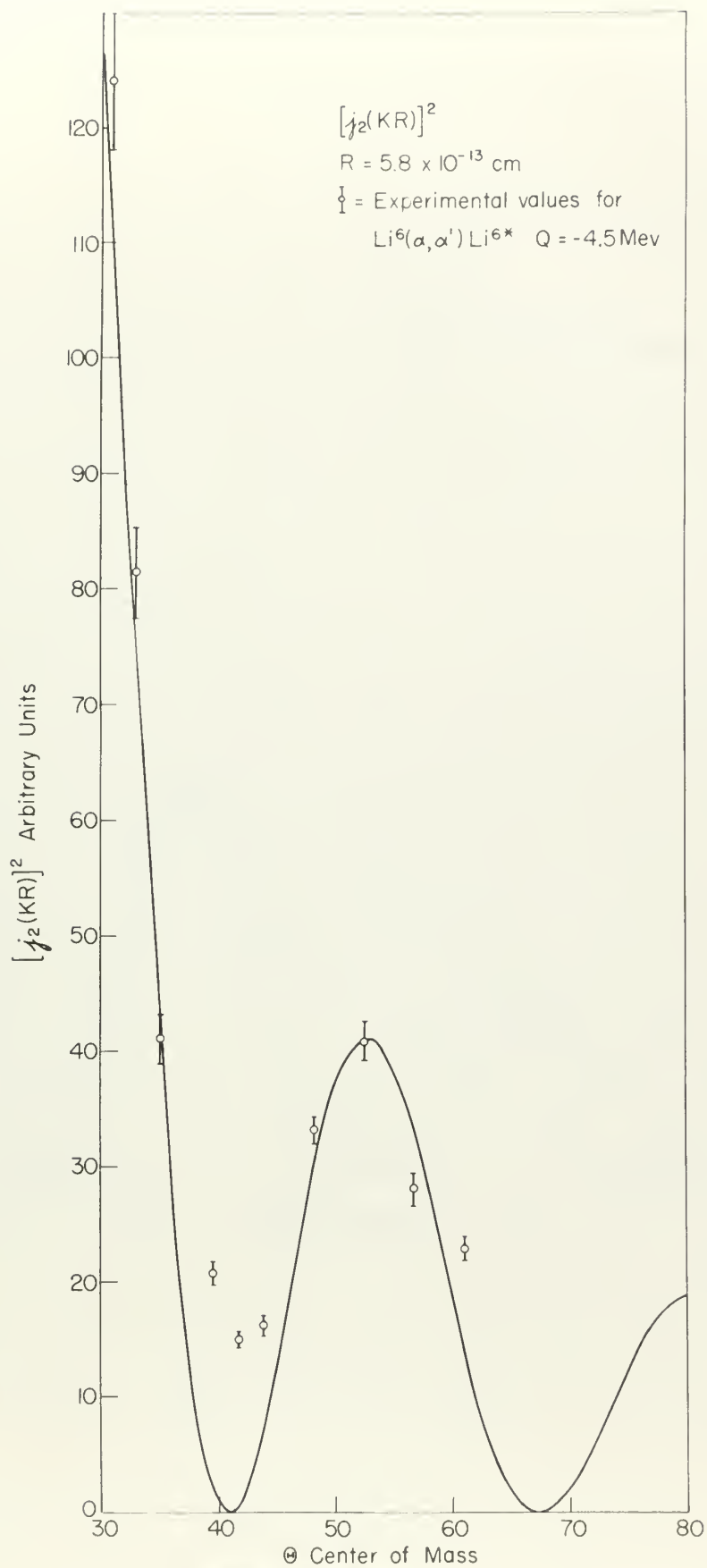


Figure B3



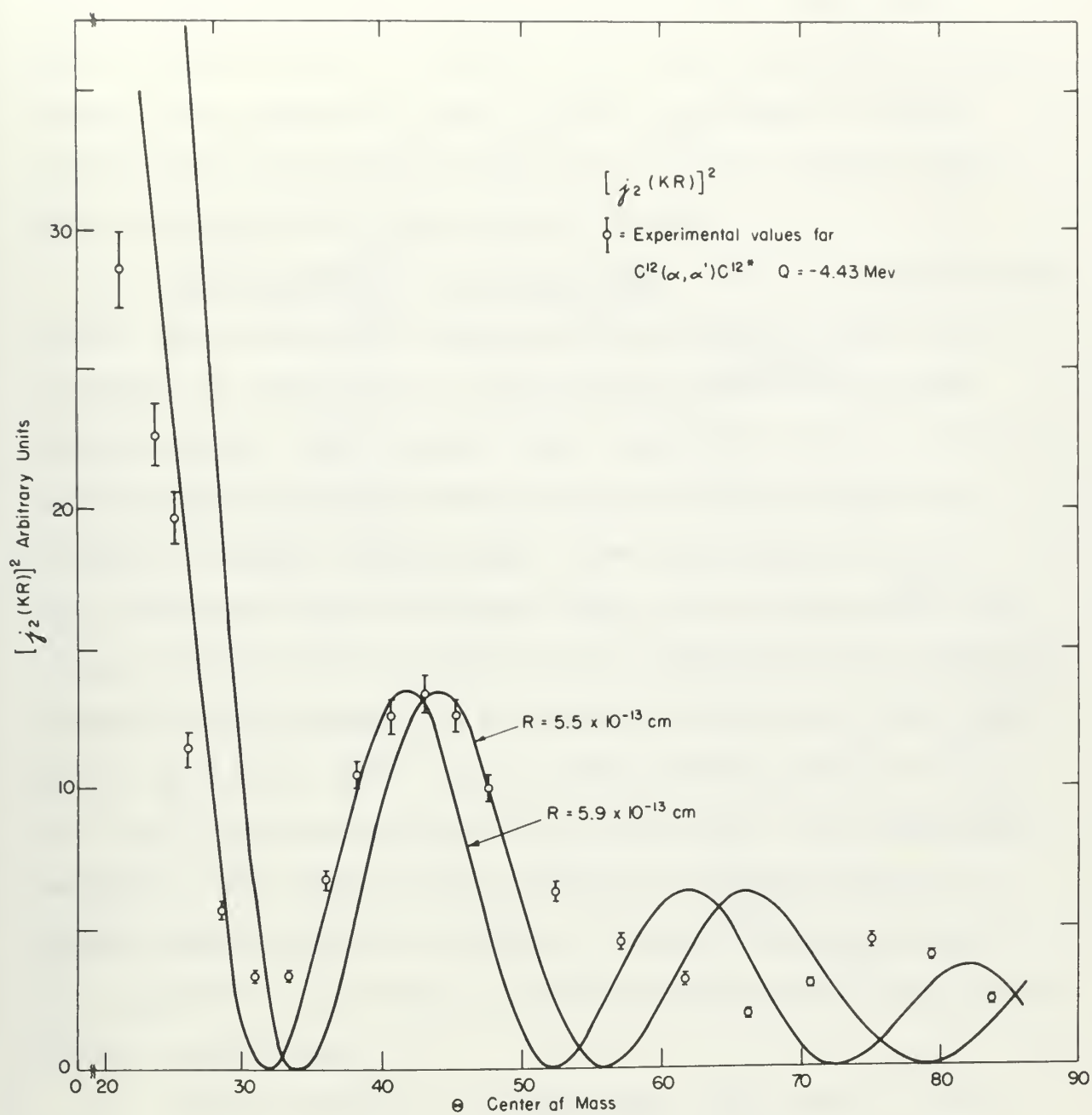


Figure 24





was used for the first excited level of  $C^{12}$ . Since the first maximum shown is actually the first maximum occurring beyond zero degrees for the  $j_0$  curve, agreement at larger angles should be somewhat better than in the previous case. This is illustrated quite well in Fig. 15.

4.  $Mg^{24}(\alpha, \alpha')Mg^{24*}$   $Q = -1.37$  Mev. Due to the kinematics of the interaction, the center-of-mass angular range of observation is increased for interactions involving heavier target nuclei. For a ground level spin of  $J = 0$  and a  $J = 2$  excited level, both of even parity, the theory predicts a  $|j_2(KR)|^2$  angular distribution. The experimental data fit the theoretical curve extremely well and this agreement continues past the third maximum of the spherical Bessel function (second maximum shown), as indicated in Fig. 16. With a unit radius  $r_0 = 1.5 \times 10^{-13}$  cm, an alpha-particle radius of  $2.1 \times 10^{-13}$  cm was required to fit the curve. By bombarding magnesium with 44-Mev alpha particles, Gugelot (H6) has obtained almost identical results. His data are approximated by a  $|j_2(KR)|^2$  and require a radius approximately the same as in the present case.

5.  $Mg^{24}(\alpha, \alpha')Mg^{24*}$   $Q = -4.12$  Mev. The level of excitation involved in this interaction is actually a doublet (H5). The lower level has been determined to be  $J = 4^+$  (A3) for which the theory would predict a  $|j_4(KR)|^2$  angular

There is illustrated with this map the

DATE OF THE REPORT

in the present case.

[illegible]

for which the theory would predict a  $1/c^2$  variation (25). The lower level has been determined to be  $1.4 \times 10^4$  cm<sup>-1</sup> (26) and is involved in this interaction as usually a virtual

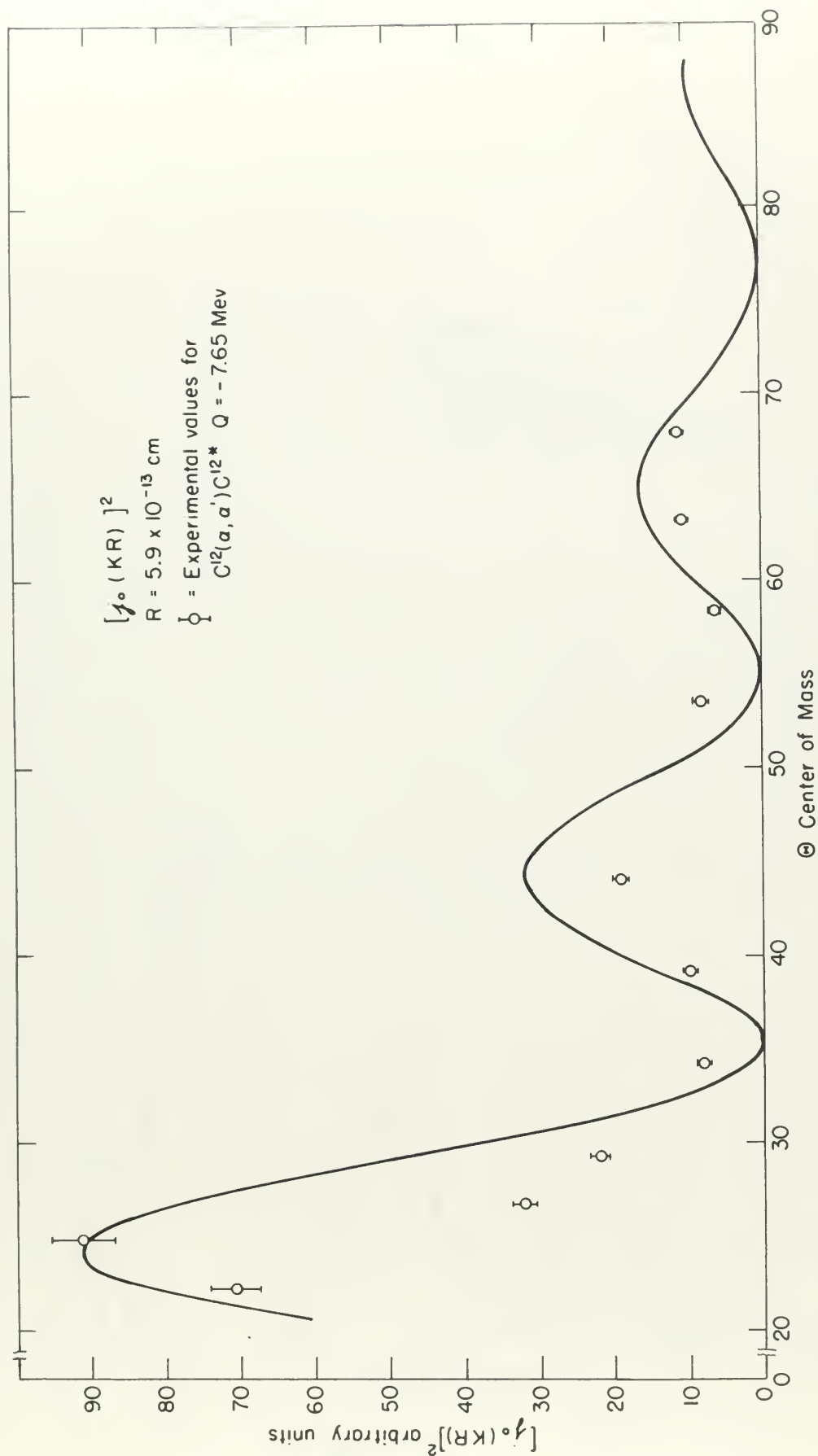


Figure 75





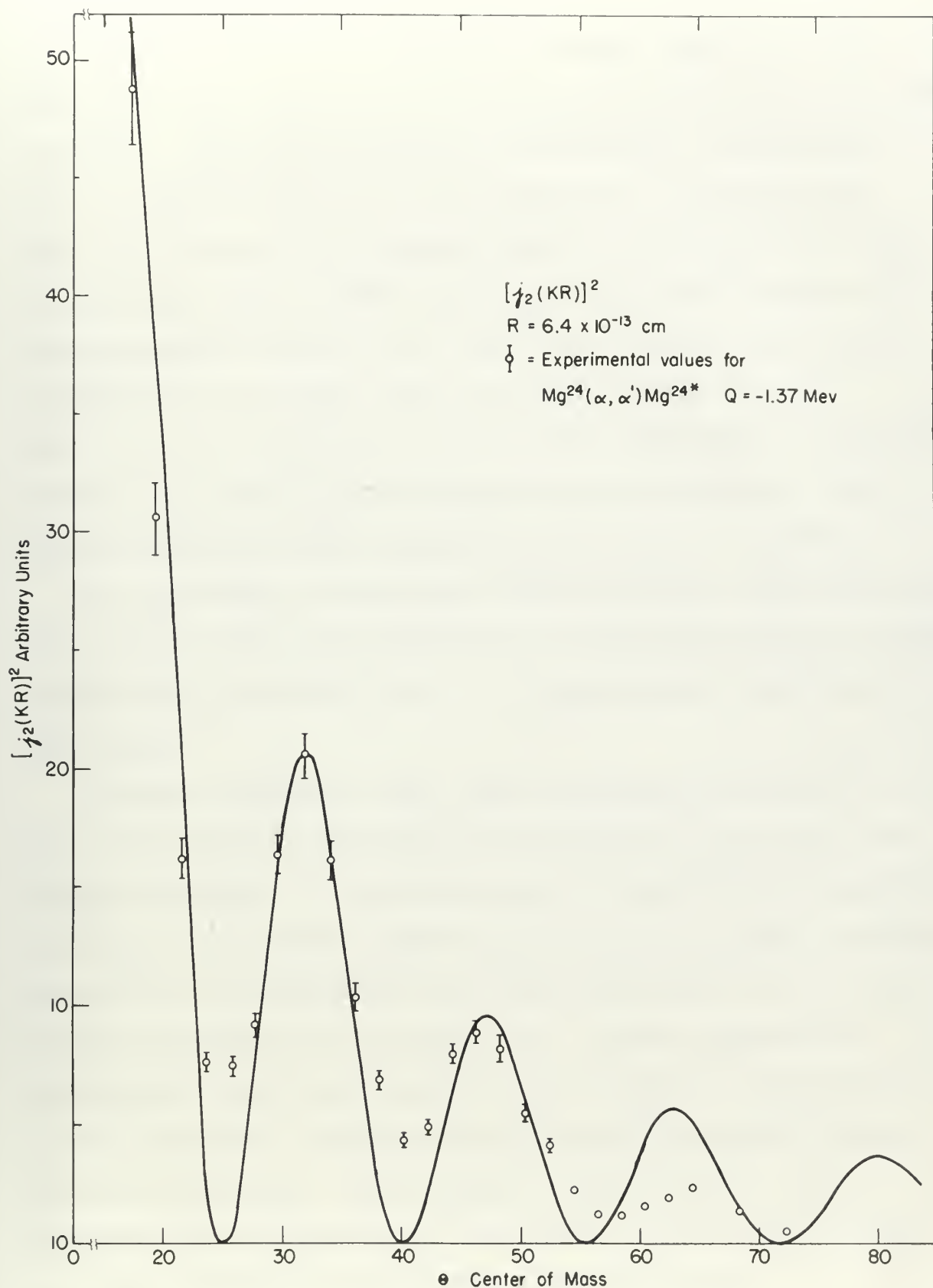


Figure 28



distribution. However, the nuclear radius required to fit the data to this curve is too large to be considered physically possible. The agreement between experimental observations and a  $j_2(KR)^2$  spherical Bessel function, illustrated in Fig. 27, is seen to be extremely good. The theoretical curve was obtained using a unit radius  $r_0 = 1.5 \times 10^{-13}$  cm and an alpha-particle radius of  $1.9 \times 10^{-13}$  cm. This result can be interpreted to indicate that the higher level, having a spin  $J = 2$ , is excited and that in this interaction, excitation of the  $J = 4$  level is discriminated against because of the higher angular momentum transfer which would be involved.

The positions of maxima and minima obtained experimentally are compared with the predictions for the direct surface interaction model in Table 2 and it is seen that the agreement is quite good.

With one exception (S2), there is no known evidence to support the direct interaction process in the inelastic scattering of protons. A study was made of the results of many of the  $(p,p')$  interactions (B7, B9, F3, F6, G2, R4, W8) and in none of these was it possible to fit the experimental data to the angular distributions predicted for a direct interaction. It appears that the  $(p,p')$  interaction proceeds by a process completely different from that which occurs in inelastic alpha-particle scattering. This could be interpreted as due to a difference in diffuseness at the nuclear surface for protons and alpha particles as discussed later in Sec. D.

distribution. However, the results shown in Fig. 10  
 the data in this figure is too large to be presented separately  
 possible. The agreement between experimental observations  
 and a  $\frac{1}{2}(kT)^{3/2}$  theoretical based formula, illustrated in  
 Fig. 10, is seen to be extremely good. The theoretical curve  
 was obtained using a unit value of  $\gamma = 1.5 \times 10^{-11}$  and an  
 alpha-particle radius of  $1.5 \times 10^{-11}$  cm. This value was  
 introduced to indicate that the alpha-particle radius is  
 equal to  $r = 1.5$ , is equal and that in this instance, the  
 of the  $r = 1$  level is distinguished against values of the  
 higher angular momentum transfer which would be involved.  
 The positions of maxima and minima obtained experimentally  
 are compared with the predictions for the direct transfer theory  
 action model in Table I and it is seen that the agreement is  
 quite good.

With one exception (22), there is no known evidence to sup-  
 port the direct transfer hypothesis in the present case.  
 being of proton. A study was made of the results of many of  
 the (p,p') reactions (23, 24, 25, 26, 27, 28, 29, 30) and in many  
 of these was it possible to fit the experimental data to the  
 angular distributions predicted for a direct reaction. It  
 appears that the (p,p') reactions proceed by a process com-  
 pletely different from that which occurs in nuclear trans-  
 fer reactions. This would be indicated by the fact that  
 differences in differences in the angular distributions of the  
 and alpha particles as discussed later in Sec. II.



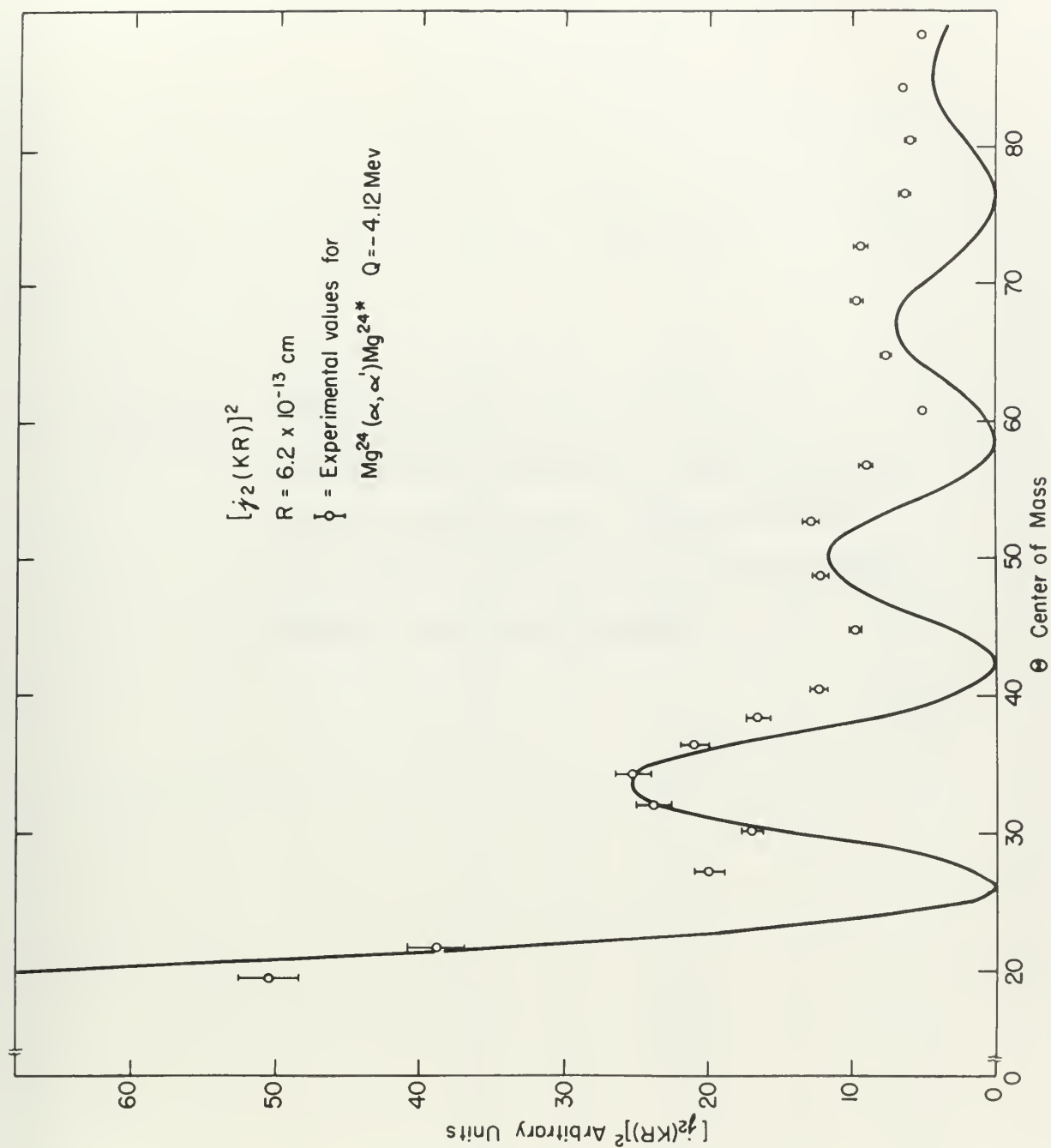


Figure 27



Table 2. Angular positions of maxima and minima of the inelastic alpha-particle angular distributions compared with theoretical predictions for the direct surface interaction model.

Table 6. Equine postures at various stages of the locomotor adjustment period with equine distributional changes for the first routine locomotion away.



POSITIONS OF MAXIMA AND MINIMA  
IN THE INELASTIC ALPHA PARTICLE ANGULAR DISTRIBUTIONS  
EXPERIMENTAL DATA  
COMPARED WITH  
PREDICTIONS OF DIRECT SURFACE INTERACTION MODEL

TARGET NUCLEUS	EXCITATION LEVEL (Mev)	MAXIMUM OR MINIMUM	CENTER OF MASS ANGLE (Deg.)	
			Experiment	Theory
$\text{Li}^6$	2.19	Min	34.5	35
	"	Max	44	45
	4.5	Min	42.5	41
	"	Max	52	53
$\text{C}^{12}$	4.43	Min	32	32
	"	Max	43	42
	"	Min	66	52
	"	Max	75	62
	7.65	Max	24.5	24.5
	"	Min	35	35.5
	"	Max	46	44.5
	"	Min	56.5	55.5
	"	Max	65	65
$\text{Mg}^{24}$	1.37	Min	25	25
	"	Max	32	32
	"	Min	40.5	40
	"	Max	46.5	47
	"	Min	57	55
	"	Max	64.5	63
	4.12	Min	29.5	26.5
	"	Max	33.5	34
	"	Min	43	42.5
	"	Max	51	50.5
	"	Min	60.5	59
	"	Max	69	67
	"	Min	80	77



### C. VALIDITY OF THE ISOTOPIC SPIN SELECTION RULE

The alpha-particle spectrum of Fig. 10 and the discussion of Sec. V indicate that there is little or no breakdown of the isotopic spin selection rule in the inelastic scattering interactions observed in this investigation. In the bombardment of  $\text{Li}^6$ , excitation of the forbidden 3.57-Mev level occurred with a probability of less than 4 percent that of either of the two allowed levels which were strongly excited. Similarly, excitation of the 2.31-Mev level in  $\text{N}^{14}$ , forbidden by this charge independence selection rule, occurred with a probability less than 6 percent that of the allowed 3.05-Mev level.

The statements of Part A of this section and the agreement between the experimental angular distributions and those theoretically predicted, for the inelastic scattering mechanism described in Sec. VIB, are clearly indicative of a direct surface interaction process.

These facts lend support to the recent proposal of Lane and Thomas (13) that isotopic spin should be conserved in a direct interaction.

The above-mentioned evidence of the fact that the induction of the  
of the V indicates that there is little or no correlation of  
the induction with selection rules in the induction mechanism  
interactions observed in this investigation. In the context  
ment of  $L^2$ , excitation of the transition  $L^2 \rightarrow L^2$  level  
coupled with a probability of less than a percent that of  
either of the two allowed levels which were strongly excited.  
Similarly, excitation of the  $L^2 \rightarrow L^2$  level in  $L^2$  is measured  
by this charge independent selection rule, occurred with a  
probability less than a percent that of the allowed  $L^2 \rightarrow L^2$  level.

The statements of Part I of this section and the agree-  
ment between the experimental angular distribution and those  
theoretically predicted, for the induction mechanism mechanism  
described in Part I, are clearly consistent with a theory  
surface induction mechanism.

These facts are consistent with the present picture of the  
and Thomas (1) that induction with selection is consistent with a  
direct interaction.



#### D. ELASTIC SCATTERING

The elastic alpha-particle angular distributions obtained in this experiment, Figs. 19-21, exhibit a structure similar to that observed in the diffraction of light by an opaque body. The reasons for the smooth cross section variation from 60-73 degrees shown in Fig. 20 are not understood. The diffraction pattern is apparently masked by interference with some other process occurring in the interaction and this appears to be worthy of future investigation. A very similar phenomenon was observed in the elastic scattering of deuterons from oxygen (F3) but no analysis of these data was attempted.

Recently, various experimenters have reported the results obtained in the elastic scattering of 10-40-Mev alpha particles by heavy nuclei (F1, G3, W2, W3). The essentially classical analyses of these data (B6, P1, W3) have had some success in qualitatively explaining the observed monotonic decrease of  $\sigma/\sigma_{\text{coulomb}}$  with increasing angle. These experimental results, however, are in direct contrast to the diffraction patterns observed in the elastic scattering of 22-Mev protons (C4, C5) and 40-Mev alpha particles (11) by light nuclei: diffraction effects, similar to those obtained in this investigation, have also been noted in other elastic alpha-particle scattering experiments (B10, E1) in which the results were interpreted in terms of an optical scattering model.

The elastic light-scattering spectra were obtained in this experiment, Fig. 1, which are similar to those observed in the diffraction of light by an opaque body. The reason for the smooth character of the curves is that the light is not scattered. The diffraction pattern is a result of interference also some other process occurring in the scattering and this appears to be a type of diffuse scattering. A very similar phenomenon was observed in the elastic scattering of neutrons from oxygen (2) and in oxygen at low temperatures. Recently, certain experiments were performed and results obtained in the elastic scattering of low-energy light scattered by heavy nuclei (3, 4, 5). The essentially classical analysis of these data (6, 7) has not been known in qualitatively explained the elastic scattering of neutrons at low energies with increasing angle. These experimental results, however, are in almost complete agreement with the results observed in the elastic scattering of light (8, 9) and low-energy neutrons (10) by light nuclei (11, 12). It is also noted in other elastic light-scattering experiments, similar to those obtained in this experiment, have also been noted in other elastic light-scattering experiments (13, 14) in which the results were interpreted in terms of an optical scattering model.

The optical model of the nucleus (58, 59) has been used with varying degrees of success in explaining the diffraction patterns observed in the elastic scattering of charged particles by nuclei (61). It is of interest that good agreement with experiment (64, 64) was obtained for such a model in the elastic scattering of 22-Mev protons by aluminum (69). The real part of the complex potential, necessary to obtain agreement in this case, was represented by the square well potential obtained when one assumes that all of the nuclear charge is essentially on the nuclear surface. By imposing the additional requirement that the target nucleus have a diffuse surface, this form of the complex potential also gave satisfactory agreement with experimental data on the elastic scattering of protons by heavy nuclei. Porter (61) has estimated this diffuseness to be of the order of  $1 \times 10^{-13}$  cm for the alpha-particle bombardment of heavy nuclei, i.e., approximately twice the value which gives satisfactory agreement when protons are used as the bombarding particles. The diffraction type phenomena occurring in the elastic angular distributions of the present investigation can also be explained in terms of an optical model which is consistent with the model employed in the analysis of the inelastic scattering data.

Large ( $\alpha, p$ ) and ( $\alpha, d$ ) cross sections observed in this investigation (Figs. 8 and 28), and others, are interpreted



The object of the present work is to study the effect of the temperature on the rate of reaction between the hydrogen and the oxygen. The results are given in the form of a series of curves showing the variation of the rate of reaction with temperature. The curves are plotted on a semi-logarithmic scale, the logarithm of the rate of reaction being plotted against the reciprocal of the absolute temperature. The curves show that the rate of reaction increases rapidly with increasing temperature, and that the activation energy of the reaction is about 10,000 calories per mole. The results are in good agreement with those obtained by other workers in this field.

The rate of reaction between the hydrogen and the oxygen is a function of the temperature, the pressure, and the concentration of the reactants. In the present work, the pressure and the concentration of the reactants are kept constant, and the effect of temperature alone is studied. The results are given in the form of a series of curves showing the variation of the rate of reaction with temperature. The curves are plotted on a semi-logarithmic scale, the logarithm of the rate of reaction being plotted against the reciprocal of the absolute temperature. The curves show that the rate of reaction increases rapidly with increasing temperature, and that the activation energy of the reaction is about 10,000 calories per mole. The results are in good agreement with those obtained by other workers in this field.

The rate of reaction between the hydrogen and the oxygen is a function of the temperature, the pressure, and the concentration of the reactants. In the present work, the pressure and the concentration of the reactants are kept constant, and the effect of temperature alone is studied. The results are given in the form of a series of curves showing the variation of the rate of reaction with temperature. The curves are plotted on a semi-logarithmic scale, the logarithm of the rate of reaction being plotted against the reciprocal of the absolute temperature. The curves show that the rate of reaction increases rapidly with increasing temperature, and that the activation energy of the reaction is about 10,000 calories per mole. The results are in good agreement with those obtained by other workers in this field.



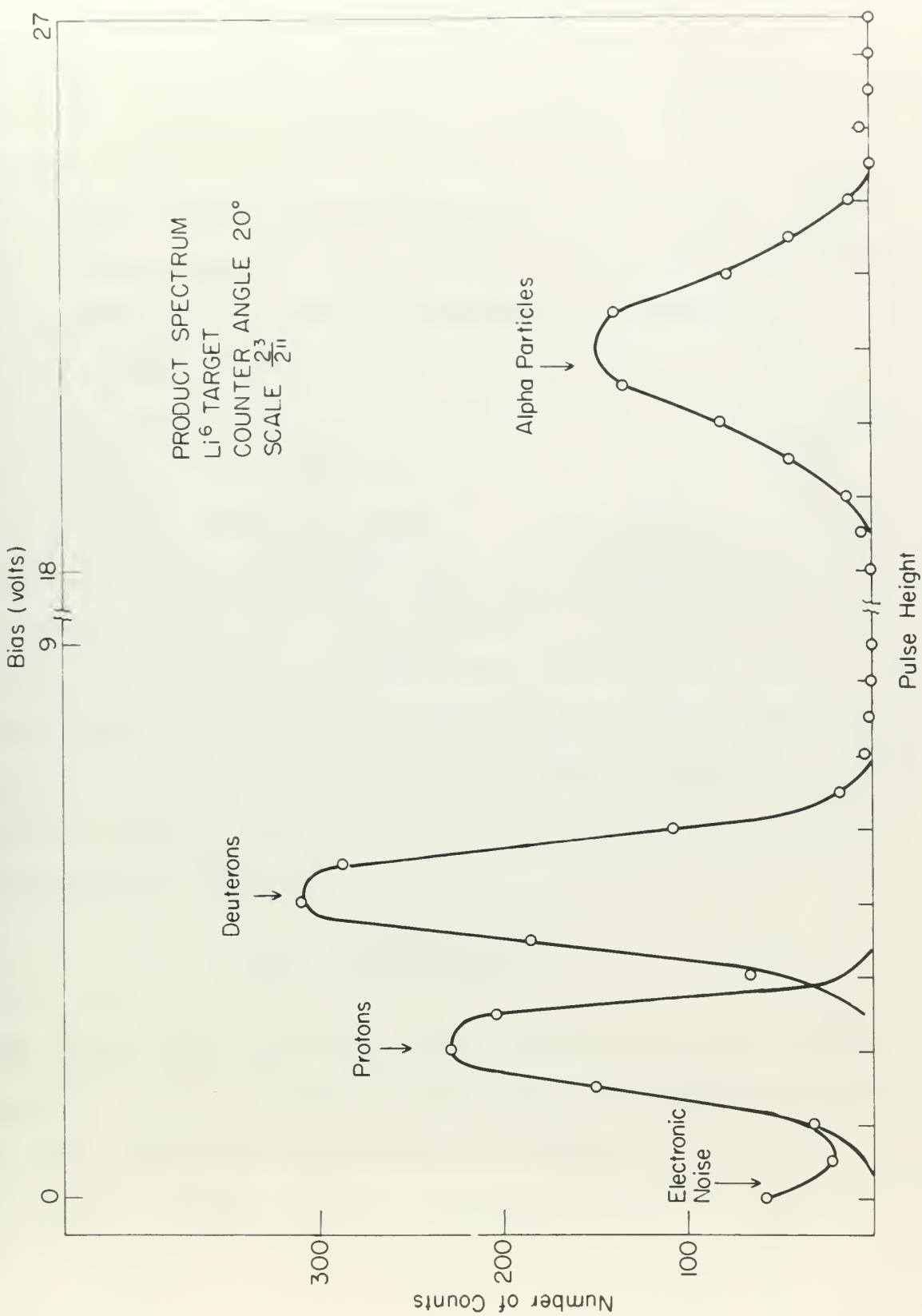


Figure 28



to indicate that nuclei are opaque to high-energy alpha particles (B12, P1, W2). The theoretical treatment of data in the elastic alpha-particle scattering previously mentioned (26) also assumed an opaque nucleus. The argument was that complete absorption occurred for partial waves with  $\ell$  values less than that corresponding to the classical angular momentum for which the distance of closest approach is equal to the sum of the alpha particle and the nuclear radii. In the treatment of the data obtained in the present investigation it is assumed that the nucleus can be represented as being completely opaque out to a radius  $R$ , with a diffuse surface of thickness  $\Delta R$ . This model is similar to the optical model which can be deduced from the results of a recent survey of total reaction cross section data (B12). In Table 3, the elastic angular distributions of the present experiment are compared with those predicted for scattering from an opaque sphere. Positions of the predicted maxima were obtained from the relation

$$\frac{d\sigma}{d\Omega} = \left| \frac{J_1(KR \sin \theta)}{KR \sin \theta} \right|^2$$

which is the exact expression for the scattering from an opaque disc and very closely approximates the angular distributions for scattering from an opaque sphere.

to indicate that model and appear to differ slightly from  
theoretical (Fig. 1). The theoretical treatment is  
also in the case of the particle scattering system  
mentioned (Fig. 2) also shown in some models. The latter  
model was that complete absorption occurred for partial waves  
with  $l$  values less than that corresponding to the classical  
angular momentum for which the distance of closest approach  
is equal to the sum of the sphere radius and the radius  
of the nucleus. In the treatment of the data obtained in the present  
investigation it is assumed that the nucleus can be treated  
as being completely opaque out to a radius  $R$ , with a  
certain value of  $\Delta R$ . This model is similar to  
the optical model which can be derived from the results of a  
recent survey of total reaction cross section data (Fig. 3). In  
Table 1, the elastic scattering distributions of the present ex-  
periment are compared with those predicted for scattering from  
an opaque sphere. Positions of the scattered maxima were ob-  
tained from the relation

$$\frac{d\sigma}{d\Omega} = \left| \frac{f_1(\theta) \sin \theta}{k \sin \theta} \right|^2$$

which is the same expression for the scattering from an op-  
aque disc and very closely approximates the angular distribu-  
tion for scattering from an opaque sphere.



Table 3. Angular positions of the maxima observed in the elastic scattering angular distributions compared with those predicted for scattering from an opaque sphere.

Natural Mg		$C^{12}$		$Li^6$	
C.M. Angular Position of Maxima (degrees)		C.M. Angular Position of Maxima (degrees)		C.M. Angular Position of Maxima (degrees)	
Opaque Sphere		Opaque Sphere		Opaque Sphere	
$R = 5.4$		$R = 4.4$		$R = 4.5$	
<u>Expt.</u>	<u><math>\times 10^{-13}</math> cm</u>	<u>Expt.</u>	<u><math>\times 10^{-13}</math> cm</u>	<u>Expt.</u>	<u><math>\times 10^{-13}</math> cm</u>
24	24	29	29	33.5	33.5
39	41	48	50		
55	55	-	69		
		83	89		



The theoretical curves were fitted using values of  $R$  which gave an exact fit at the position of the first experimental maximum. These values of  $R$  are compared with the mean values of the interaction radii required to fit the inelastic scattering theory to the experimental data. This comparison yields the following values for the diffuseness  $\Delta R$  of the nuclear surface:  $\text{Li}^6 - 1.7 \times 10^{-13}$  cm,  $\text{C}^{12} - 1.3 \times 10^{-13}$  cm, natural Mg -  $0.9 \times 10^{-13}$  cm. These results are of the order of magnitude estimated by Porter (P1) and are in agreement with results obtained in recent analysis of total reaction cross section data (B17). The increase in diffuseness with decreasing atomic number is not incompatible with the concept that the light nuclei are less concentrated.

The difference in diffuseness of the nuclear surface to protons and to alpha particles was mentioned earlier in this section. It has also been pointed out that angular distributions obtained in the inelastic scattering of protons do not, in general, show the structure characteristic of a direct surface interaction which is observed in this experiment. It is not inconsistent with these considerations to speculate that the relatively thick diffuse edge of the nucleus, as seen by an alpha particle, represents a larger effective direct interaction "surface". to alpha particles

The experimental results are listed in Table I. The values of  $\Delta n$  of the various samples are  $1.7 \times 10^{-3}$  cm,  $1.1 \times 10^{-3}$  cm, and  $0.9 \times 10^{-3}$  cm. These results are of the order of magnitude expected by theory (7) and are in agreement with results obtained in other experiments of total reflection angle (8). The difference in thickness with decreasing atomic number is not incompatible with the concept that the light medium is less dense.

The difference in appearance of the two types of  
protons and of alpha particles was mentioned earlier in this  
section. It has also been pointed out that regular light-  
microscopy is the method of choice for the study of protons and  
alpha particles, while the electron microscope is a  
direct method of investigation which is necessary in the study  
of alpha particles with these modifications to  
speculate that the relatively high electron energy of the low  
voltage, as well as the alpha particle, is a factor  
effective direct investigation "electron" in alpha particles



than to protons.

As illustrated in Table 1, the concept of a diffuse surface opaque nucleus, which is consistent with the model assumed for the inelastic scattering process, gives results in close agreement with the elastic scattering data. This cannot be interpreted, however, as verification of the validity of the elastic scattering model, since similar agreement with the data can be obtained using a completely different representation of the elastic interaction. Consider the nucleus as being represented by a square well potential with the coulomb potential cut off at the nuclear radius  $R_n$ . In this case a differential scattering cross section  $\frac{d\sigma}{d\Omega} \sim |f(\theta)|^2$  is obtained in which

$$f(\theta) = \frac{1}{K^3} [V_0 \sin KR - (V_0 KR + 2e^2 K) \cos KR]$$

where  $K = \sqrt{k_1^2 + k_f^2 - 2k_1 k_f \cos \theta}$

$k_1$  = initial interaction wave number

$k_f$  = final interaction wave number

$\theta$  = center-of-mass scattering angle

$R$  = interaction radius

$V_0$  = depth of potential well

This reduces to

University of California, San Diego, La Jolla, California 92037

© 1998 by The McGraw-Hill Companies, Inc. All rights reserved. Printed in the United States of America. This book is protected by copyright. No part of this publication may be reproduced, stored in a retrieval system, or transmitted, in any form or by any means, electronic, mechanical, photocopying, recording, or by any information storage and retrieval system, without permission in writing from The McGraw-Hill Companies, Inc.

1. The first part of the document is a list of names and titles, including "The Hon. Mr. Justice" and "The Hon. Mr. Justice".

$$\left[ \partial_t \exp (X^T u_t + X_{-2}^T V) = 0 \text{ a.s. } \forall \frac{t}{n} \in \mathcal{I} \right] \frac{f}{\mathcal{I}} = \langle \phi \rangle?$$

$$= 200\sqrt{2} \approx 282.84 \approx 283$$

[illegible]

$$f(\theta) \approx \frac{V_0 R^2}{K} \left[ j_1(KR) - \frac{2e^2}{KR^2 V_0} \cos(KR) \right]$$

where  $j_1$  is the spherical Bessel function of order one. For any reasonable value for  $V_0^*$ , it can be shown (W7) that the second term, due entirely to the coulomb effect, has a negligible effect on the angular positions of the maxima, and that the differential cross section may be approximated by

$$\frac{d\sigma}{d\Omega} \approx \frac{V_0 R^2}{K} |j_1(KR)|^2$$

A rigorous treatment of this problem (F5), based on the general phase shift representation of the scattering matrix, has been published complete with tables. The predictions of the above equation are compared with the experimental data in Table 4 where the agreement is seen to be as good as that illustrated in Table 3. From these results, it is concluded that the close agreement with experiment obtained for the opaque nucleus concept is insufficient evidence to validate the use of the model. The fact that the model is consistent with the one employed to describe the inelastic scattering process may be entirely fortuitous. The theoretical curves were fitted using values for  $R$  which correspond to the mean values of the interaction radii required to fit the inelastic scattering theory to the experimental data. These radii are comparable with the ones obtained in the computation of total reaction cross sections calculated by Shapiro (S4) for a totally black square well potential.

---

\* A reasonable value of 20-30 Mev was used. There is evidence (T5) for a larger well depth.



$$\left[ \langle \sigma \rangle = \frac{\langle \sigma^2 \rangle}{\langle \sigma \rangle} - \langle \sigma \rangle \right] \frac{\langle \sigma^2 \rangle}{\langle \sigma \rangle} \approx \langle \sigma \rangle$$

where  $\langle \sigma \rangle$  is the spectral density function of order  $\sigma$ . For any reasonable value for  $\langle \sigma^2 \rangle$ , it can be shown that the spectral density, and similarly the spectral density, and the effect on the spectral density of the system, and the differential cross section can be approximated by

$$\left[ \langle \sigma \rangle \right] \frac{\langle \sigma^2 \rangle}{\langle \sigma \rangle} \approx \frac{\langle \sigma^2 \rangle}{\Omega_D}$$

A rigorous treatment of this problem (77), based on the spectral density representation of the scattering matrix, has been presented in the literature. The derivation of the above equation is compared with the experimental data in Table 1. Where the agreement is seen to be as good as that illustrated in Table 1. The above results, it is concluded that the above agreement with experiment obtained for the above results may be in significant evidence as to the validity of the model. The fact that the model is consistent with the experimental results, the elastic scattering process may be entirely topological. The theoretical results with the above results for a system compared to the above values of the interaction with the system to the elastic scattering theory to the experimental data. These results are compared with the above results in the calculation of total reaction cross section calculated by

$$\sigma_{\text{total}} = \sigma_{\text{elastic}} + \sigma_{\text{inelastic}} \quad (78)$$

\* A reasonable value of  $\Omega_D$  is not known. There is evidence (77) for a lower value.



Table 4. Angular positions of the maxima observed in the elastic scattering angular distributions compared with those predicted for elastic scattering from a square well potential.

Natural Mg		$C^{12}$		$Li^6$	
C.M. Angular Position of Maxima (degrees)		C.M. Angular Position of Maxima (degrees)		C.M. Angular Position of Maxima (degrees)	
<u>Expt.</u>	<u>Square well</u>	<u>Expt.</u>	<u>Square well</u>	<u>Expt.</u>	<u>Square well</u>
24	25.6	29	31.6	33.5	34
39	39.5	46	49		
55	54	-	69.6		
		83	91.3		

Table 4. Angular positions of the various members in the elastic restoring angles. Illustrations are provided for those members for elastic restoring angles.

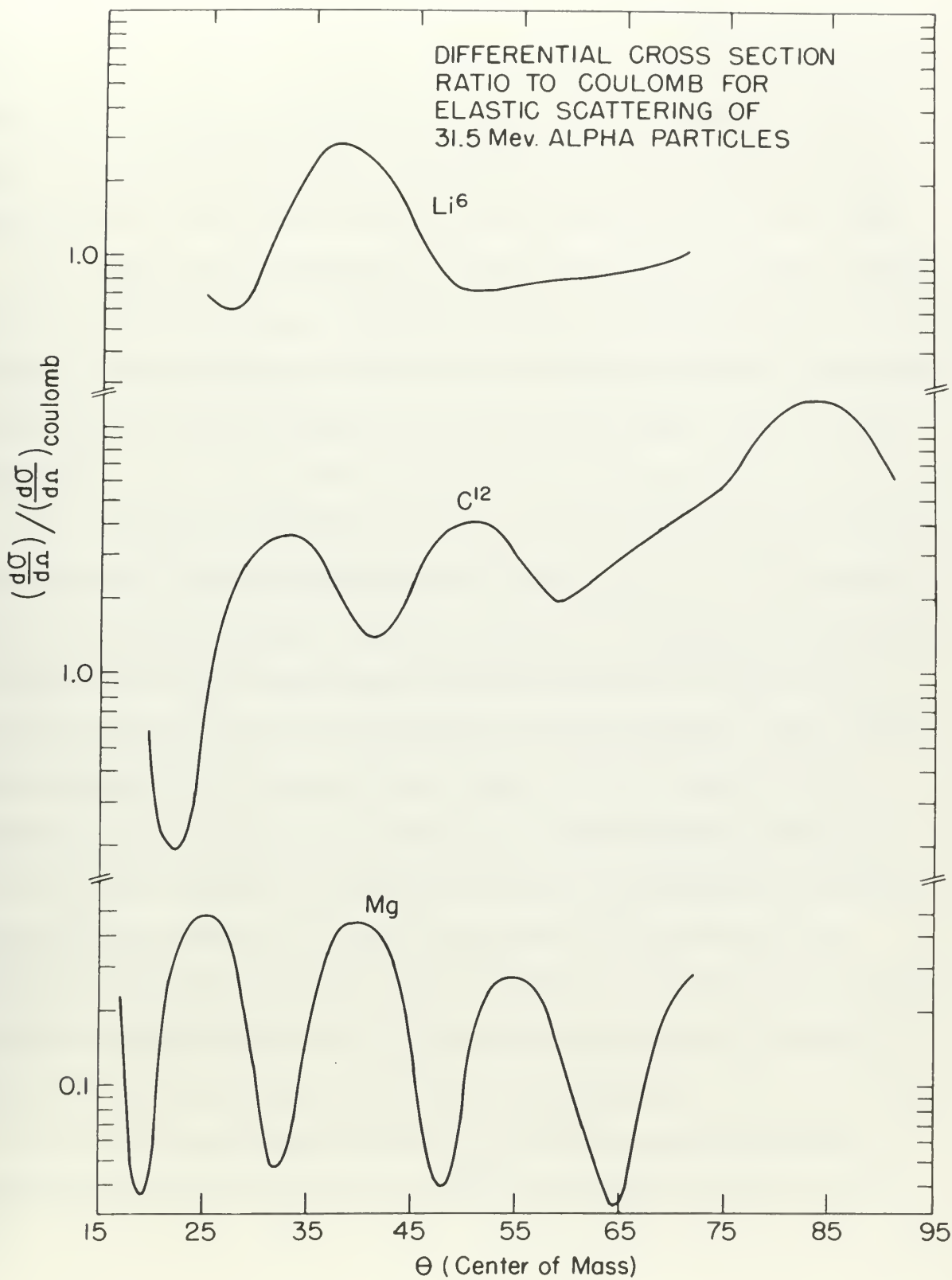
A recent, and as yet unpublished, elastic alpha-particle scattering experiment was performed to study the angular dependence of  $(\frac{d\sigma}{d\Omega})/(\frac{d\sigma}{d\Omega})_{\text{coulomb}}$  at 40 Mev over a range of elements from carbon to silver (11). A composite plot of these data shows the details of the gradual change from the diffraction to the exponential behavior with increasing atomic number. The data obtained in the present investigation are illustrated in this same form in Fig. 29 to facilitate comparison of the behavior at the bombarding energy of 31.5 Mev used in this experiment. The general characteristics of both composite plots are quite similar.

## VII. CONCLUSIONS

The data obtained in this investigation and the discussion of Sec. VIA clearly indicate that the mechanisms of compound nucleus formation and electric excitation are not of primary importance in an analysis of the inelastic scattering of 31.5-Mev alpha particles by light nuclei. The angular distributions are similar to those predicted by Austern et al. (A4) for an interaction in which the bombarding particle transfers an amount of energy to a nucleon at the surface of the nucleus,









the so-called direct surface interaction. Experimental agreement with the predictions of a theory based on this model is quite good. Nevertheless, the following statements must be considered as imposing a limit on the validity of this model.

1. The theory assumes an interaction with a single nucleon in the target nucleus. However, from purely kinematic considerations it can be shown (H6) that the momentum transfer involved requires that the energy be transferred to more than a single nucleon.

2. The Born approximation is probably quite good for the interactions under consideration, i.e.,  $E_0 \sim 30$  Mev compared with a maximum coulomb barrier of 8 Mev. Similar agreement obtained with the use of coulomb wave functions would give strong support to the applicability of the model. This will be attempted in the near future (T5) and the effect on the theoretical predictions should be of considerable interest.

3. The electric interaction theory is subject to certain refinements which may or may not affect the magnitude and angular dependence of the cross sections predicted for this method of excitation. One of the most important of these is the use of an arbitrary radius of interaction.

4. It was assumed that the compound nucleus type of interaction did not occur for the following reasons:

1. The theory assumes an interaction with a virtual medium in the target nucleus. However, from purely kinematical considerations it can be shown (22) that the maximum transfer involved requires that the energy be transferred to more than a single

1. The electric interaction energy is subject to certain theoretical predictions which are of considerable interest. It is accepted in the present paper (19) that the effect on the energy of the spin-orbit interaction of the nucleus. This will agree with the use of Coulomb wave functions would give obtained with the use of Coulomb wave functions would give with a maximum column error of 2 per cent. This is consistent with the use of Coulomb wave functions. 1.4.  $\epsilon_{\text{C}}$  is the Coulomb interaction energy. The same interaction is present in the case of the

TO THE DIRECTOR, BUREAU OF INVESTIGATION, U.S. DEPARTMENT OF JUSTICE



- (a) The variation of intensity with angle was not smooth but showed a well defined structure.
- (b) There was no angular symmetry about 90 degrees.
- (c) No back angle maxima were found and the majority of the inelastic scattering was confined to the forward quadrant.
- (d) The angular distributions were insensitive to significant variations in the incident beam energy.
- (e) The differential cross sections observed were large compared with those previously obtained for interactions known to proceed by compound nucleus formation.

The development of a formal compound nucleus theory, which predicts the inelastic angular distributions resulting from the excitation of discrete levels, could affect the above considerations.

On the basis of the present evidence, however, it is concluded that the inelastically scattered alpha particles, observed in the present investigation, result from a direct interaction at the nuclear surface. Due to experimental limitations, it was not possible to obtain data at angles smaller than 14.8 degrees. As a result, even though good agreement with theory was found at larger angles, it was not possible to verify the position of the first predicted maxima except

(a) The variation of intensity with angle was

measured by means of a slit collimator.

(b) The intensity was measured by means of a slit collimator.

(c) The beam width was measured by means of a slit collimator.

(d) The intensity was measured by means of a slit collimator.

(e) The intensity was measured by means of a slit collimator.

(f) The intensity was measured by means of a slit collimator.

(g) The intensity was measured by means of a slit collimator.

(h) The intensity was measured by means of a slit collimator.

(i) The intensity was measured by means of a slit collimator.

(j) The intensity was measured by means of a slit collimator.

(k) The intensity was measured by means of a slit collimator.

(l) The intensity was measured by means of a slit collimator.

(m) The intensity was measured by means of a slit collimator.

(n) The intensity was measured by means of a slit collimator.

(o) The intensity was measured by means of a slit collimator.

(p) The intensity was measured by means of a slit collimator.

(q) The intensity was measured by means of a slit collimator.

(r) The intensity was measured by means of a slit collimator.

(s) The intensity was measured by means of a slit collimator.

(t) The intensity was measured by means of a slit collimator.

(u) The intensity was measured by means of a slit collimator.

(v) The intensity was measured by means of a slit collimator.

(w) The intensity was measured by means of a slit collimator.

(x) The intensity was measured by means of a slit collimator.

(y) The intensity was measured by means of a slit collimator.

(z) The intensity was measured by means of a slit collimator.

in one level of  $C^{12}$ . If these experimental difficulties can be overcome, it is possible that  $(\alpha, \alpha')$  angular distributions can yield valuable information about the properties of a number of nuclei in which the quantum numbers of the energy levels are as yet undetermined.

In the two cases investigated, it was seen that the excitation of levels prohibited by the isotopic spin selection rule occurred with a probability of less than about 5 percent that of the allowed levels. These experimental results lend support to the statement that isotopic spin is conserved in direct interactions (L3).

The diffraction phenomena, occurring in the angular distributions of elastically scattered alpha particles, are suggestive of the use of an optical model in the description of elastic nuclear events. The large  $(\alpha, p)$  and  $(\alpha, d)$  cross sections observed in this experiment can be interpreted as requiring the use of a large absorption coefficient in the complex scattering potential employed in the optical model. Both statements are compatible with the results of others (B6, B12, P1, S4, W9). The elastic angular distributions can be interpreted in terms of a model consistent with the one employed in describing the inelastic scattering data, although this evidence is insufficient to verify the validity of the model. The results of this experiment support the increasing



in the level of  $C_{10}$ . It shows experimental difficulties  
of previous, it is possible that  $(C_{10})$  might be  
can yield valuable information about the properties of a  
number of points in which the question arises of the energy  
levels are as yet undetermined.  
In the two cases investigated, it was seen that the ex-  
citation of levels predicted by the independent spin interaction  
rule occurred with a probability of less than about 5 percent  
that of the allowed levels. These experimental results are  
in accord with the statement that the probability is decreased in  
direct interactions  $(S_1 S_2)$  and  $(S_1 S_3)$  compared to the  
indirect interactions  $(S_1 S_2 S_3)$  occurring in the doublet spin-  
triplet states of the  $2p^2$  configuration. The results are in  
agreement with the use of an orbital model in the calculation of  
electronic energy levels. The  $2p^2$  and  $(p, d)$  cases are  
shown observed in this experiment and are interpreted as re-  
sulting from the use of a large orbital contribution in the  
complex configuration interaction analysis in the orbital model.  
Both experiments are consistent with the results of the  
( $2p, 3d$ ), ( $3p, 4d$ ), and ( $3d, 4d$ ) cases. The atomic energy levels are  
calculated in terms of a single configuration  $2p^2$  and  
employed in describing the energy levels of the  $2p^2$  configuration.  
This method is insufficient to yield the results of the  
model. The results of this experiment support the use of the



evidence that the elastic scattering of alpha particles can be described in terms of an optical model in which the imaginary potential is extensive and rather intense.

The conclusions which can be drawn from the data obtained in this experiment are summarized as follows:

1. The inelastic alpha-particle scattering proceeds primarily by a direct surface interaction process, with the possibility of some small contributions from compound nucleus formation or electric excitation.

2. It is possible to obtain useful information about the properties of the energy levels of nuclei from a study of the  $(\alpha, \alpha')$  angular distributions.

3. Isotopic spin is conserved in these interactions.

4. The  $(p, p')$  and  $(\alpha, \alpha')$  reactions proceed by completely different processes.

5. The elastic alpha-particle scattering can be interpreted in terms of a potential square well scattering center or in terms of an optical model and a complex scattering potential.

distance from the elastic scattering of light particles and  
 be described in terms of an optical model in which the  
 scattering potential is assumed to be a function of the  
 distance which can be taken from the data obtained  
 in this experiment and compared as follows:

1. The elastic scattering potential is assumed to be  
 identical to a direct optical potential, with the  
 possibility of some small corrections to the optical model  
 formation of elastic scattering.

2. It is possible to obtain optical scattering from the  
 properties of the energy levels of nuclei from a study of the  
 (a) regular structure.

3. Elastic scattering is considered in these experiments.  
 4. The (a) and (b) reactions proceed by completely  
 different processes.

5. The elastic scattering scattering can be taken  
 from the form of a potential energy well which is  
 or in terms of an optical model and a complex potential  
 potential.

## APPENDIX I

THE CONVERSION OF EXPERIMENTAL ANGULAR DISTRIBUTION DATA TO  
THE CENTER-OF-MASS COORDINATE SYSTEM

Experimental data must be converted from the laboratory to the particle or center-of-mass frame of reference for comparison with theoretical angular distribution predictions. The form of the corrections to be applied to the experimental data is summarized by Schiff (83). A compilation of these corrections, suitable for interpolation, has been prepared (M5) and a nomogram, suitable for rough but rapid conversion, has been published (F7). To eliminate an additional source of error in the results of the present experiment, conversion to the particle coordinate system was accomplished using correction curves plotted from the exact formulae. The following symbols are used in this appendix, where the required corrections are derived from elementary principles:

- $m_1$  mass of bombarding particle
- $m_2$  mass of target nucleus
- $m_3$  mass of observed particle
- $m_4$  mass of residual nucleus

## APPENDIX I

THE THEORY OF CORRELATION ANALYSIS  
THE CORRELATION ANALYSIS

Experimental data must be converted from the form

to the form of correlation analysis (Table I).

When the data are converted to the form of correlation analysis, the form of the correlation is as follows:

data is converted by using (1). A correlation of

correlation, which is the correlation, is the

(2) and a correlation, which is the correlation, is the

has been defined (3). It is defined as follows:

of error in the form of the present experiment, which

to the form of correlation analysis is as follows:

correlation error which is the correlation, is the

which is the correlation, is the correlation, is the

correlation is the correlation, is the correlation, is the

1. Form of correlation analysis

2. Form of correlation analysis

3. Form of correlation analysis

4. Form of correlation analysis



- $v_1 \dots v_4$  the velocities of  $m_1 \dots m_4$  measured in the laboratory frame of reference
- $v_c$  velocity of the center of mass measured in the laboratory coordinate system
- $V_1 \dots V_4$  the velocities of  $m_1 \dots m_4$  measured in the center-of-mass system
- $Q$  the reaction  $Q$  value as calculated from the mass tables and expressed in Mev
- $E_0$  the total initial kinetic energy measured in the laboratory
- $E$  the total initial kinetic energy of the system measured in the center of mass
- $\Theta_0$  the laboratory angle of observation of particle  $m_3$
- $\Theta$  the center-of-mass angle corresponding to the laboratory angle  $\Theta_0$
- $d\omega$  the unit solid angle measured in the laboratory coordinates
- $d\Omega$  the unit solid angle measured in the center-of-mass coordinates
- $\gamma$  defined by equation (4)
- $g(\Theta_0)$  defined by equation (12)

the velocities of  $v_1 \dots v_n$  measured in the  
laboratory frame of reference  
velocity of the center of mass measured in the  
laboratory coordinate system  
the velocities of  $v_1 \dots v_n$  measured in the center-  
of-mass system  
the reaction  $Q$  value as determined from the mass  
tables and measured in MeV  
the total initial kinetic energy measured in the  
laboratory  
the total initial kinetic energy of the system  
measured in the center of mass  
the laboratory angle of emission of particle  $i$   
the center-of-mass angle corresponding to  $\theta_i$   
laboratory angle  $\phi_i$   
the unit vector defined in the laboratory  
coordinate  
the unit vector defined in the center-of-  
mass coordinate  
 $\gamma$  defined by equation (1)  
 $\alpha(\phi_i)$  defined by equation (2)

# 1. RELATIONS BETWEEN ANGLES IN THE LABORATORY AND CENTER OF MASS

In the laboratory the bombarding particle of mass  $m_1$  moving with velocity  $v_1$  collides with a target nucleus of mass  $m_2$  at rest. The center of mass of the two particles moves with a velocity  $v_c$  so that the linear momentum of the system is  $m_1 v_1 = (m_1 + m_2) v_c$ . Therefore

$$v_c = \alpha v_1 \quad \text{where } \alpha = \frac{m_1}{m_1 + m_2} \quad (1)$$

In the center of mass, prior to the collision the velocity of  $m_1$  is

$$V_1 = (v_1 - v_c) = v_1(1 - \alpha)$$

Since  $m_2$  is initially at rest in the laboratory system, the center-of-mass velocity of  $m_2$  is simply

$$V_2 = -v_c$$

The center of mass is, by definition, stationary in the center-of-mass frame of reference. Therefore, in the center-of-mass coordinates, the total linear momentum is zero. After the collision, this requires that

$$m_3 V_3 = m_4 V_4 \quad \text{or} \quad V_4 = \frac{m_3}{m_4} V_3$$

where  $m_3$  and  $V_3$  refer to the scattered or observed particle and  $m_4$  and  $V_4$  refer to the residual particle.

1. Relative motion is the motion of one body with respect to another.

In the laboratory the horizontal velocity of mass  $m_1$  before the collision is  $v_1$  and the velocity of mass  $m_2$  is zero. The center of mass of the two particles moves with a velocity  $v_c$  so that the linear momentum of the system is  $m_1 v_1 = (m_1 + m_2) v_c$ . Therefore

$$(A) \quad v_c = \frac{m_1 v_1}{m_1 + m_2}$$

In the center of mass, before the collision the velocity of  $m_1$  is

$$v_1 - v_c = (v_1 - \frac{m_1 v_1}{m_1 + m_2}) = \frac{m_2 v_1}{m_1 + m_2}$$

Since  $m_2$  is initially at rest in the laboratory system, the center-of-mass velocity of  $m_2$  is simply

$$v_c = \frac{m_1 v_1}{m_1 + m_2}$$

The center of mass is at a constant velocity in the center-of-mass frame of reference. Therefore, in the center-of-mass frame, the total linear momentum is zero. After the collision, this remains true

$$m_1 v_1' + m_2 v_2' = 0 \quad \text{or} \quad v_2' = -\frac{m_1}{m_2} v_1'$$

where  $m_1 v_1'$  and  $m_2 v_2'$  are the momenta of masses  $m_1$  and  $m_2$  relative to the center of mass.



From energy conservation considerations

$$\frac{1}{2}m_1v_1^2 + \frac{1}{2}m_2v_2^2 = \frac{1}{2}m_3v_3^2 + \frac{1}{2}m_4v_4^2 - Q$$

which reduces to

$$\frac{1}{2}m_1v_1^2 \left( \frac{m_2}{m_1 + m_2} \right) = \frac{1}{2}m_3v_3^2 \left( 1 + \frac{m_3}{m_4} \right) - Q$$

However

$$\frac{1}{2}m_1v_1^2 \left( \frac{m_2}{m_1 + m_2} \right) = \left( \frac{m_2}{m_1 + m_2} \right) E_0 = E$$

the total initial center-of-mass kinetic energy of the system, therefore

$$v_3^2 = \frac{E + Q}{\frac{1}{2}m_3 \left( \frac{m_3 + m_4}{m_4} \right)} \quad (?)$$

In Fig. 30 the uniform motion  $v_c$  of the center of mass in the laboratory system is superimposed on the angular and velocity relations in the center-of-mass coordinate system. It is seen that laboratory velocities can be obtained by vectorially adding  $v_c$  to the center of mass

$$\psi = \frac{1}{\sqrt{2}} \left( \psi_1 + \psi_2 \right)$$

where  $\psi_1$  and  $\psi_2$  are

$$\psi_1 = \left( \frac{2}{\pi} \right)^{1/4} e^{-\frac{1}{2} x^2} \quad \psi_2 = \left( \frac{2}{\pi} \right)^{1/4} e^{-\frac{1}{2} x^2} \cos x$$

However

$$\psi = \frac{1}{\sqrt{2}} \left( \frac{2}{\pi} \right)^{1/4} e^{-\frac{1}{2} x^2} (1 + \cos x)$$

The total initial center-of-mass kinetic energy of the system

therefore

$$(3) \quad \frac{1}{2} M v_0^2 = \frac{1}{2} M \left( \frac{v_0}{2} \right)^2$$

in the initial center of mass  $v_0$  of the system of mass

in the laboratory system is determined by the initial and

velocity relations in the center-of-mass coordinate system.

It is seen that laboratory velocity can be obtained by

reversibly adding  $v_0$  to the center of mass

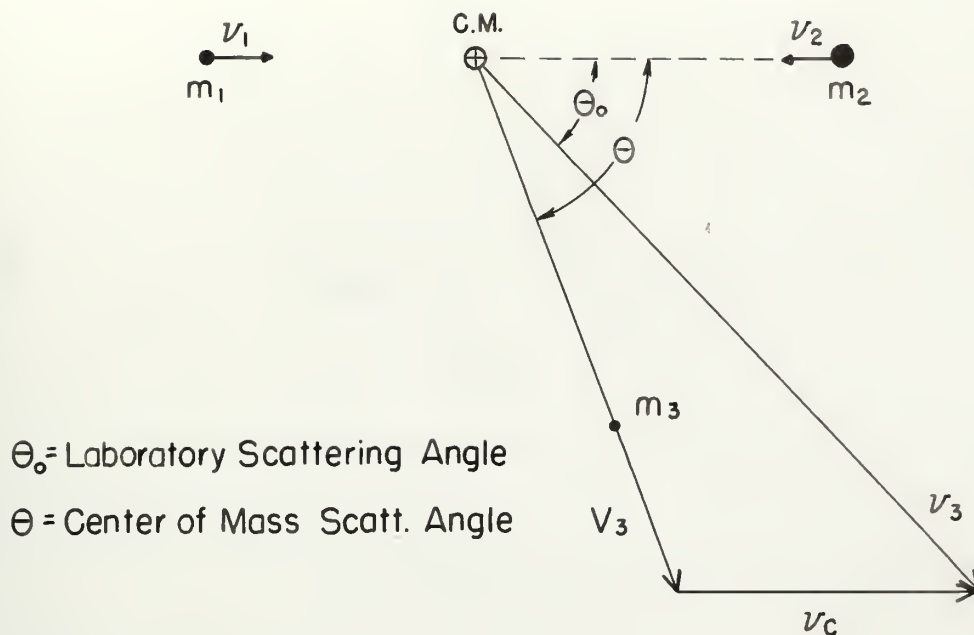


Figure 30

Applying the law of sines to Fig. 30

$$\frac{\sin \Theta_0}{V_3} = \frac{\sin (\Theta - \Theta_0)}{v_c}$$

or

$$\sin (\Theta - \Theta_0) = \frac{v_c}{V_3} \sin \Theta_0 \quad (3)$$

Considering only nonrelativistic interactions, where  $Q = (m_1 + m_2 - m_3 - m_4)$  is small compared with the rest energy  $m_1 c^2$  of any of the particles involved, it is assumed that  $m_1 + m_2 \approx m_3 + m_4$ . Substituting  $v_c$  from equation (1) and  $V_3$  from equation (2)

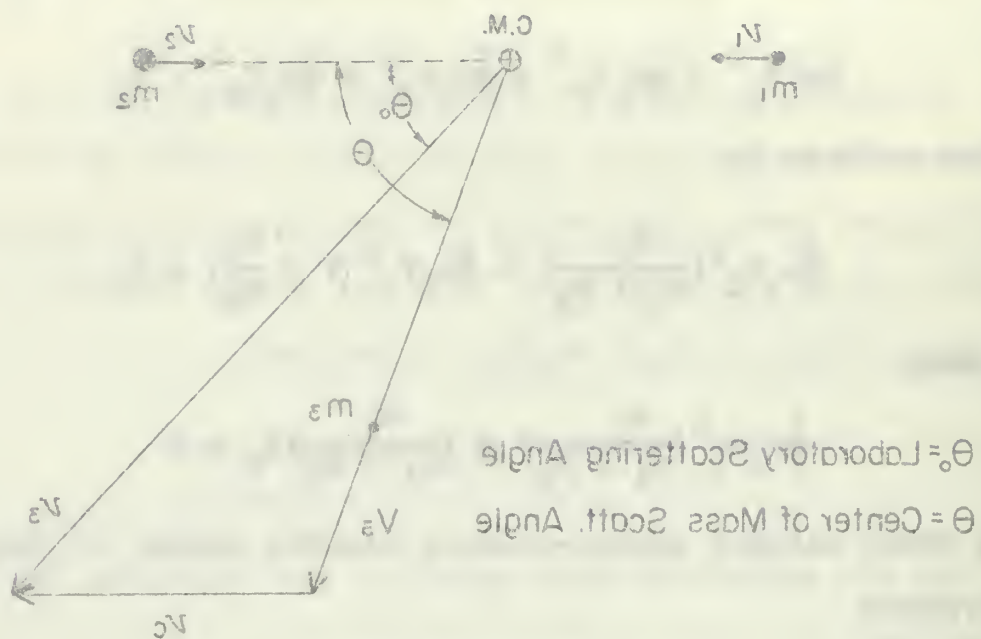


Figure 30

Applying the law of sines to Fig. 30

$$\frac{\sin \theta_0}{v_C} = \frac{\sin (\theta - \theta_0)}{v_2}$$

or

$$\sin (\theta - \theta_0) = \frac{v_2}{v_C} \sin \theta_0 \quad (3)$$

Considering only nonrelativistic interactions, where  $E = (m_1 + m_2 - m_3 - m_4) c^2$  is small compared with the rest energy  $m_1 c^2$  of any of the particles involved, it is assumed that  $m_1 + m_2 \approx m_3 + m_4$ . Substituting  $v_C$  from equation (1) and  $v_2$  from equation (2)



$$\frac{v_c}{V_3} = \left[ \frac{m_1 m_3}{m_2 m_4} \frac{E}{E + Q} \right]^{1/2} = \gamma \quad (4)$$

and equation (3) reduces to the useful form

$$\sin (\Theta - \Theta_0) = \gamma \sin \Theta_0 \quad (5)$$

In the case of scattering,  $m_3 = m_1$  and  $m_4 = m_2$  so that

$$\gamma = \frac{m_1}{m_2} \left[ \frac{E}{E + Q} \right]^{1/2}$$

By use of the trigonometric identity for the difference of two angles, equation (5) reduces to

$$\tan \Theta_0 = \frac{\sin \Theta}{\gamma + \cos \Theta} \quad (6)$$

which is identical with equation 18.4 of Schiff (83) and can be conveniently represented as shown in Fig. 31.

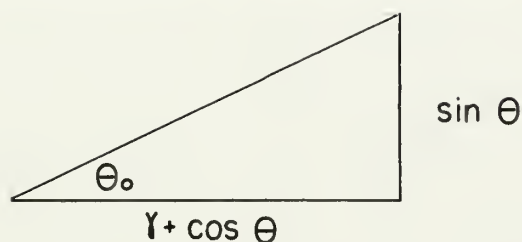


Figure 31

Equation (5) can then be plotted for each value of  $\gamma$  determined by the energy levels of the target nucleus as illustrated in Fig. 32. The conversion from laboratory to center-of-mass angle can be obtained directly from the curve with an accuracy of better than  $\pm 0.25$  degree.

(1)

$$r = \sqrt{\frac{a^2}{b^2} + \frac{b^2}{a^2}}$$

and equation (2) reduces to the identity

(2)

$$a^2 - b^2 = a^2 - b^2$$

In the case of rectangles,  $a = b$ , and  $r = \sqrt{2}$  in both

$$r = \sqrt{\frac{a^2}{b^2} + \frac{b^2}{a^2}}$$

By use of the Pythagorean theorem, the two different

and angles, equation (2) reduces to

(3)

$$\frac{a^2}{b^2} = \frac{a^2}{b^2}$$

which is identical with equation (2) of part (1) and

the corresponding expression is given in (2) - (3)



Figure 31

Equation (2) can then be written in the form of a  
definition of the angle theta in the right triangle as  
illustrated in Fig. 31. The corresponding two equations in  
center-of-mass units can be written similarly. The two  
with an accuracy of better than 0.1%.

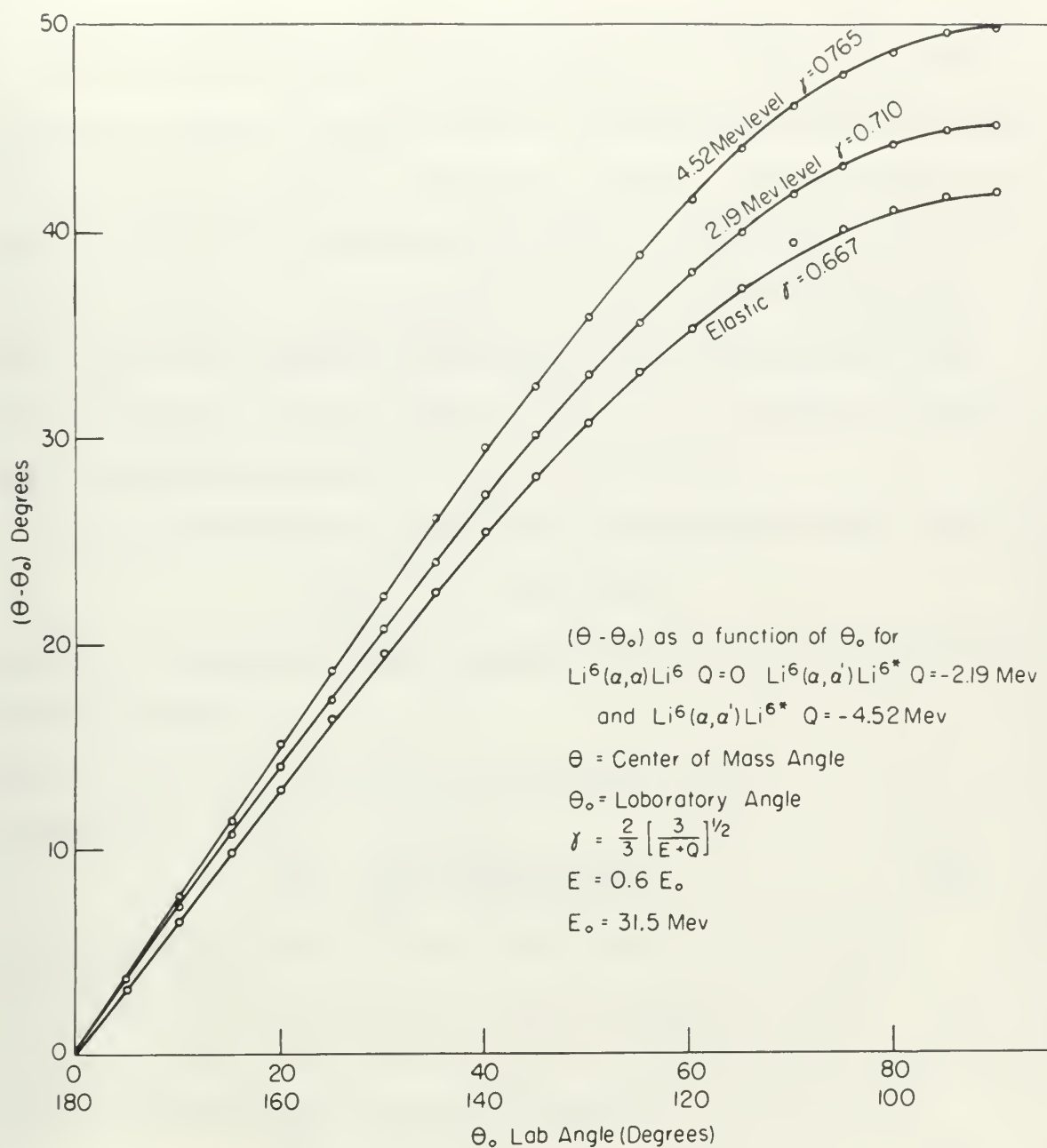


Figure 32





## 2. RELATION BETWEEN LABORATORY AND CENTER-OF-MASS DIFFERENTIAL CROSS SECTIONS

At a forward angle of observation, the finite counter aperture subtends a larger solid angle in the center-of-mass coordinates than in the laboratory system. This effect is most important in reactions involving light nuclei since it is due entirely to the velocity of the center of mass in the laboratory frame of reference. The relation between the differential cross section in the two reference frames can be obtained directly from its definition.

In the laboratory system, the differential solid angle is

$$d\omega = 2\pi \sin \theta_0 d\theta_0$$

since  $\phi$  is common to both reference frames. In the center-of-mass system

$$d\Omega = 2\pi \sin \theta d\theta$$

therefore

$$\frac{d\omega}{d\Omega} = \frac{\sin \theta_0 d\theta_0}{\sin \theta d\theta} \quad (7)$$

From Fig. 31

$$\cot \theta_0 = \gamma \csc \theta + \cot \theta \quad (8)$$

and by differentiation of equation (8)

$$\frac{d\theta_0}{d\theta} = \frac{\sin^2 \theta_0}{\sin^2 \theta} (1 + \gamma \cos \theta) \quad (9)$$

# RELATION BETWEEN LABORATORY AND CENTER-OF-MASS SYSTEMS

As a typical case of consideration, the linear motion of a particle is considered. In the laboratory system, the particle moves with a constant velocity  $v$ . This velocity is most important in reactions involving light nuclei since it is due entirely to the velocity of the center of mass in the laboratory frame of reference. The relation between the differential cross section in the two reference frames can be obtained directly from the definition.

In the laboratory system, the differential cross section is

$$\frac{d\sigma}{d\Omega} = \frac{d\sigma}{d\Omega_0} \frac{d\Omega_0}{d\Omega}$$

since  $\Omega$  is common to both reference frames. In the center-of-mass system

$$d\Omega = \sin\theta d\theta d\phi$$

therefore

$$(7) \quad \frac{d\sigma}{d\Omega} = \frac{d\sigma}{d\Omega_0} \frac{\sin\theta_0 d\theta_0 d\phi_0}{\sin\theta d\theta d\phi}$$

from fig. 12

$$(8) \quad \cos\theta_0 = \frac{v}{v_0} \cos\theta + \frac{V}{v_0}$$

and by differentiation of equation (8)

$$(9) \quad \frac{d\theta_0}{d\theta} = \frac{1}{\sin\theta} \left( \frac{v}{v_0} \sin\theta - \frac{V}{v_0} \right)$$

Figure 33 can be obtained directly from equation (8):

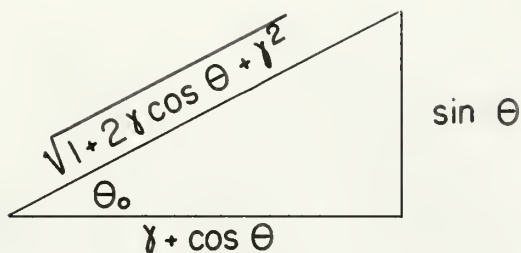


Figure 33

and Fig. 34 is obtained directly from equation (5):

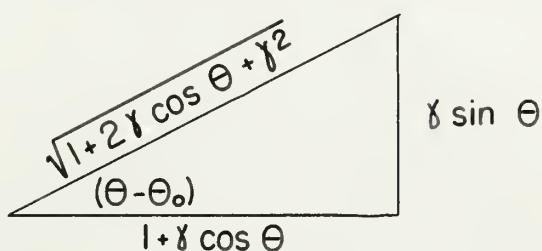


Figure 34

Substituting equation (9) into equation (7)

$$\frac{d\omega}{d\Omega} = \frac{\sin^3 \theta_0}{\sin^3 \theta} (1 + \gamma \cos \theta) \quad (10)$$

It is necessary to obtain the value of  $(\theta - \theta_0)$  in converting from laboratory to center-of-mass angle.

Equation (10) is easily expressed in terms of  $(\theta - \theta_0)$  by use of the following relation obtained from Fig. 33:

Figure 33 can be obtained directly from equation (5):

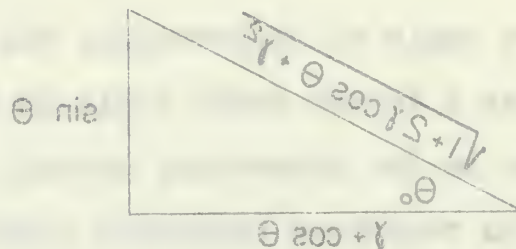


Figure 33

and Fig. 34 is obtained directly from equation (6):

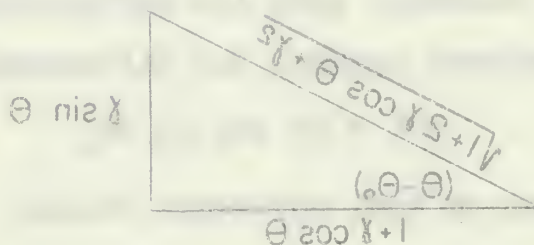


Figure 34

Substituting equation (6) into equation (4)

$$\frac{\partial \omega}{\partial \lambda} = \frac{\partial \omega}{\partial \lambda} \cdot \frac{\partial \lambda}{\partial \theta} \quad (10)$$

It is necessary to obtain the value of  $(\theta - \theta_0)$  in

converting from laboratory to center-of-mass angle.

Equation (10) is easily expressed in terms of  $(\theta - \theta_0)$  by

use of the following relation derived from Fig. 34:



$$\sin \vartheta_0 = \frac{\sin \vartheta}{\sqrt{1 + 2\gamma \cos \vartheta + \gamma^2}} \quad (11)$$

Substitution of equation (11) into equation (10) yields

$$\frac{d\omega}{d\Omega} = \frac{\sin^2 \vartheta_0}{\sin^2 \vartheta} \cos (\vartheta - \vartheta_0) \equiv g(\vartheta_0) \quad (12)$$

The intensity in the center-of-mass system is found by multiplying the measured intensity by the factor  $g$  which for a given reaction depends on  $\gamma$  and  $\vartheta_0$ . A plot of  $g(\vartheta_0)$ , computed for three levels of excitation of the  $\text{Li}^6$  nucleus, is illustrated in Fig. 35.



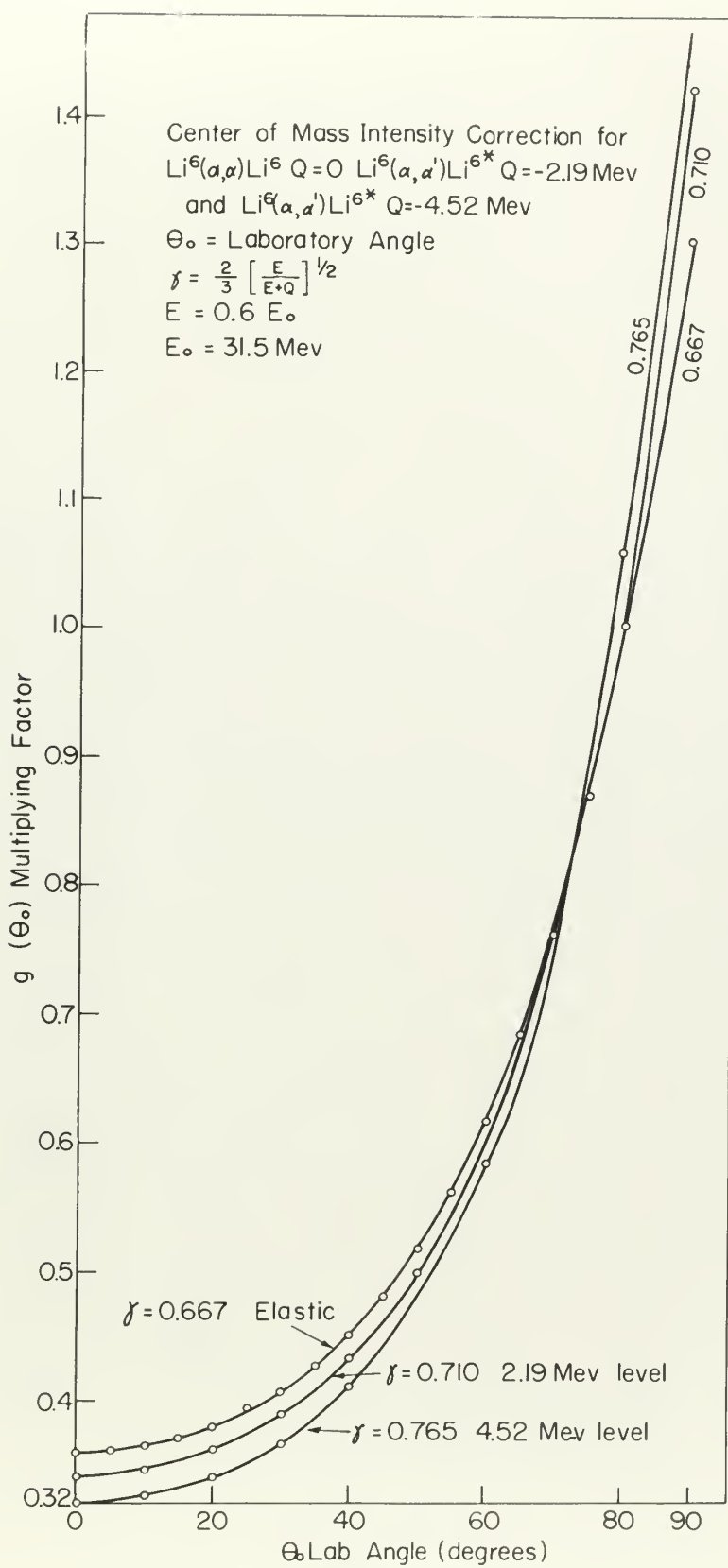


Figure 35





## BIBLIOGRAPHY

- A1 F. A. Aschenbrenner, Phys. Rev. 93, 657 (1953), and  
Ph.D. Thesis, M.I.T., May 1954.
- A2 W. A. Aron, B. G. Hoffman, and F. C. Williams, AECU 663,  
Radiation Laboratory, Univ. of Calif. May 1951.
- A3 F. Ajzenberg and T. Lauritsen, Revs. Modern Phys. 27,  
77 (1955).
- A4 N. Austern, S. T. Butler, and H. McManus, Phys. Rev. 92,  
350 (1953).
- A5 R. K. Adair, Phys. Rev. 87, 1041 (1952).
- A6 R. K. Adair, Phys. Rev. 86, 155 (1952).
- B1 H. A. Bethe, Revs. Modern Phys. 2, 69 (1937).
- B2 E. S. Bieler, Proc. Roy. Soc. (London), A105, 424 (1924).
- B3 P. R. Dyerly and W. E. Stephens, Phys. Rev. 21, 473 (1951).
- B4 E. Bleuler, A. K. Stebbins, and D. J. Tendam, Phys. Rev.  
90, 460 (1953).
- B5 A. B. Bhatia and K. Huang, reported by R. Kuby, Nature,  
186, 554 (1950).
- B6 J. S. Blair, Phys. Rev. 95, 1818 (1954).
- B7 C. J. Baker, J. N. Dodd, and D. H. Simmons, Phys. Rev.  
85, 1051 (1952).
- B8 S. Bashkin, F. P. Mooring and S. Petree, Phys. Rev. 81,  
378 (1951).
- B9 W. E. Burcham, W. M. Gibson, A. Hossain, and J. Rotblat,  
Phys. Rev. 92, 1266 (1953).

## BIBLIOGRAPHY

- 41 F. A. Thompson, *Phys. Rev.* 50 (1942), 202.
- 42 W. D. Thomas, *Phil. Mag.* 35 (1947), 100.
- 43 W. A. Brown, R. G. Holman, and V. G. Williams, *Phys. Rev.* 60 (1946), 100.
- 44 Radiation Laboratory, Univ. of Calif., *Phys. Rev.* 61 (1947), 100.
- 45 F. A. Thompson and V. G. Williams, *Phys. Rev.* 61 (1947), 100.
- 46 W. A. Thompson, R. G. Holman, and V. G. Williams, *Phys. Rev.* 61 (1947), 100.
- 47 W. A. Thompson, *Phys. Rev.* 61 (1947), 100.
- 48 W. A. Thompson, *Phys. Rev.* 61 (1947), 100.
- 49 W. A. Thompson, *Phys. Rev.* 61 (1947), 100.
- 50 W. A. Thompson, *Phys. Rev.* 61 (1947), 100.
- 51 W. A. Thompson, *Phys. Rev.* 61 (1947), 100.
- 52 W. A. Thompson, *Phys. Rev.* 61 (1947), 100.
- 53 W. A. Thompson, *Phys. Rev.* 61 (1947), 100.
- 54 W. A. Thompson, *Phys. Rev.* 61 (1947), 100.
- 55 W. A. Thompson, *Phys. Rev.* 61 (1947), 100.
- 56 W. A. Thompson, *Phys. Rev.* 61 (1947), 100.
- 57 W. A. Thompson, *Phys. Rev.* 61 (1947), 100.
- 58 W. A. Thompson, *Phys. Rev.* 61 (1947), 100.
- 59 W. A. Thompson, *Phys. Rev.* 61 (1947), 100.

- B10 E. Bleuler and D.J. Tandan, Phys. Rev. 70, 1205 (1955).
- B11 "Statistical Aspects of the Nucleus", a conference held at the Brookhaven National Laboratory, Jan. 14-26, 1955.
- B12 H. G. Blosser and T. E. Samsley, Phys. Rev. 100, 1348 (1955).
- C1 B. L. Cohen, Phys. Rev. 82, 1945 (1953).
- C2 E. D. Courant, Phys. Rev. 82, 703 (1951).
- C3 G. Chew, Phys. Rev. 80, 196 (1955).
- C4 B. L. Cohen and R. V. Neidigh, Rev. Sci. Instr. 25, 755 (1954).
- C5 B. L. Cohen and R. V. Neidigh, Phys. Rev. 93, 282 (1954).
- D1 S. Devons, Proc. Roy. Soc. (London), A172, 127 (1939).
- D2 E. C. Diven and G. M. Almy, Phys. Rev. 80, 407 (1950).
- E1 R. M. Eisberg, C. Igo, and H. E. Wegner, Phys. Rev. 92, 1606 (1955).
- E2 P. M. Endt and J. C. Kluyver, Revs. Modern Phys. 26, 95 (1954).
- F1 G. M. Farwell and H. E. Wegner, Phys. Rev. 92, 356 (1954).
- F2 Y. Fujimoto and A. Hossain, Phil. Mag. 46, 542 (1955).
- F3 R. G. Freemantle, D. J. Prowse, and J. Rotblatt, Phys. Rev. 96, 1268 (1954); R. G. Freemantle, W. M. Gibson, D. J. Prowse, and J. Rotblatt, Phys. Rev. 92, 1268 (1953); W. E. Burcham, W. M. Gibson, A. Hossain, and J. Rotblatt, Phys. Rev. 92, 1268 (1953).
- F4 H. Feshbach, C. E. Porter, and V. F. Weisskopf, Phys. Rev. 96, 448 (1954).
- F5 A. J. Ferguson, "The Elastic Scattering of Charged Particles b Nuclei", AEC of Canada, Ltd. AECL 157, August 1954.



1. W. H. Rouse Ball, Elementary Principles of Mathematics, 1892, 1893, 1894, 1895, 1896, 1897, 1898, 1899, 1900, 1901, 1902, 1903, 1904, 1905, 1906, 1907, 1908, 1909, 1910, 1911, 1912, 1913, 1914, 1915, 1916, 1917, 1918, 1919, 1920, 1921, 1922, 1923, 1924, 1925, 1926, 1927, 1928, 1929, 1930, 1931, 1932, 1933, 1934, 1935, 1936, 1937, 1938, 1939, 1940, 1941, 1942, 1943, 1944, 1945, 1946, 1947, 1948, 1949, 1950, 1951, 1952, 1953, 1954, 1955, 1956, 1957, 1958, 1959, 1960, 1961, 1962, 1963, 1964, 1965, 1966, 1967, 1968, 1969, 1970, 1971, 1972, 1973, 1974, 1975, 1976, 1977, 1978, 1979, 1980, 1981, 1982, 1983, 1984, 1985, 1986, 1987, 1988, 1989, 1990, 1991, 1992, 1993, 1994, 1995, 1996, 1997, 1998, 1999, 2000, 2001, 2002, 2003, 2004, 2005, 2006, 2007, 2008, 2009, 2010, 2011, 2012, 2013, 2014, 2015, 2016, 2017, 2018, 2019, 2020, 2021, 2022, 2023, 2024, 2025, 2026, 2027, 2028, 2029, 2030, 2031, 2032, 2033, 2034, 2035, 2036, 2037, 2038, 2039, 2040, 2041, 2042, 2043, 2044, 2045, 2046, 2047, 2048, 2049, 2050, 2051, 2052, 2053, 2054, 2055, 2056, 2057, 2058, 2059, 2060, 2061, 2062, 2063, 2064, 2065, 2066, 2067, 2068, 2069, 2070, 2071, 2072, 2073, 2074, 2075, 2076, 2077, 2078, 2079, 2080, 2081, 2082, 2083, 2084, 2085, 2086, 2087, 2088, 2089, 2090, 2091, 2092, 2093, 2094, 2095, 2096, 2097, 2098, 2099, 2100, 2101, 2102, 2103, 2104, 2105, 2106, 2107, 2108, 2109, 2110, 2111, 2112, 2113, 2114, 2115, 2116, 2117, 2118, 2119, 2120, 2121, 2122, 2123, 2124, 2125, 2126, 2127, 2128, 2129, 2130, 2131, 2132, 2133, 2134, 2135, 2136, 2137, 2138, 2139, 2140, 2141, 2142, 2143, 2144, 2145, 2146, 2147, 2148, 2149, 2150, 2151, 2152, 2153, 2154, 2155, 2156, 2157, 2158, 2159, 2160, 2161, 2162, 2163, 2164, 2165, 2166, 2167, 2168, 2169, 2170, 2171, 2172, 2173, 2174, 2175, 2176, 2177, 2178, 2179, 2180, 2181, 2182, 2183, 2184, 2185, 2186, 2187, 2188, 2189, 2190, 2191, 2192, 2193, 2194, 2195, 2196, 2197, 2198, 2199, 2200, 2201, 2202, 2203, 2204, 2205, 2206, 2207, 2208, 2209, 2210, 2211, 2212, 2213, 2214, 2215, 2216, 2217, 2218, 2219, 2220, 2221, 2222, 2223, 2224, 2225, 2226, 2227, 2228, 2229, 2230, 2231, 2232, 2233, 2234, 2235, 2236, 2237, 2238, 2239, 2240, 2241, 2242, 2243, 2244, 2245, 2246, 2247, 2248, 2249, 2250, 2251, 2252, 2253, 2254, 2255, 2256, 2257, 2258, 2259, 2260, 2261, 2262, 2263, 2264, 2265, 2266, 2267, 2268, 2269, 2270, 2271, 2272, 2273, 2274, 2275, 2276, 2277, 2278, 2279, 2280, 2281, 2282, 2283, 2284, 2285, 2286, 2287, 2288, 2289, 2290, 2291, 2292, 2293, 2294, 2295, 2296, 2297, 2298, 2299, 2300, 2301, 2302, 2303, 2304, 2305, 2306, 2307, 2308, 2309, 2310, 2311, 2312, 2313, 2314, 2315, 2316, 2317, 2318, 2319, 2320, 2321, 2322, 2323, 2324, 2325, 2326, 2327, 2328, 2329, 2330, 2331, 2332, 2333, 2334, 2335, 2336, 2337, 2338, 2339, 2340, 2341, 2342, 2343, 2344, 2345, 2346, 2347, 2348, 2349, 2350, 2351, 2352, 2353, 2354, 2355, 2356, 2357, 2358, 2359, 2360, 2361, 2362, 2363, 2364, 2365, 2366, 2367, 2368, 2369, 2370, 2371, 2372, 2373, 2374, 2375, 2376, 2377, 2378, 2379, 2380, 2381, 2382, 2383, 2384, 2385, 2386, 2387, 2388, 2389, 2390, 2391, 2392, 2393, 2394, 2395, 2396, 2397, 2398, 2399, 2400, 2401, 2402, 2403, 2404, 2405, 2406, 2407, 2408, 2409, 2410, 2411, 2412, 2413, 2414, 2415, 2416, 2417, 2418, 2419, 2420, 2421, 2422, 2423, 2424, 2425, 2426, 2427, 2428, 2429, 2430, 2431, 2432, 2433, 2434, 2435, 2436, 2437, 2438, 2439, 2440, 2441, 2442, 2443, 2444, 2445, 2446, 2447, 2448, 2449, 2450, 2451, 2452, 2453, 2454, 2455, 2456, 2457, 2458, 2459, 2460, 2461, 2462, 2463, 2464, 2465, 2466, 2467, 2468, 2469, 2470, 2471, 2472, 2473, 2474, 2475, 2476, 2477, 2478, 2479, 2480, 2481, 2482, 2483, 2484, 2485, 2486, 2487, 2488, 2489, 2490, 2491, 2492, 2493, 2494, 2495, 2496, 2497, 2498, 2499, 2500, 2501, 2502, 2503, 2504, 2505, 2506, 2507, 2508, 2509, 2510, 2511, 2512, 2513, 2514, 2515, 2516, 2517, 2518, 2519, 2520, 2521, 2522, 2523, 2524, 2525, 2526, 2527, 2528, 2529, 2530, 2531, 2532, 2533, 2534, 2535, 2536, 2537, 2538, 2539, 2540, 2541, 2542, 2543, 2544, 2545, 2546, 2547, 2548, 2549, 2550, 2551, 2552, 2553, 2554, 2555, 2556, 2557, 2558, 2559, 2560, 2561, 2562, 2563, 2564, 2565, 2566, 2567, 2568, 2569,



- F6 R. G. Freemantle, D. J. Prowse, A. Rossin, and J. Rotblatt, Phys. Rev. 96, 1470 (1954).
- F7 F. J. M. Farley, Nucleonics, 12, 56 (October 1954).
- F8 S. Fernbach, R. Serber, and T. E. Taylor, Phys. Rev. 75, 1352 (1949).
- F9 N. C. Francis and K. M. Watson, Am. J. Phys. 21, 659 (1953).
- G1 E. Guth, Phys. Rev. 68, 280 (1945).
- G2 H. E. Cove and H. F. Stoddart, Phys. Rev. 86, 572 (1952).
- G3 H. E. Cove, Phys. Rev. 99, 1353 (1955).
- G4 P. C. Gugelot, Phys. Rev. 87, 575 (1952).
- G5 H. Geiger and E. Marsden, Proc. Roy. Soc. (London), A85, 495 (1909).
- H1 J. W. Haffner, Ph.D. Thesis, M.I.T., 1955.
- H2 R. Euby and H. C. Newns, Phil. Mag. 42, 1448 (1951).
- H3 W. Hauser and H. Feshbach, Phys. Rev. 87, 366 (1952).
- H4 R. Euby and H. C. Newns, Proc. Phys. Soc. (London), A64, 618 (1951).
- H5 H. J. Hausman, A. J. Allen, J. S. Arthur, R. F. Bender, and C. J. McDole, Phys. Rev. 88, 1296 (1952).
- H6 Private communication, E. Henley, Univ. of Washington.
- I1 "Elastic Scattering of 40-Mev Alpha Particles from Light Elements", G. Igo, H. E. Wegner, and R. M. Eisberg; preprint to be published in Physical Review.



- L1 M. S. Livingston, J. Appl. Phys. 15, 2 (1944).
- L2 M. S. Livingston and H. A. Bethe, Revs. Modern Phys. 9, 263 (1937).
- L3 A. M. Lane and R. G. Thomas, "The Compound Nucleus Theory of Nuclear Reactions", to be published.
- L4 R. E. LeLevier and D. S. Saxon, Phys. Rev. 87, 45 (1953).
- M1 Private communication, D. W. Miller, Indiana University.
- M2 H. McManus and A. T. Sharp, Phys. Rev. 87, 128 (1953).
- M3 C. J. Mullin and E. Guth, Phys. Rev. 82, 141 (1951).
- M4 M. A. Melkanoff, S. A. Moszkowski, J. Nedvik, and D. S. Saxon, University of California, unpublished.
- M5 M. Moskow, Master's Degree Essay, Johns Hopkins University, May 1948.
- P1 C. E. Porter, Phys. Rev. 99, 1400 (1955).
- P2 J. Prentki, Cahiers de Phys. 55, 37 (1955). Contains a review of theories for the excitation of nuclei by charged particles.
- R1 E. Rutherford, Phil. Mag. 21, 869 (1911).
- R2 V. K. Rasmussen, D. W. Miller, and M. B. Sampson, Phys. Rev. 100, 181 (1955).
- R3 W. Reizler, Proc. Roy. Soc. (London), A134, 154 (1931).
- R4 E. H. Rhoderick, Proc. Roy. Soc. (London), A201, 348 (1950).
- R5 Private communication, L. S. Rodberg, M.I.T.



- [illegible]



- S1 H. F. Stoddart and R. E. Cove, Phys. Rev. 87, 961 (1953).
- S2 G. Schrank, P. C. Engelot, and I. B. Layton, Palmer Physical Laboratory, Princeton University, September 27, 1954 (unpublished).
- S3 L. I. Schiff, "Quantum Mechanics", pp. 87-101, McGraw-Hill Book Co., Inc., 1949.
- S4 M. M. Shapiro, Phys. Rev. 90, 171 (1953).
- T1 C. J. Taylor, W. K. Jentschke, M. E. Renley, F. S. Eby, and P. C. Kruger, Phys. Rev. 84, 1034 (1951).
- T2 E. Bleuler and D. J. Tendam, Bull. Am. Phys. Soc. 30, No. 4, 26 (1955).
- T3 This computation was done by W. Tobocean, Institute for Advanced Study, Princeton University.
- T4 H. A. Tolhoek and P. J. Brussard, Physica, XXI, 449 (1955).
- T5 Private communication, W. Tobocean, Institute for Advanced Study, Princeton, University.
- W1 N. S. Wall, Ph.D. Thesis, M.I.T. 1953.
- W2 H. E. Wegner, R. M. Eisberg, and G. Igo, Phys. Rev. 99, 825 (1955).
- W3 N. S. Wall, J. R. Rees, and K. W. Ford, Phys. Rev. 97, 726 (1955).
- W4 V. F. Weisskopf, and D. H. Ewing, Phys. Rev. 57, 473 (1940).

- 61 E. J. Boudier and G. J. Boudier, *Ann. Bot. (Paris)* 1904.
- 62 G. Boudier, *Ann. Bot. (Paris)* 1904.
- 63 Botanical Laboratory, University of Wisconsin, Madison, Wis.
- 64 1904 (unpublished).
- 65 E. J. Boudier, *Ann. Bot. (Paris)* 1904.
- 66 E. J. Boudier, *Ann. Bot. (Paris)* 1904.
- 67 E. J. Boudier, *Ann. Bot. (Paris)* 1904.
- 68 E. J. Boudier, *Ann. Bot. (Paris)* 1904.
- 69 E. J. Boudier, *Ann. Bot. (Paris)* 1904.
- 70 E. J. Boudier, *Ann. Bot. (Paris)* 1904.
- 71 E. J. Boudier, *Ann. Bot. (Paris)* 1904.
- 72 E. J. Boudier, *Ann. Bot. (Paris)* 1904.
- 73 E. J. Boudier, *Ann. Bot. (Paris)* 1904.
- 74 E. J. Boudier, *Ann. Bot. (Paris)* 1904.
- 75 E. J. Boudier, *Ann. Bot. (Paris)* 1904.
- 76 E. J. Boudier, *Ann. Bot. (Paris)* 1904.
- 77 E. J. Boudier, *Ann. Bot. (Paris)* 1904.
- 78 E. J. Boudier, *Ann. Bot. (Paris)* 1904.
- 79 E. J. Boudier, *Ann. Bot. (Paris)* 1904.
- 80 E. J. Boudier, *Ann. Bot. (Paris)* 1904.
- 81 E. J. Boudier, *Ann. Bot. (Paris)* 1904.
- 82 E. J. Boudier, *Ann. Bot. (Paris)* 1904.
- 83 E. J. Boudier, *Ann. Bot. (Paris)* 1904.
- 84 E. J. Boudier, *Ann. Bot. (Paris)* 1904.
- 85 E. J. Boudier, *Ann. Bot. (Paris)* 1904.
- 86 E. J. Boudier, *Ann. Bot. (Paris)* 1904.
- 87 E. J. Boudier, *Ann. Bot. (Paris)* 1904.
- 88 E. J. Boudier, *Ann. Bot. (Paris)* 1904.
- 89 E. J. Boudier, *Ann. Bot. (Paris)* 1904.
- 90 E. J. Boudier, *Ann. Bot. (Paris)* 1904.

- W5 T. R. Wilkins, Phys. Rev. 60, 365 (1941).
- W6 J. M. Blatt and V. F. Weisskopf, "Theoretical Nuclear Physics", John Wiley and Sons, N. Y., 1951.
- W7 Private communication, N. S. Wall.
- W8 G. A. Wrenshall, Phys. Rev. 61, 58 (1943).
- W9 R. D. Woods and D. S. Eaxon, Phys. Rev. 96, 577 (1954).

- 45 J. B. Williams, *ibid.*, p. 100 (1961).
- 46 J. B. Williams and J. F. Williams, *Theoretical Physics*, John Wiley and Sons, N. Y. 1961.
- 47 Private communication, to J. B. Williams.
- 48 G. A. H. Roberts, *ibid.*, p. 100 (1961).
- 49 J. B. Williams and J. F. Williams, *ibid.*, p. 100 (1961).



## BIOGRAPHICAL NOTE

The author was born August 19, 1930 in Indianapolis, Indiana. He was called to active duty as a member of the U. S. Naval Reserve in 1940, commissioned an Ensign in 1943 and subsequently served on board the USS BRAINE (DD630) in the South Pacific until 1945. In December 1945 he was assigned as Operations Officer, Commander Destroyer Squadron 4 and later served as Executive Officer, USS GEARING (DE710). In 1947, in accordance with the U. S. Navy Five Term Program, he was enrolled as an undergraduate at Purdue University and in 1949 was awarded the B.S. degree with Highest Distinction.

He attended the U. S. Naval Postgraduate School, Annapolis, Md. during the academic year 1950-51, as a student in the Ordnance Engineering (Special Physics) curriculum, and was enrolled in the M.I.T. Graduate School, Department of Physics, in June 1951. After obtaining the degree of Master of Science at M.I.T. in June 1953 he was assigned as Commanding Officer, USS C. T. O'BRIEN (DE421). In September 1954 he returned to M.I.T. and was enrolled in the Graduate School of Physics under the provisions of The Advanced Science Program sponsored by the Office of Naval Research.

Publication: "The Radionuclides of Arsenic Produced by Deuteron Bombardment of Germanium", Phys. Rev. 95, 148 (1951), with Lt. J. F. Fagan, Jr.





AMERICAN MEDICAL ASSOCIATION  
PUBLISHED WEEKLY

CHICAGO, ILL., U.S.A.  
1914

Subscription price, Five Dollars Per Annum in Advance.  
Single Copies, Fifteen Cents.

Entered as Second-Class Matter, May 2, 1882.  
Postpaid.

Acceptance for mailing at special rate of postage provided for in  
Act of October 3, 1917, authorized on July 16, 1918.

Postage paid at Chicago, Ill., and at additional mailing offices.  
Postmaster: Send address changes to THE JOURNAL OF THE  
AMERICAN MEDICAL ASSOCIATION, 535 N. Dearborn St., Chicago, Ill.

Copyright, 1914, by American Medical Association.  
Printed at the Chicago Press & Publishing Co., Chicago, Ill.

Published by the American Medical Association, 535 N. Dearborn St., Chicago, Ill.  
Subscription orders, notices of change of address, and all correspondence  
should be sent to the Editor, at the above address.













JA 17 58

BINDERY

Thesis  
W268

Watters

36226

Angular distributions  
of alpha particles scat-  
tered by light nuclei.

JA 17 58

BINDERY

Thesis  
W268

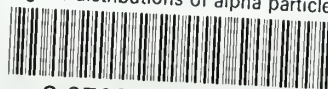
Watters

36226

Angular distributions of alpha  
particles scattered by light  
nuclei.

thesW268

Angular distributions of alpha particles



3 2768 001 93020 9

DUDLEY KNOX LIBRARY